Regulation of Telomere Maintenance by the Shelterin Complex in Fission Yeast *Schizosaccharomyces pombe*

By

Ya-Ting Chang
B.S., National Taiwan University, 1999
M.S., National Yang-Ming University, 2003

THESIS

Submitted as partial fulfillment of the requirements
for the degree of Doctor of Philosophy in Biochemistry and Molecular Genetics
in the Graduate College of the
University of Illinois at Chicago, 2014

Chicago, Illinois
Defense Committee:

Toru M. Nakamura, Chair and Advisor
Pradip Raychaudhuri, Biochemistry and Molecular Genetics
Vadim Gaponenko, Biochemistry and Molecular Genetics
Maxim Frolov, Biochemistry and Molecular Genetics
Yee-Kin Ho, Biochemistry and Molecular Genetics
Amy L. Kenter, Microbiology and Immunology

This thesis is dedicated to my family, especially my parents Yu-Shui Chang and Liao-Chu Su (張玉水, 蘇廖珠), as well as my dearest friend 小羊子. Without them it would ever have been accomplished.

Acknowledgements

This research could not have been completed without the help of many people. First of all, I would like to thank my advisor, Dr. Toru M. Nakamura, for his support and his adventure with me. Our weekly discussion helped me to develop my own ideas and became a better graduate student. I especially want to express my great appreciation to my committee members for their valuable and constructive suggestions during the development of this research work. The deepest gratitude is also due to Dr. Vadim Gaponenko, who shared his great experience and wisdom. Without his help, I wouldn't successfully develop the optimal protocol for Tpz1 purification and identify Tpz1 phosphorylation sites. My gratitudes also extend to Dr. Yen-Kin Ho and Dr. Pradip Raychaudhuri, for their encouragement and support. They have helped me, as a foreign student, to stand on my own feet and finish my long journey of science exploration. In addition, I want to thank Dr. Bettina Moser for sharing the experimental skills and useful suggestions for both scientific experiments and life. Special thanks also goes to my collaborator Dr. Aaron Aslanian from Dr. John Yates the third laboratory of the Scripps Research Institute. Without his spectacular skills and knowledge of the mass spectrometry analysis, this study would never have been completed. I also would like to express my heartfelt thanks to my very good friend Dr. Lakxmi Subramanian, my best friends in Taiwan: Teata Chang, Iris Li, Cheng Huang, Catherine Tsai, Amber Lin, and Natasha Tsai, for their wonderful friendship and the way that they have always been there for me. I am very lucky to have them in my life. Finally, I really wish to express my love and gratitude to my family for their support and blessings for my studies. My

mother is my inspiration, who finished her high school in her 60s. I wouldn't finish this study without her as a role model.

The portion of chapter 2 in this work has been published previously in PLoS Genetics.

Copyright and License Policies of PLoS Genetics

Open access agreement. Upon submission of an article, its authors are asked to indicate their agreement to abide by an open access Creative Commons Attribution (CC BY) license. Under the terms of this license, authors retain ownership of the copyright of their articles. However, the license permits any user to download, print out, extract, reuse, archive, and distribute the article, so long as appropriate credit is given to the authors and source of the work. The license ensures that the authors' article will be available as widely as possible and that the article can be included in any scientific archive.

Contribution of Authors

Chapter 1 is a literature review that places my dissertation question in the context of the larger field and highlights the significance of my research question. Chapter 2 represents a published manuscript for which I was the primary author and major driver of the research. Dr. Bettina Moser finished the experiments shown in Figures 2.14C. My research advisor, Dr. Toru M. Nakamura contributed to the writing of the manuscript. Chapter 3 represents a series of my own unpublished data directed at answering the question of how Tpz1 hyperphosphorylation involves in telomere maintenance. I anticipate that this line of research will be continued in the laboratory after I leave and that this work will ultimately be published as part of a co-authored manuscript.

Table of Contents

List of Figures

List of Tables

Abbreviation

a.a.	Amino acid
APMSF	4-Amidinophenylmethanesulfonyl fluoride hydrochloride
bp	Base pair
cDNA	Complementary DNA
ChIP	Chromatin Immunoprecipitation
DDRs	DNA damage responses
DSB	Double Stranded Break
dsDNA	Double stranded DNA
HR	Homologous recombination
NHEJ	Non-homologous end joining
OB fold	oligonucleotide/oligosaccharide fold
PMG	Pombe Glutamate medium
PMSF	Phenylmethylsulfonyl fluoride
RPA	Replication Protein A
ssDNA	Single stranded DNA
STE	Subtelomeric repeat element
TCA	Trichloroacetic Acid
Tpz1	TPP1 homolog in *Schizosaccharomyces pombe*

Summary

Telomere replication is tightly controlled during cell cycle progression, especially in late S/G_2 phase when 3'-overhang of telomere is extended by telomerase, a specialized reverse transcriptase crucial for compensating DNA loss from the incomplete duplication of telomeric DNA by replicative DNA polymerases. Studies in fission yeast have previously identified evolutionarily conserved shelterin and Stn1-Ten1 complexes, and established that $Rad3^{ATR}$/$Tel1^{ATM}$-dependent phosphorylation of the shelterin complex subunit Ccq1 at Thr93 as a critical post-translational modification for telomerase recruitment to telomeres. Furthermore, the shelterin complex subunits Poz1, Rap1 and Taz1 have been identified as negative regulators of Ccq1 Thr93 phosphorylation and telomerase recruitment. However, it remained unclear how telomere maintenance is dynamically regulated during the cell cycle.

In the first part of my study, I therefore investigated how loss of Poz1, Rap1 and Taz1 affects cell cycle regulation of Ccq1 Thr93 phosphorylation and telomere association of telomerase ($Trt1^{TERT}$), DNA polymerases, Replication Protein A (RPA) complex, $Rad3^{ATR}$-$Rad26^{ATRIP}$ checkpoint kinase complex, $Tel1^{ATM}$ kinase, shelterin subunits (Tpz1, Ccq1 and Poz1) and Stn1. Furthermore, I examined how telomere shortening, caused by *trt1⊿* or catalytically dead *trt1-D743A*, affects cell cycle-regulated telomere association of telomerase and DNA polymerases. Based on these findings, I then proposed that fission yeast shelterin maintains telomere length homeostasis by coordinating the differential arrival of leading (Polε) and lagging (Polα) strand DNA polymerases at telomeres to modulate $Rad3^{ATR}$ association, Ccq1 Thr93 phosphorylation and telomerase recruitment. In the second part of my study, I

determined that Ccq1-interacting protein, Tpz1 is hyper-phosphorylated by Rad3^{ATR}/Tel1^{ATM} kinases in strains with highly elongated telomeres due to lack of telomerase inhibitors (*poz1Δ*, *rap1Δ*, and *taz1Δ*) as well as in strains with shorter telomeres due to a defect in telomerase mediated telomere extension by telomerase (*trt1Δ* and *ccq1-T93A*). The increase in Tpz1-telomerase interactions mirrored the increase in Tpz1 hyper-phosphorylation observed in *poz1Δ*, *rap1Δ* and *taz1Δ* cells, raising the possibility that Tpz1 phosphorylation might be important in promoting telomerase-shelterin interaction and telomerase mediated telomere extension. Furthermore, deletion of the *ccq1* gene abolished Tpz1 hyper-phosphorylation, suggesting that Ccq1 functions as an adaptor to mediate Rad3^{ATR}/Tel1^{ATM}-dependent phosphorylation of Tpz1. However, abolishment of all six high consensus Rad3^{ATR}/Tel1^{ATM} phosphorylation sites with the preferred SQ/TQ motif did not completely eliminate Tpz1 hyper-phosphorylation in *rap1Δ* cells nor did it lead to any defect in telomere length maintenance, suggesting that non-SQ/TQ sites within Tpz1 must be phosphorylated.

Therefore, to more comprehensively determine Tpz1 phosphorylation sites and examine functional significance of Tpz1 phosphorylation in telomere maintenance, I identified *in vivo* Tpz1 phosphorylation sites by mass spectrometry analysis and carried out mutational analysis of these sites. My analysis revealed that a non-Rad3^{ATR}/ Tel1^{ATM} phosphorylation site Ser138 negatively regulated telomere extension, while multiple phosphorylation sites within a central S/T rich region of Tpz1 positively regulated both telomere extension and phosphorylation-dependent mobility shift of Tpz1 observed in

rap1Δ cells. These findings thus established that phosphorylation of Tpz1 contributes to telomere length homeostasis.

1. Introduction

1.1 Early history of telomere studies

A specialized nucleoprotein structure called telomere protects ends of linear chromosomes in eukaryotes. Pioneering studies carried out by Herman Müller and Barbara McClintock in 1930s established importance of telomeres in genome stability. Müller analyzed fruit fly *Drosophila* chromosomes, and found X ray-induced chromosome break sites are prone to rearrangement but natural chromosome ends are protected from rearrangement. Therefore, he concluded that "the terminal gene must have a special function that of sealing the end of the chromosome" and that "for some reason, a chromosome cannot persist indefinitely without having its ends thus sealed (Müller, 1938). He named this structure "telomere" (from Greek *telos* = end and *meros* = part). Through studies of Maize chromosomes, McClintock found that newly generated chromosome break sites frequently underwent multiple rounds of fusion-breakage cycles. If broken ends from different chromosomes are fused, such fused chromosomes can break again when two centromeres are pulled toward the opposite poles during mitosis. However broken ends could eventually be "healed" and protected from further fusion-breakage cycles much like ends of chromosomes (McClintock, 1941).

Studies in subsequent years have determined that telomeric DNA is comprised of repetitive GT-rich sequences in most eukaryotic species, and specific proteins recognize and bind to these telomeric repeats (Baumann and Cech, 2001; Liu et al., 2004; Miyoshi et al., 2008; Ye et al., 2004; Zhong et al., 1992). Telomere proteins are critical for protecting chromosome ends from nuclease degradation, fusions and rearrangements events by DNA repair factors, and being recognized by DNA damage

checkpoint proteins that can induce permanent cell cycle arrest or apoptosis (Lydall, 2009)

Since replicative DNA polymerases (which can only extend DNA strands in a 5' to 3' direction) cannot fully duplicate ends of linear DNA molecule, telomeric DNA is lost every cell cycle unless cells have an alternative mechanism to overcome this "end replication problem" (Fig. 1.1) (Olovnikov, 1971; Watson, 1972). In the 1980s, studies carried out by Elizabeth Blackburn and Carol Greider identified a specialized reverse transcriptase known as telomerase from *Tetrahymena* that is capable of extending GT-rich telomeric repeats *de novo* by using its tightly associated RNA subunit as a template. (Greider and Blackburn, 1985, 1989; Yu et al., 1990). Understanding how telomeric proteins regulate recruitment of telomerase to telomeres remains to be highly active area of research, as studies in recent years have found that failure to properly maintain telomeres can lead to premature aging and various types of cancer in humans (Armanios and Blackburn, 2012; Martinez and Blasco, 2010)

1.2 Fission yeast as a model organism for telomere research

Fission yeast *Schizosaccharomyces pombe* is a unicellular eukaryotic organism that is evolutionarily as distant from more commonly used budding yeast *Saccharomyces cerevisiae* as from humans (Hedges, 2002; Sipiczki, 2000). However, proteins involved in ensuring stable maintenance of telomeres in *S. pombe* are much better conserved with humans than in *S. cerevisiae* (Figure 1.2 and Table 1.1) (Baumann and Cech, 2001; de Lange, 2005; Miyoshi et al., 2008) Furthermore, the fact that *S. pombe* cells

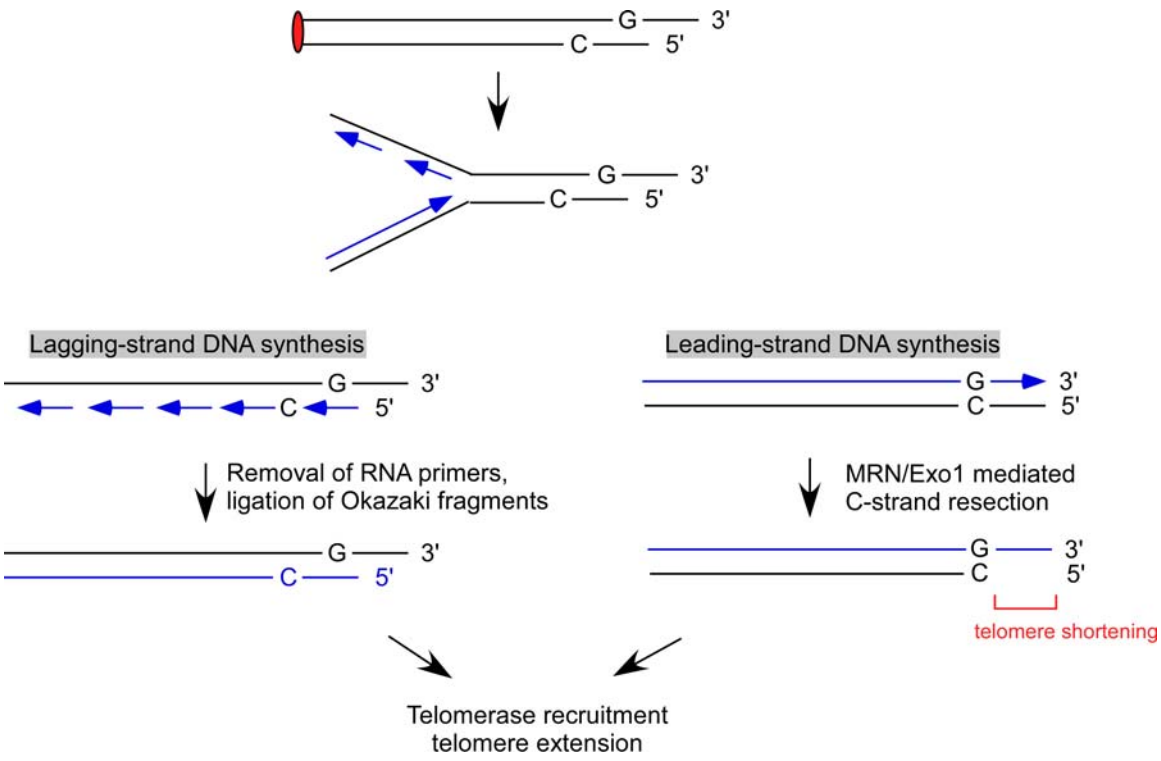

Figure 1.1 The end replication problem at telomeres

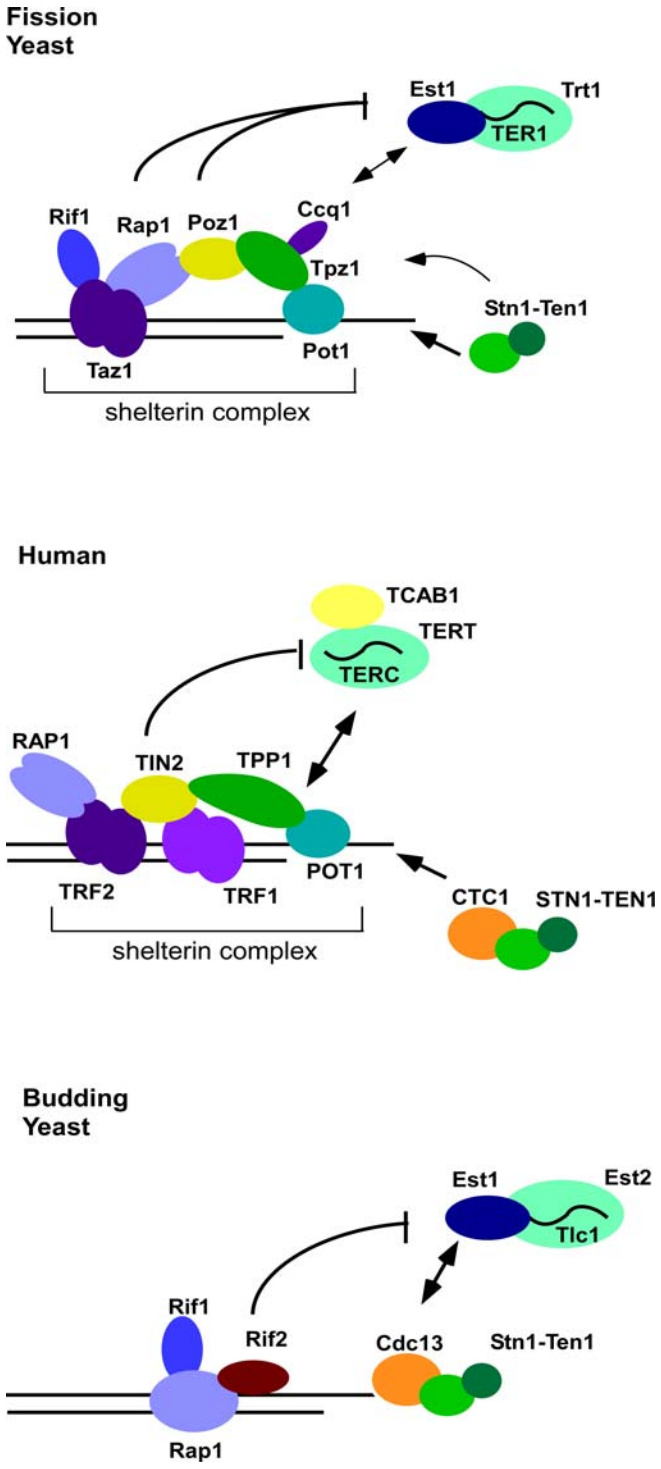

Figure 1.2 Proteins involved in telomere maintenance in fission yeast, human and budding yeast.

Table 1.1 Protein involves in telomere maintenance in human, fission yeast and budding yeast.

	Human	Fission Yeast	Budding Yeast	Biological Function
Protein components of the telomere				
Telomerase	TERT	Trt1	Est1	Telomerase catalytic subunit
	Est1	Est1	Est1A/B	Telomerase regulatory subunit
	TERC	TER1	TLC1	RNA component; function as template of telomere extension
CST complex	CTC1		Cdc13	G-tail binding protein for end protection; work together with Stn1/Ten1, named CST complex
		Stn1	Stn1	
		Ten1	Ten1	
Shelterin complex	Pot1	Pot1		G-tail capping protein
		Ccq1		Required for telomerase recruitment in fission yeast
	Tpp1	Tpz1		Pot1 interacting protein; Tpz1 is an adapter of Pot1 complex and required for telomerase recruitment
	Tin2	Poz1		Bridging protein required to connect ssDNA and dsDNA binding proteins
dsDNA binding proteins	Rap1	Rap1	Rap1	dsDNA telomere repeat binding proteins. Prevent DNA damage repair responses (HR, NHEJ) at telomeres; negative regulation in telomere lengthening
	Trf1/Trf2	Taz1		
		Rif1	Rif1/Rif2	
DNA damage proteins				
Signal modifier	Mre11/Rad 50/Nbs1	Rad32/Rad 50/Nbs1	Mre11/Rad50/ Xrs2	Recognize DNA damages and initiate DNA damage response (Homologous recombination); also involved in ATM/Tel1 recruitment to DNA damage sites and initiate DNA damage responses
Sensor/PIKK	ATM	Tel1	Tel1	Phosphorylate target proteins at DNA damage sites
	ATR	Rad3	Mec1	
PIKK interacting protein	ATRIP	Rad26	Lcd1/Ddc2	Required for ATR binding to RPA coated ssDNA
	Ku	Ku	Ku	Required for Non-Homologous End Joining

Table 1.1 Proteins involve in telomere maintenance.

can survive telomere dysfunction by circularizing all three chromosomes allows researchers to more easily characterize telomere dysfunction in this organism than in other organisms that carry more chromosomes and cannot easily survive telomere dysfunction due to a high occurrence of inter-chromosome fusions (Baumann and Cech, 2001; Naito et al., 1998; Nakamura et al., 1998). Highly developed molecular genetics tools also make it easy to introduce mutations and epitope tags into fission yeast cells to generate strains suitable for carrying out detailed functional studies. These characteristics thus make fission yeast an attractive model system for studying telomere biology.

1.2.1 Telomeric and sub-telomeric DNA in fission yeast

In fission yeast, proximal telomeric DNA consists of a ~300bp repetitive consensus DNA sequence TTAC(A) (C)$G_{2\text{-}8}$, that is mostly double stranded. Telomeric DNA terminates with 3' single stranded DNA structures, known as G-tails. The G-tail provides the binding sites for telomeric proteins to protect and execute telomere functions. The G-tail also serves as a primer for DNA synthesis by telomerase (Figure 1.3A). The loosely conservative 86bp repeats (Sub-telomeric repeat element, STE) reside in sub-telomeric regions on each arm of Chromosome I and II (Figure 1.3B).

Both telomeric and sub-telomeric DNA sequences behave as buffers against telomeric DNA loss caused by the end replication problem and degradation by nucleases. Telomeric and sub-telomeric regions can also "silence" transcription by RNA Polymerase II due to formation of heterochromatin (Nimmo et al., 1994). On the other hand, studies have found that sub-telomeric DNA is transcribed as

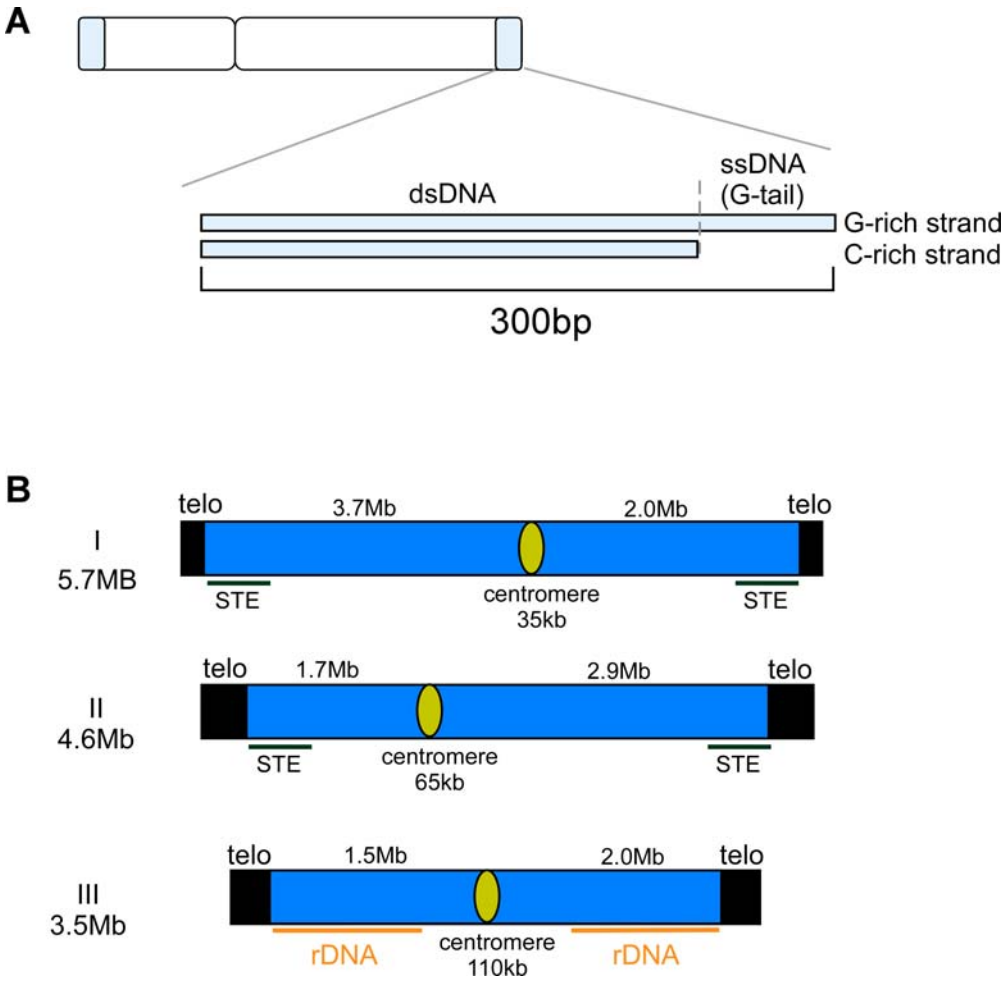

Figure 1.3 Telomere DNA structure
(**A**) Telomeric DNA (~300bp) at chromosome ends. (**B**) Telomere sequence arrangement in fission yeast chromosomes (Adapted from De Lange,T., Lundblad, T., Blackburn, E. (2006). Telomeres, Second Ed. In Julia Promisel Cooper, Yasushi Hiraoka Chapter 16. “Fission Yeast Telomeres”, pp 495-523, Long Island, New York: Cold Spring Harbor Laboratory Press.)

non-coding RNA in fission yeast (Bah et al., 2012; Greenwood and Cooper, 2012). While the functional significance of sub-telomeric non-coding RNA in fission yeast is not known, related telomeric repeat-containing RNA (TERRA) from budding yeast and humans have been shown to regulate telomere extension by telomerase and homologous recombination DNA repair proteins (Azzalin et al., 2007; Luke et al., 2008; Schoeftner and Blasco, 2008).

1.2.2 Telomere proteins in fission yeast

The telomeric repeat DNA in fission yeast is bound by the shelterin complex, which is comprised of the G-tail binding protein Pot1, double-stranded DNA binding protein Taz1, bridging proteins Rap1, Poz1 and Tpz1, which connect Taz1 to Pot1 via Taz1-Rap1, Rap1-Poz1, Poz1-Tpz1 and Tpz1-Pot1 interactions, and another Tpz1 interacting protein Ccq1 (Miyoshi et al., 2008) (Figure 1.2 and Table 1.1). These proteins are essential in protection of chromosome ends against nucleolytic degradation and activation of DNA damage response (DDRs) at the telomeres. Among fission yeast shelterin subunits, Ccq1 has been found to promote telomere recruitment and telomere extension, while Taz1, Rap1 and Poz1 have been found to function as negative regulators of telomerase.

Pot1 contains OB folds (oligonucleotide/oligosaccharide folds) which provide ssDNA binding ability and allow Pot1 to cap and to prevent nuclease degradation at the G-tails. Loss of Pot1 or Tpz1 leads to severe and immediate telomere loss and cell death for a majority of cells. A few cells manage to survive by circularizing their chromosomes (Baumann and Cech, 2001; Miyoshi et al., 2008; Tomita and Cooper,

2008). Taz1 (ortholog of human shelterin subunits TRF1 and TRF2) directly binds to telomere dsDNA by using its C-terminal myb motif domain. Taz1 and its interacting partner Rap1 are important for inhibiting homologous recombination (HR) and non-homologous end fusion (NHEJ) at telomeres (Cooper et al., 1998; Miller and Cooper, 2003; Miller et al., 2005).

In addition to the shelterin complex, protection of fission yeast telomeres requires the function of another evolutionarily well conserved Stn1-Ten1 complex (Figure 1.2). Similar to *pot1Δ* or *tpz1Δ* cells, deletion of either Stn1 or Ten1 leads to immediate telomere loss/fusion, cell death and generation of circular chromosome survivors. (Martin et al., 2007). While it remains to be determined why *stn1Δ* and *ten1Δ* cells fail to protect telomeres in fission yeast, the Stn1-Ten1 complex has been shown to interact with Tpz1 by yeast 2-hybrid assays (Chang et al., 2013). The Stn1-Ten1 complex in fission yeast may also contain a third subunit that has not yet been identified. In budding yeast and human, Stn1-Ten1 containing complexes include a third subunit Cdc13 and CTC1, respectively. The third subunit is also the largest subunit. (Figure 1.2 and Table 1.1) (Grandin et al., 2001; Grandin et al., 1997; Miyake et al., 2009).

While not yet shown in fission yeast, the CST (Cdc13/CTC1-Stn1-Ten1) complex in budding yeast and humans have been found to interact with the DNA polymerase α-primase complex (Chen et al., 2013; Grossi et al., 2004; Huang et al., 2012; Qi and Zakian, 2000) and regulate lagging strand synthesis at telomeres (Nakaoka et al., 2012; Wang et al., 2012; Wu et al., 2012). In fact, the CST complex has been proposed to be a RPA-like complex based on structural similarities of Stn1 and Ten1 shared with the middle and small subunits of the RPA complex (Gao et al., 2007; Gelinas et al., 2009;

Sun et al., 2009). There is also evidence that another RPA-like complex (but distinct from the CST complex) is involved in telomerase and DNA polymerase stimulation in *Tetrahymena* (Min and Collins, 2009; Sakaguchi et al., 2009). These findings thus raise the possibility that the CST complex might have co-evolved from a common ancestor of the RPA complex to either compete or cooperate with the RPA complex at telomeres (Price et al., 2010; Sakaguchi et al., 2009).

1.3 Protection of telomeres against DNA damage responses

Two major DNA repair pathways respond to double stranded breaks (DSBs): non-homologous end joining (NHEJ) fuses broken ends in G_1 phase, and homologous recombination (HR) uses homology of neighboring sequence to repair damage DNAs in the S/G_2 phase. NHEJ repairs damage by re-ligating blunt ends, while HR uses the homologous sequence to restore the broken DNAs more precisely.

In the NHEJ pathway, human Ku heterodimer (Ku70-Ku80) recognizes blunt ends of DSBs and activates DNA-PKcs (catalytic subunit of DNA-PK) to initiate NHEJ. XRCC4/LIG4 and stimulatory factor XLF are then recruited to facilitate the re-ligation of the broken ends (Mahaney et al., 2009). Homologous recombination repair pathway mainly depends on MRN-ATM and RPA-ATR. Human MRN complex (MRE11-RAD50-NBS1) recognizes DSBs and promotes sensor ATM kinase activation. MRE11 contains endonuclease and exonuclease activity, which is crucial to initiate DNA resection (Williams et al., 2007). RPA accumulates on ssDNA to stabilize during DNA repair. ATRIP (ATR interacting protein) binds to ssDNA and recruits ATR kinase to promote HR. ATM and ATR kinases act redundantly to promote HR. They regulate target

proteins via phosphorylation, which is a common and essential modification in this signal transduction pathway.

It has been shown that DSBs internally inserted next to a telomere have less potential to cause cell cycle arrest (Michelson et al., 2005), suggesting that telomere structure is capable of preventing inappropriate DNA damage responses (DDRs). Conserved telomeric proteins binding to chromosome ends exclude DDRs, like Taz1 and Pot1 in fission yeast (Baumann and Cech, 2001; Cooper et al., 1997), TRF2/RAP1 and POT1 in human (Bae and Baumann, 2007), and Rap1 and Cdc13 in budding yeast (Jia et al., 2004; Nugent et al., 1998; Pardo and Marcand, 2005; Zubko and Lydall, 2006) (Table 1.1).

On the other hand, DDR proteins such as checkpoint kinases ATM and ATR also play positive and critical roles in stable maintenance of telomeres in both fission and budding yeasts, plants, *Drosophila*, *Xenopus* and mammalian cells (Bi et al., 2005; Boltz et al., 2012; Deng et al., 2009; Moser et al., 2011; Nakamura et al., 2002; Tseng et al., 2006; Vespa et al., 2005; Wu et al., 2007; Yamazaki et al., 2012a). In fission yeast, $Rad3^{ATR}$ and $Tel1^{ATM}$ kinases phosphorylate telomeric protein Ccq1 in order to facilitate recruitment of telomerase to telomeres (Moser et al., 2011; Yamazaki et al., 2012a). The regulation of how these kinases are recruited to telomeres was unclear. In Chapter 2, I will show that Poz1, Rap1 and Taz1 negatively regulate recruitment of $Rad3^{ATR}$-$Rad26^{ATRIP}$ to telomeres to limit Ccq1 Thr93 phosphorylation and thus maintain telomere length homeostasis.

1.4 Regulation of telomerase recruitment and telomere length homeostasis

As mentioned earlier, due to the end replication problem, without telomerase, telomere length would gradually shorten after each DNA replication process. The telomerase complex minimally consists of a catalytic subunit TERT (telomerase reverse transcriptase) and telomerase RNA (Feng et al., 1995; Singer and Gottschling, 1994; Webb and Zakian, 2008) (Figure 1.3). It also requires additional regulatory subunits such as Est1 for recruitment/activation of telomerase at telomeres (Beernink et al., 2003; Evans and Lundblad, 1999; Hughes et al., 1997; Reichenbach et al., 2003; Snow et al., 2003)

In budding yeast, only a small fraction (~7%) of telomeres is extended in a given cell cycle, and extension frequently and preferentially occurs at short telomeres as a preferred substrate for telomerase (Bianchi and Shore, 2007b; Teixeira et al., 2004). It has also been shown that shorter telomeres in budding yeast are replicated earlier than longer telomeres (Bianchi and Shore, 2007a) In addition, checkpoint kinase $Tel1^{ATM}$ has been found to be recruited preferentially to shorter telomeres in a MRX complex dependent manner, suggesting their roles in establishing preferential extension of shorter telomeres (Bianchi and Shore, 2007b; Hector et al., 2007; Sabourin et al., 2007). In Chapter 2, I will show evidence that fission yeast telomerase is also preferentially recruited to shorter telomeres, and shorter telomeres are replicated earlier (Chang et al., 2013).

Fission yeast telomere extension and telomerase recruitment are restricted to late S phase in a cell cycle-dependent manner (Moser et al., 2009a). Est1 is proposed to recruit telomerase to telomeres and stimulate telomerase activity through interaction

with telomeric protein Ccq1 and telomerase RNA TER1 (Moser et al., 2011; Webb and Zakian, 2008, 2012). Checkpoint kinases Rad3^{ATR} and Tel1^{ATM} are redundantly required for telomere maintenance and telomerase recruitment (Moser et al., 2009b; Naito et al., 1998), since the interaction between Ccq1 and the 14-3-3-like domain of Est1 is facilitated by Rad3^{ATR}/Tel1^{ATM}-dependent phosphorylation of Ccq1 on Thr93 (Chang et al., 2013; Moser et al., 2011; Yamazaki et al., 2012a). Poz1, Rap1, and Taz1 are necessary to limit Ccq1 phosphorylation and uncontrolled telomere extension by telomerase (Chang et al., 2013; Moser et al., 2011). In Chapter 2, I will show that fission yeast shelterin complex regulates the coordination of the differential arrival of DNA polymerase δ and α for leading- and lagging-stranded DNA synthesis at telomeres, and modulate Rad3^{ATR} association, Ccq1 Thr93 phosphorylation and telomerase recruitment to limit telomere extension (Chang et al., 2013).

As mentioned earlier, evolutionarily conserved ssDNA binding complex CST has also been found to regulate telomere replication and telomere extension by telomerase (Chandra et al., 2001; Chen et al., 2012; Miyake et al., 2009; Pennock et al., 2001; Price et al., 2010; Surovtseva et al., 2009). Studies have found that post-translational modifications of the CST complex play critical regulatory roles in CST function. For example, cell cycle-dependent Thr308 phosphorylation of budding yeast Cdc13 by Cdk1 in late S/G_2 phase facilitate telomerase recruitment by promoting Cdc13-Est1 interaction and preventing Cdc13-Stn1 interaction (Li et al., 2009). Phosphorylation of budding yeast Stn1 on Thr223 and Ser250 by Cdk1 has also been shown recently to be important for promoting formation of CST complex and preventing telomerase association with telomeres (Liu et al., 2014). Furthermore, SUMOylation of budding

yeast Cdc13 has been shown to promote Cdc13-Stn1 interaction and prevent recruitment of telomerase recruitment (Hang et al., 2011).

Post-translational modifications also play critical roles in regulation of shelterin complex in mammalian cells. For example, dsDNA telomere proteins TRF1 and TRF2 have been found to be regulated by phosphorylation, SUMOylation, Ubiquitylation, PARsylation and Methylation on multiple distinct sites with roles in regulating association of TRF1/TRF2 with telomeres, controlling telomere extension by telomerase and regulating DNA damage checkpoint responses (Walker and Zhu, 2012). In addition, CDK1 kinase-dependent phosphorylation of human TPP1 Ser111 was recently found to promote telomerase recruitment and telomere extension (Zhang et al., 2013). In Chapter 3, I will present evidence that fission yeast Tpz1 (TPP1 ortholog) is also phosphorylated at multiple sites, and Tpz1 phosphorylation contributes to telomere length homeostasis in fission yeast.

2. Fission Yeast Shelterin Regulates DNA Polymerases and Rad3^{ATR} Kinase to Limit Telomere Extension[1]

2.1 Introduction

In eukaryotic cells, dynamic cell cycle-regulated protein-DNA complexes formed at telomeres play key roles in the maintenance of genome stability (Gilson and Geli, 2007; Verdun and Karlseder, 2007). Using Chromatin immunoprecipitation (ChIP) assays, our laboratory has previously established cell cycle-regulated changes in telomere association of telomere-specific proteins (telomerase catalytic subunit Trt1^{TERT}, Taz1, Rap1, Pot1 and Stn1), DNA replication proteins (DNA polymerases, MCM and RPA), the checkpoint protein Rad26^{ATRIP} (a regulatory subunit of checkpoint kinase Rad3^{ATR}) and DNA repair protein Nbs1 (a subunit of Mre11-Rad50-Nbs1 complex) in fission yeast (Moser et al., 2009a). Unexpectedly, the leading strand DNA polymerase Polε arrived at telomeres significantly earlier than the lagging strand DNA polymerases Polα and Polδ in late S-phase. Temporal recruitments of RPA and Rad26^{ATRIP} matched the arrival of Polε, while recruitments of Trt1^{TERT}, Pot1 and Stn1 matched the arrival of Polα (Moser et al., 2009a; Moser et al., 2009b). However, it has not yet been established if the delayed arrival of Polα/Polδ represents a C-strand fill-in reaction after extension of the G-strand by telomerase, or if it might be part of the regulatory mechanism that controls recruitment of telomerase by regulating Rad3^{ATR}/Tel1^{ATM} accumulation and Ccq1 Thr93 phosphorylation (Moser et al., 2011). Furthermore, while previous studies have established that Taz1 and mammalian TRF1 contribute to

[1]This Chapter has been adapted from Chang, Y.-T., Moser, B.M. and Nakamura, T.M. (2013) PLoS Genet. 9(11): e1003936. (doi: 10.1371/journal.pgen.1003936)

efficient replication of telomeric repeats (Miller et al., 2006; Sfeir et al., 2009), very little was known how the loss of Taz1 or TRF1 affects behaviors of replicative DNA polymerases at telomeres. In addition, it has not been established how cell cycle-regulated dynamic binding patterns of checkpoint kinases, shelterin and CST are affected by challenges posed by replicating highly extended telomeric repeats as found in *poz1Δ*, *rap1Δ*, and *taz1Δ* cells.

Therefore, I investigated how loss of the shelterin subunits Poz1, Rap1 and Taz1 affects cell cycle-regulated recruitment timings of telomerase catalytic subunit $Trt1^{TERT}$, DNA polymerases (Polα and Polε), the Replication Protein A (RPA) complex subunit Rad11, the $Rad3^{ATR}$-$Rad26^{ATRIP}$ checkpoint kinase complex, $Tel1^{ATM}$ kinase, shelterin subunits (Tpz1 Ccq1 and Poz1), and Stn1. In addition, I investigated how telomere shortening, caused either by deletion of $Trt1^{TERT}$ or introduction of catalytically dead $Trt1^{TERT}$, affected cell cycle-regulated telomere association of telomerase and DNA polymerases. These detailed ChIP analyses have provided new insights into the dynamic coordination of DNA replication, DNA damage kinase recruitment, and telomerase recruitment in fission yeast, and thus I will present here a new and more dynamic model of telomere length regulation in fission yeast.

2.2 Results

2.2.1 Epistasis analysis of telomerase inhibitors Poz1, Rap1 and Taz1

To better understand how Poz1, Rap1 and Taz1 function together in telomere maintenance, I performed epistasis analysis among single, double and triple deletion mutant cells for telomere length, cold sensitivity, and protection of telomeres against

telomere fusion in G_1 arrested cells, and recruitment of $Trt1^{TERT}$ to telomeres (Chikashige and Hiraoka, 2001; Kanoh and Ishikawa, 2001; Miller et al., 2005; Miyoshi et al., 2008). Telomere length distribution of *poz1Δ*, *rap1Δ* and *poz1Δ rap1Δ* cells closely resembled one another (Figures 2.1A and 2.1B #1), suggesting that *poz1Δ* and *rap1Δ* cause similar defect(s) in telomere length regulation. The distribution of telomere length was broader and skewed toward shorter telomeres in *taz1Δ* cells than *rap1Δ* or *poz1Δ* cells (Figure 2.1B #2-3), and *rap1Δ taz1Δ* and *poz1Δ rap1Δ taz1Δ* cells showed identical telomere length distributions as *taz1Δ* cells (Figure 2.1B #4), suggesting that Taz1 carries out both Poz1/Rap1-dependent and -independent roles in telomere length regulation. Interestingly, since telomere length distribution in *poz1Δ taz1Δ* was much broader than in *poz1Δ rap1Δ taz1Δ* cells (Figure 2.1B #3-4), it appears that Rap1 could also affect telomere length independently of Poz1 and Taz1. In support for such independent function, Rap1 binding to telomeres was significantly reduced but not entirely eliminated in *poz1Δ taz1Δ* cells (Figure 2.1C). Previously, our laboratory have also found that Rap1 contributes to recombination-based telomere maintenance independently of Taz1 and Poz1 (Khair et al., 2009).

I also found that *poz1Δ* and *taz1Δ* cells, but not *rap1Δ* cells, show reduced cell growth at lower temperature (Figure 2.1D). Cold sensitivity of *taz1Δ* cells (Miller et al., 2005) was more severe than *poz1Δ* cells, and *poz1Δ taz1Δ* cells were more sensitive than *taz1Δ* cells. Interestingly, while *rap1Δ taz1Δ* cells showed the most severe cold sensitivity among all mutant combinations tested, cold sensitivity of *poz1Δ rap1Δ taz1Δ* cells was milder, suggesting that the presence of Poz1 in *rap1Δ taz1Δ* cells is

detrimental to cell growth at low temperature. In addition, *rap1Δ* and *taz1Δ* cells, but not *poz1Δ* cells, showed telomere-telomere fusion (Ferreira and Cooper, 2001; Fujita et al., 2012; Miller et al., 2005) when cells are grown in low nitrogen media to arrest cells in G_1 phase (Figure 2.1E). Among double and triple mutant cells, all cells that lack Rap1 and/or Taz1 underwent telomere fusion. Thus, only Rap1 and Taz1 (but not Poz1) are involved in protection of telomeres against fusions in G_1-phase arrested cells.

Based on ChIP analysis utilizing the hybridization of a telomeric probe to dot blotted samples, I found that $Trt1^{TERT}$ showed progressive increase in telomere association in the order of *poz1Δ*, *rap1Δ* and *taz1Δ* cells (Moser et al., 2011) (Figure 2.1F). Further analysis of double and triple mutant cells revealed that *poz1Δ rap1Δ* cells have similar levels of $Trt1^{TERT}$ binding as *rap1Δ* cells, and *poz1Δ taz1Δ*, *rap1Δ taz1Δ* and *poz1Δ rap1Δ taz1Δ* cells have similar levels of $Trt1^{TERT}$ binding as *taz1Δ* cells. Thus, regarding its inability to limit telomerase binding to telomeres, *taz1Δ* is epistatic over *rap1Δ* or *poz1Δ*, and *rap1Δ* is epistatic over *poz1Δ*.

2.2.2 Changes in cell cycle-regulated telomere association of $Trt1^{TERT}$ in wt, *poz1Δ*, *rap1Δ*, and *taz1Δ* cells

$Trt1^{TERT}$ binding to telomeres is cell cycle-regulated, and maximal association of $Trt1^{TERT}$ occurs in late-S phase when telomeres are replicated (Moser et al., 2009a). To better understand the roles of Poz1, Rap1 and Taz1 in limiting $Trt1^{TERT}$ binding to telomeres, I examined changes in $Trt1^{TERT}$ association in *poz1Δ*, *rap1Δ* and *taz1Δ* cells by ChIP using *cdc25-22* synchronized cell cultures. Since asynchronous ChIP analysis

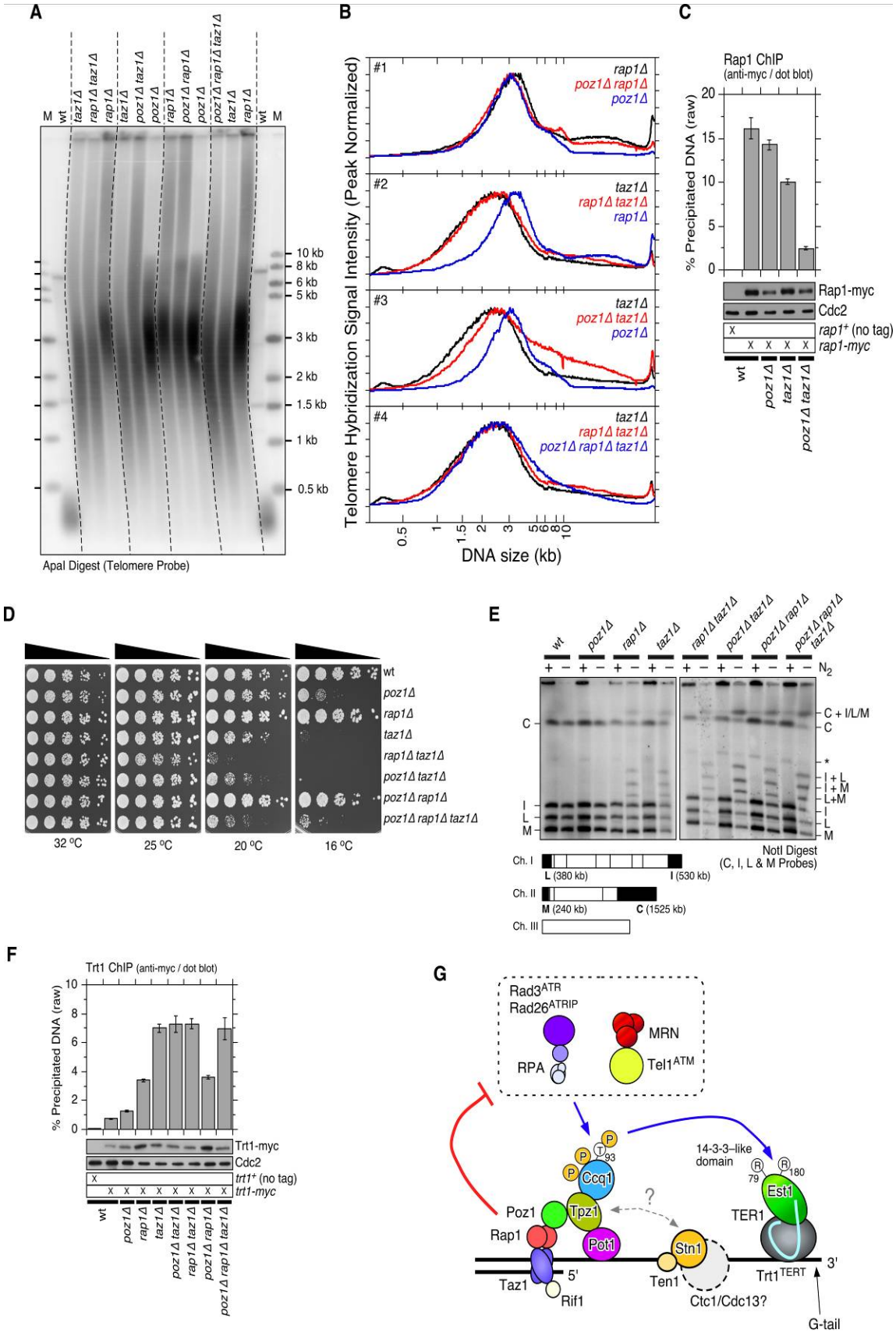
A
M wt taz1Δ rap1Δ taz1Δ rap1Δ taz1Δ poz1Δ taz1Δ poz1Δ rap1Δ poz1Δ rap1Δ taz1Δ poz1Δ rap1Δ taz1Δ taz1Δ rap1Δ wt M
10 kb
8 kb
6 kb
5 kb
3 kb
2 kb
1.5 kb
1 kb
0.5 kb
ApaI Digest (Telomere Probe)
B
#1 rap1Δ poz1Δ rap1Δ poz1Δ
#2 taz1Δ rap1Δ taz1Δ rap1Δ
#3 taz1Δ poz1Δ taz1Δ poz1Δ
#4 taz1Δ rap1Δ taz1Δ poz1Δ rap1Δ taz1Δ
Telomere Hybridization Signal Intensity (Peak Normalized)
0.5 1 1.5 2 3 5 6 8 10
DNA size (kb)
C
Rap1 ChIP
(anti-myc / dot blot)
% Precipitated DNA (raw)
20 15 10 5 0
Rap1-myc
Cdc2
rap1+ (no tag)
rap1-myc
wt poz1Δ taz1Δ poz1Δ taz1Δ
D
wt
poz1Δ
rap1Δ
taz1Δ
rap1Δ taz1Δ
poz1Δ taz1Δ
poz1Δ rap1Δ
poz1Δ rap1Δ taz1Δ
32 °C 25 °C 20 °C 16 °C
E
wt poz1Δ rap1Δ taz1Δ rap1Δ taz1Δ poz1Δ taz1Δ poz1Δ rap1Δ poz1Δ rap1Δ taz1Δ
+ − + − + − + − + − + − + − N2
C
I
L
M
C + I/L/M
C
*
I + L
I + M
L+M
I
L
M
NotI Digest
(C, I, L & M Probes)
Ch. I
L (380 kb)
I (530 kb)
Ch. II
M (240 kb)
C (1525 kb)
Ch. III
F
Trt1 ChIP (anti-myc / dot blot)
% Precipitated DNA (raw)
10 8 6 4 2 0
Trt1-myc
Cdc2
trt1+ (no tag)
trt1-myc
wt poz1Δ rap1Δ taz1Δ poz1Δ taz1Δ rap1Δ taz1Δ poz1Δ rap1Δ poz1Δ rap1Δ taz1Δ
G
Rad3ATR
Rad26ATRIP
RPA
MRN
Tel1ATM
P
T93
Ccq1
14-3-3–like domain
R79
R180
Est1
TER1
Poz1
Tpz1
?
Rap1
Pot1
Stn1
Taz1
5'
Ten1
Trt1TERT
3'
Rif1
Ctc1/Cdc13?
G-tail

Figure 2.1 Epistasis analysis of *poz1Δ*, *rap1Δ, and taz1Δ* cells.
(**A**) Telomere length analysis for indicated strains. Genomic DNA was prepared after extensive restreaks on YES plates to ensure telomere length equilibrium. After digestion with restriction enzyme *ApaI*, DNA was fractionated on a 1% agarose gel and processed for Southern blot analysis with a telomere probe. (**B**) Quantification of telomere length distribution for Southern blot analysis shown in Figure 2.1A. (**C**, **F**) Recruitments of Rap1 (**C**) and $Trt1^{TERT}$ (**F**) to telomeres were monitored by dot blot-based ChIP assays. Compared to wt cells, Rap1 showed statistically significant reductions in binding to telomeres in *taz1Δ* ($p=2.5x10^{-3}$) and *poz1Δ taz1Δ* ($p=2.6x10^{-5}$) cells. Rap1 still showed statistically significant binding to telomeres even in *poz1Δ taz1Δ* cells compared to no tag control strain ($p=1.4x10^{-5}$). Error bars correspond to the standard error of the mean (SEM) from multiple independent experiments. Anti-myc western blot analysis indicated comparable expression levels in different genetic backgrounds. Cdc2 western blot served as a loading control. . (**D**) Analysis of cell growth at lower temperatures. Five-fold serial dilution of the indicated strains are plated on YES, and grown at indicated temperatures. (**E**) Chromosome fusion analysis of G1 arrested cells. Genomic DNA was prepared in agarose plugs from G1 arrested cells, digested with NotI, fractionated on a 1% agarose gel by pulsed-field gel electrophoresis, and processed for Southern blot analysis with probes specific for C, I, L and M NotI chromosomal fragments. A NotI restriction map of S. pombe chromosomes is shown below, with telomeric C, I, L, and M fragments marked as black boxes. (**G**) Schematic model of telomere maintenance regulation in fission yeast.

indicated that Trt1^{TERT} recruitment to telomeres is similar in single and double/triple mutant cells, I limited my cell cycle ChIP analysis to single mutant cells. After incubating *cdc25-22* cells at non-permissive temperature (36 ^{o}C) for 3 hours, late G_2-phase arrested cells were shifted to permissive temperature (25 ^{o}C) for synchronous cell cycle re-entry, and samples were collected every 20 minutes and processed for ChIP analysis.

In previous cell cycle ChIP analyses, our laboratory has utilized quantitative real-time PCR with primers that amplify a unique sub-telomeric DNA sequence directly adjacent to telomeric repeats (Moser et al., 2009a; Moser et al., 2009b). Since wild-type (wt) telomeres are only ~300 bp and the size of DNA fragments after sonication is estimated to be in the 0.5~1 kb range, the use of sub-telomeric primers provides a convenient means to determine the association of various factors to telomeres. However, since *poz1Δ*, *rap1Δ* and *taz1Δ* cells carry much longer telomeres, sub-telomeric PCR primer pairs would be too distant from the actual chromosome ends, and thus protein binding to telomeres had to be monitored using dot blotted samples and utilizing telomeric repeat DNA as hybridization probe (Moser et al., 2011).

For analysis of dot blot-based ChIP assays, I processed raw data (% precipitated DNA) in two different ways. First, to compare overall temporal binding patterns, we normalized ChIP data to the peak of binding within the first complete cell cycle (40-200 min) after release from the G_2 arrest. Second, I attempted to obtain an approximate fold-increase in protein association “per chromosome end” by correcting for changes in telomeric tract length (Materials and Methods and Table 2.1). This correction was necessary as raw % precipitated DNA values reflect the density of a given protein within

the telomeric tract, and thus significantly underestimate the actual increase in protein binding at chromosome ends for cells carrying long telomeric repeat tracts. Telomere length corrected ChIP data were normalized to values from wt cells for asynchronous ChIP assays, and normalized to the peak binding values of wt cells in late S/G_2-phase for cell cycle ChIP assays. (See Figures 2.2 for telomere length correction of Trt1^{TERT} asynchronous ChIP data as example.)

Based on changes in % septated cells, *poz1Δ*, *rap1Δ* and *taz1Δ* cells showed similar re-entries into cell cycle as wt cells (Figure 2.3C), with the first S-phase occurring 60-140 min and the second S-phase starting 200-220 min after the temperature shift. BrdU incorporation data indicated that telomeres in wt, *poz1Δ* and *rap1Δ* cells are replicated in late S-phase (100-140 min after the temperature shift), while replication of telomeres in *taz1Δ* cells occurred much earlier (60-100 min after the temperature shift) (Figure 2.4B). Furthermore, hydroxyurea (HU) treatment completely abolished telomere replication in wt, *poz1Δ* and *rap1Δ* cells, but not in *taz1Δ* cells. These data are consistent with previous findings that Taz1 is required to enforce late S-phase replication at telomeres (Dehe et al., 2012; Tazumi et al., 2012).

Consistent with our previous analysis (Moser et al., 2009a), Trt1^{TERT} showed maximal binding to telomeres in late S-phase (120-140 min) in wt cells (Figure 2.5A). In *poz1Δ* and *rap1Δ* cells, Trt1^{TERT} showed nearly identical cell cycle-regulated association patterns with a substantial delay in maximal binding (160-180 min) (Figure 2.5A). In agreement with a recent report (Dehe et al., 2012), I found that Trt1^{TERT} is bound to telomeres throughout the cell cycle in *taz1Δ* cells with much broader and persistent maximal binding at 120-180 min (Figures 2.5B and 2.3A-B). Consistent with

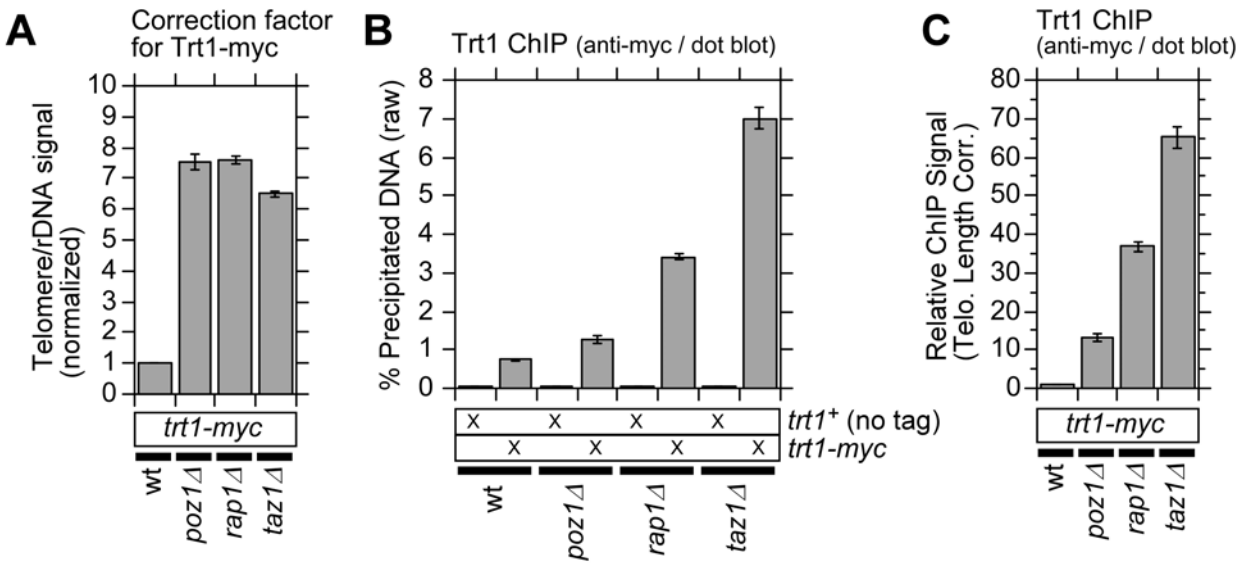

Figure 2.2 Analysis of Trt1^{TERT} recruitment to telomeres by dot blot-based asynchronous ChIP assays with telomeric DNA probe.

(**A**) Telomere correction factors for Trt1-myc strains were established by determining telomere/rDNA hybridization signal ratios relative to wt cells. Telomere correction factors for other epitope tagged strains are shown in Table 2.1. (**B**) Raw % precipitated DNA values for dot blot-based Trt1-myc ChIP assays for the indicated genotypes. (**C**) Telomere length corrected ChIP data for Trt1-myc. (See Materials and Methods section for details.) Error bars correspond to SEM.

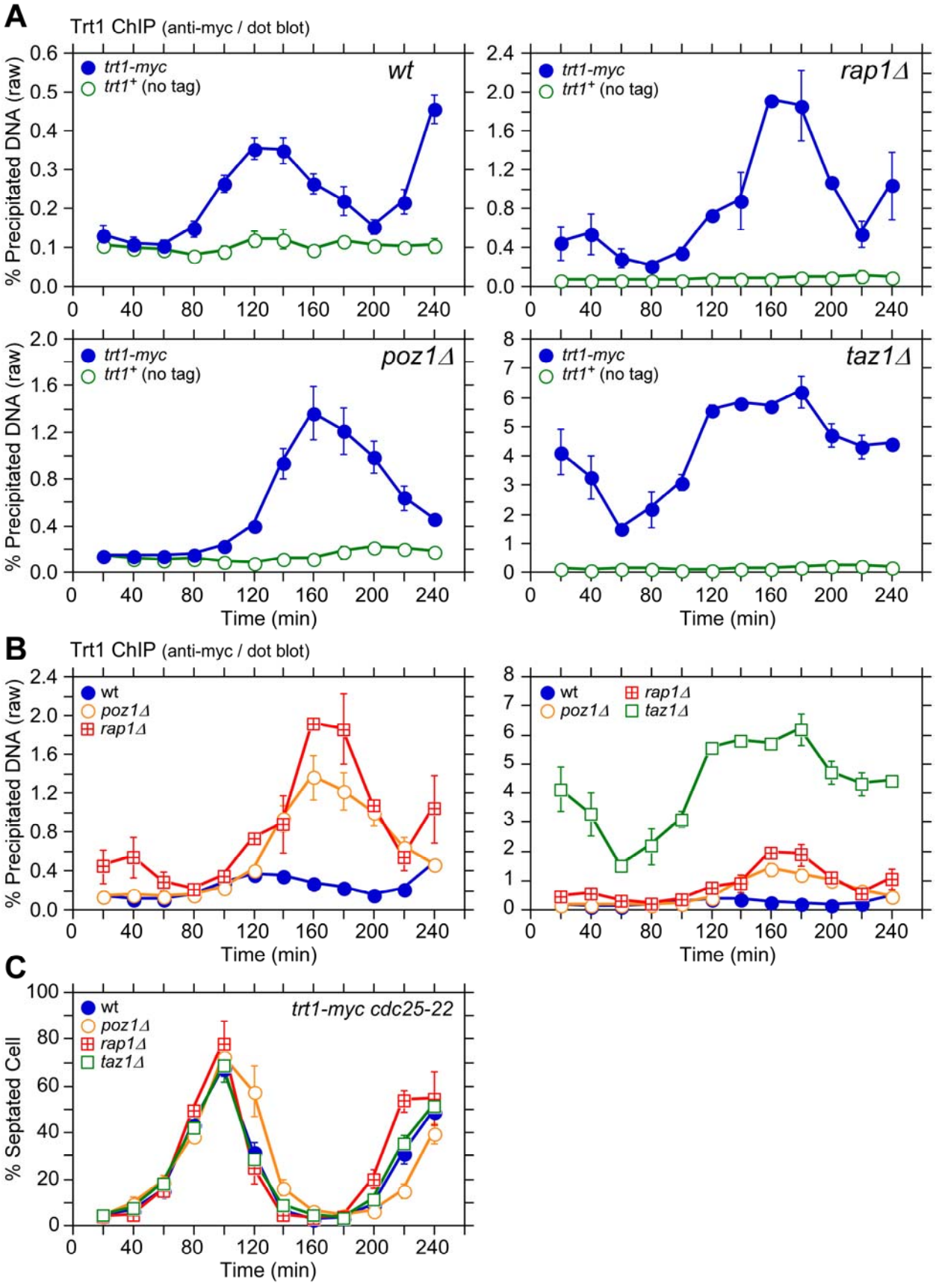
A
Trt1 ChIP (anti-myc / dot blot)
% Precipitated DNA (raw)
trt1-myc
trt1+ (no tag)
wt
rap1Δ
poz1Δ
taz1Δ
Time (min)
B
Trt1 ChIP (anti-myc / dot blot)
% Precipitated DNA (raw)
wt
poz1Δ
rap1Δ
taz1Δ
Time (min)
C
% Septated Cell
trt1-myc cdc25-22
wt
poz1Δ
rap1Δ
taz1Δ
Time (min)

Figure 2.3 Raw data of dot blot-based cell cycle ChIP assays for Trt1^{TERT}.
(**A**, **B**) Cell cycle ChIP assays were performed with *cdc25-22* synchronized cell cultures for wt, *poz1Δ*, *rap1Δ* or *taz1Δ* cells, and % precipitated DNA was determined by hybridization of a telomeric probe to dot blotted input and ChIP samples. (**C**) % septated cells were measured to monitor cell cycle progression of *cdc25-22* synchronized cell cultures for the indicated genotypes. Error bars correspond to SEM.

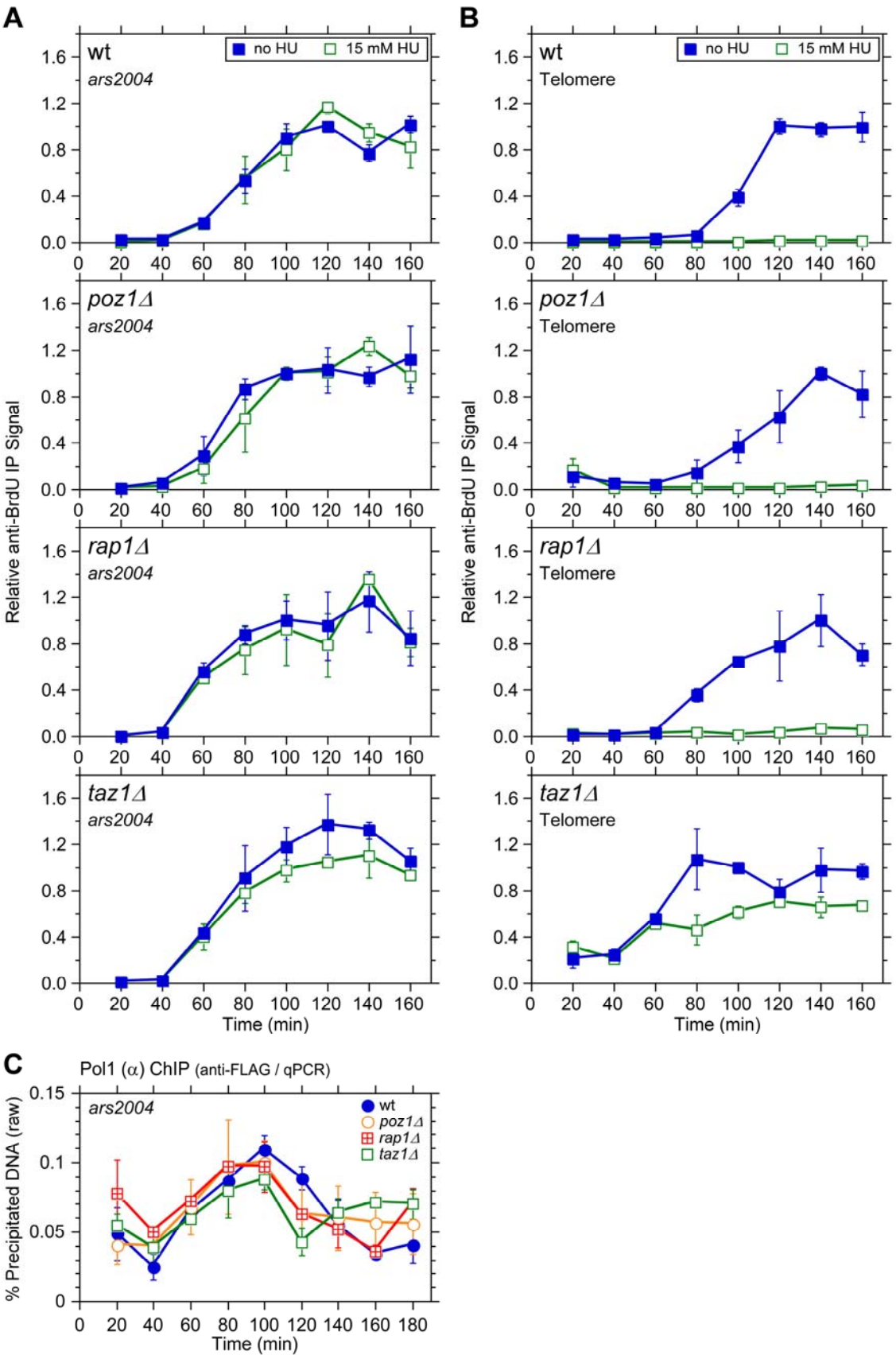
A
B
wt
ars2004
no HU
15 mM HU
poz1Δ
rap1Δ
taz1Δ
Telomere
Relative anti-BrdU IP Signal
Time (min)
C
Pol1 (α) ChIP (anti-FLAG / qPCR)
% Precipitated DNA (raw)
wt
poz1Δ
rap1Δ
taz1Δ

Figure 2.4 DNA replication timing monitored by incorporation of BrdU in cdc25-22 synchronized cells.
(**A**) ars2004 and (**B**) telomeres (Moser et al., 2009a). BrdU incorporation at telomeres is inhibited by addition of 15 mM HU for wt, *poz1Δ* and *rap1Δ* cells but not for *taz1Δ* cells. BrdU is incorporated into ars2004 with similar kinetics in the presence or absence of HU for all genetic backgrounds tested. (**C**) Pol1 (α) showed similar timing of recruitment to ars2004 in all genetic backgrounds tested. Error bars correspond to SEM.

asynchronous ChIP data, relative peak binding values (telomere length corrected) for Trt1^{TERT} increased in the order of *poz1Δ* (~40-fold), *rap1Δ* (~59-fold) and *taz1Δ* (~167-fold) over wt cells (Figure 2.5B).

2.2.3 Poz1, Rap1 and Taz1 control cell cycle-dependent association of DNA polymerases to telomeres

Real-time PCR-based ChIP assays have previously established that the leading strand DNA polymerase Polε arrives at telomeres significantly earlier than the lagging strand DNA polymerases Polα and Polδ, and that the timing of maximal Trt1^{TERT} association matches more closely to that of Polα and Polδ (~140 min) than Polε (~120 min) (Moser et al., 2009a). Dot blot-based ChIP re-confirmed the differential timing in peak association for Polα and Polε in wt cells (Figures 2.5C and 2.6). In *poz1Δ* and *rap1Δ* cells, binding of Polα was delayed ~40 min without affecting the temporal binding pattern of Polε. The delay of Polα appears to be restricted to telomeres, as the timing of Polα association with *ars2004* (early replication origin) was similar among wt, *poz1Δ* and *rap1Δ* cells (Figure 2.4C). Overall, the cell cycle-regulated association patterns of both polymerases were nearly identical in *poz1Δ* and *rap1Δ* cells, but both Polα and Polε showed increased association with telomeres in *poz1Δ* cells than *rap1Δ* cells (Figures 2.5C and 2.6A-B).

In *taz1Δ* cells, the difference in telomere binding patterns for the leading and lagging strand DNA polymerases was more dramatic. As expected based on the fact that *taz1Δ* cells replicate telomeres much earlier in S-phase (Tazumi et al., 2012) (Figure 2.4B), Polε was recruited to telomeres earlier (peak binding ~100 min) (Figure

2.6B). When corrected for telomere length, we found a ~6 fold increase in peak ChIP precipitation for Polε in *taz1Δ* cells over wt cells (Figure 2.5C). Surprisingly, Polα was constitutively bound to telomeres throughout the cell cycle in *taz1Δ* cells at ~1.5 fold above the peak binding in wt cells (Figures 2.5C and 2.6A). On the other hand, overall cell cycle progression (Figure 2.6E-F) and the association timing of Polα to *ars2004* (Figure 2.4C) were not affected in *taz1Δ* cells. Taken together, I concluded that Poz1 and Rap1 are required primarily to maintain timely recruitment of Polα to telomeres, and Taz1 is required to both (1) delay arrival of Polε to enforce late S-phase replication of telomeres and (2) enforce cell cycle-regulated association of Polα with telomeres.

2.2.4 Comparison of cell cycle-regulated association patterns for telomerase and DNA polymerases

Previous ChIP analysis using real-time PCR found largely overlapping temporal association patterns for the telomerase catalytic subunit $Trt1^{TERT}$ and Polα with both showing maximal binding at ~140 min in wt cells (Moser et al., 2009a). However, the initial increase in detectable binding to telomeres was earlier for $Trt1^{TERT}$ (~80 min) than Polα (~100 min) and treatment with HU caused much greater inhibition of Polα and Polε binding than $Trt1^{TERT}$, suggesting that $Trt1^{TERT}$ binding could occur prior to the arrival of replicative polymerases at telomeres (Moser et al., 2009a).

With dot blot-based ChIP analysis, the overall binding pattern of $Trt1^{TERT}$ was broader than in our previous analysis (Figure 2.5A) (Moser et al., 2009a). Thus, when

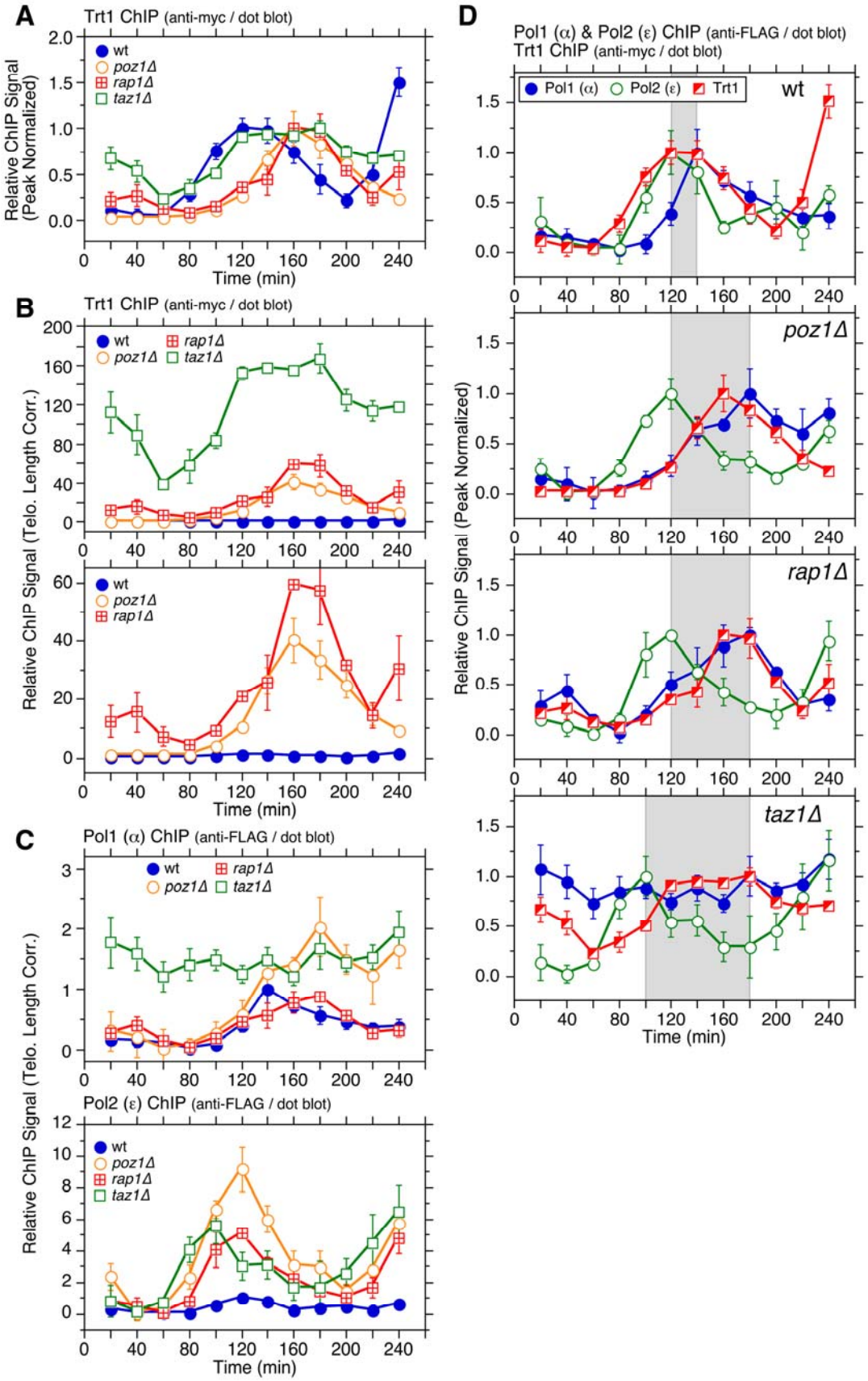
A
Trt1 ChIP (anti-myc / dot blot)
Relative ChIP Signal (Peak Normalized)
wt
poz1Δ
rap1Δ
taz1Δ
Time (min)
B
Trt1 ChIP (anti-myc / dot blot)
Relative ChIP Signal (Telo. Length Corr.)
C
Pol1 (α) ChIP (anti-FLAG / dot blot)
Pol2 (ε) ChIP (anti-FLAG / dot blot)
D
Pol1 (α) & Pol2 (ε) ChIP (anti-FLAG / dot blot)
Trt1 ChIP (anti-myc / dot blot)
Pol1 (α)
Pol2 (ε)
Trt1
wt
poz1Δ
rap1Δ
taz1Δ

Figure 2.5 Cell cycle ChIP analysis to monitor association of Trt1^{TERT} and DNA polymerases with telomeres.

(**A**) Peak normalized and (**B**) telomere length adjusted ChIP data for Trt1^{TERT} in wt, *poz1Δ*, *rap1Δ,* and *taz1Δ* cells. For (A), *poz1Δ* and *rap1Δ* cells showed statistically significant increases in Trt1^{TERT} association ($p<0.03$) compared to wt cells at 100 min and 120 min. Raw ChIP data and % septated cells to monitor cell cycle progression are shown in Figure 2.4. (**C**) Telomere length adjusted ChIP data for Pol1 (α) and Pol2 (ε) in wt, *poz1Δ*, *rap1Δ*, and *taz1Δ* cells. Peak normalized ChIP data, raw ChIP data, and % septated cells to monitor cell cycle progression are shown in Figure 2.7. Anti-FLAG western blot analysis indicated comparable expression levels in different genetic backgrounds (Figure 2.7G). (**D**) Comparison of peak normalized ChIP data for Pol1 (α), Pol2 (ε) and Trt1^{TERT}. Shaded area in wt, *poz1Δ*, and *rap1Δ* graphs corresponds to the interval between Pol2 (ε) and Pol1 (α) peaks, while shaded area in *taz1Δ* graph corresponds to the interval between Pol2 (ε) peak and the last time point of Trt1^{TERT} at peak binding before it shows reduction. Error bars correspond to SEM.

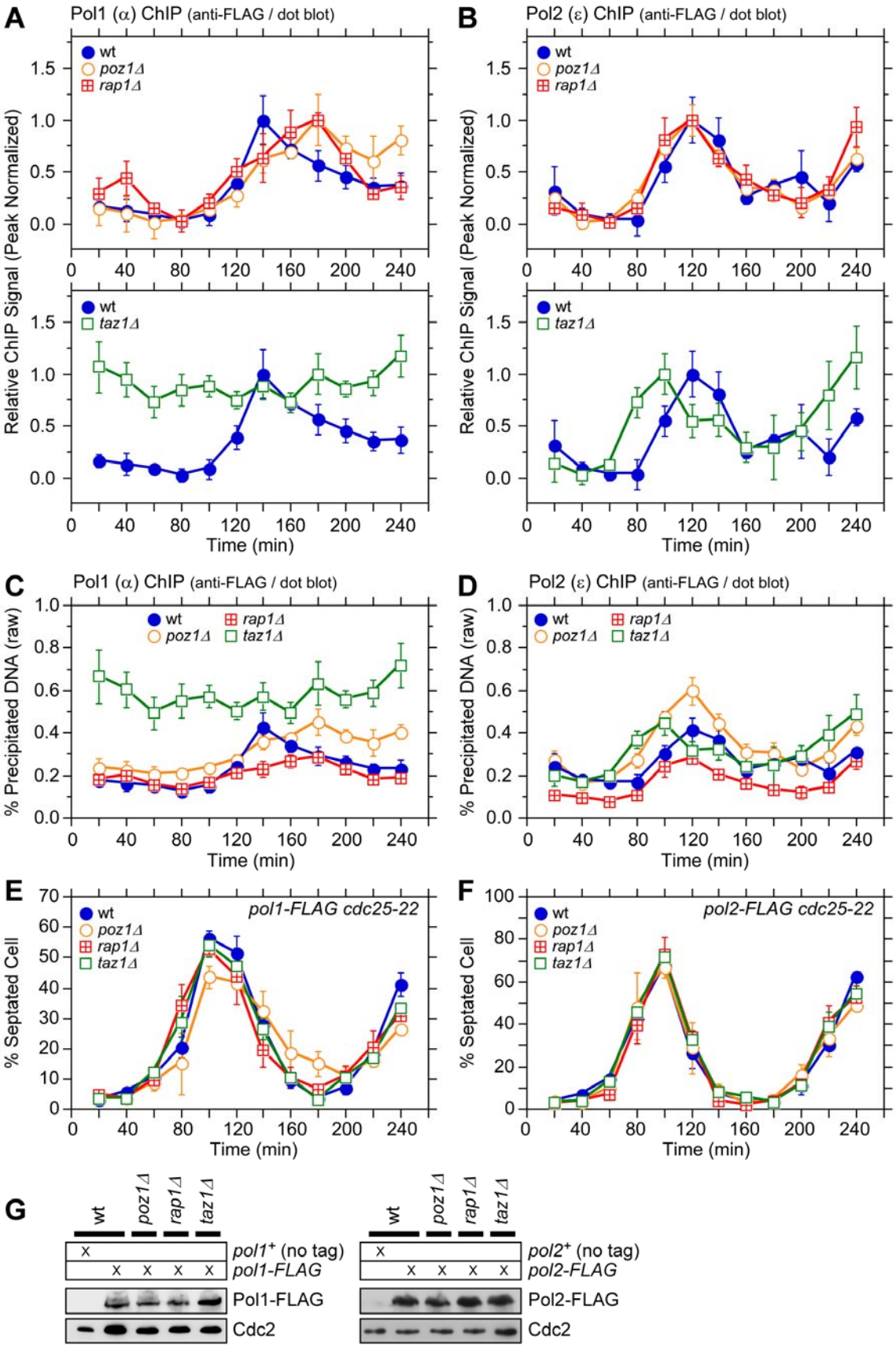
A
Pol1 (α) ChIP (anti-FLAG / dot blot)
wt
poz1Δ
rap1Δ
taz1Δ
Relative ChIP Signal (Peak Normalized)
Time (min)
B
Pol2 (ε) ChIP (anti-FLAG / dot blot)
C
Pol1 (α) ChIP (anti-FLAG / dot blot)
% Precipitated DNA (raw)
D
Pol2 (ε) ChIP (anti-FLAG / dot blot)
E
pol1-FLAG cdc25-22
% Septated Cell
F
pol2-FLAG cdc25-22
G
pol1+ (no tag)
pol1-FLAG
Pol1-FLAG
Cdc2
pol2+ (no tag)
pol2-FLAG
Pol2-FLAG
Cdc2

Figure 2.6 Cell cycle ChIP assays for DNA polymerases.
(**A**, **B**) Peak normalized cell cycle ChIP data for Pol1 (α) (**A**) and Pol2 (ε) (**B**). For Pol2 (ε), Student's t-test found a statistically significant difference in telomere binding at 80 min (p=0.03) for wt vs. *taz1Δ* cells. (**C**, **D**) Raw data of dot blot-based cell cycle ChIP assays for Pol1 (α) (**C**) and Pol2 (ε) (**D**), performed with *cdc25-22* synchronized cell cultures and telomeric DNA probe. (**E**, **F**) % septated cells were measured to monitor cell cycle progression of cdc25-22 synchronized cell cultures for Pol1 (α) (**E**) and Pol2 (ε) (**F**) ChIP assays. Error bars correspond to SEM. (**G**) Anti-FLAG western blot analysis indicated comparable expression levels in different genetic backgrounds for both Pol1 (α) and Pol2 (ε). Cdc2 western blot served as loading control.

data for Trt1^{TERT}, Polα and Polε were plotted together (Figure 2.5D), the increase in Trt1^{TERT} binding prior to arrival of Polα became more evident. On the other hand, reductions in the binding of Trt1^{TERT} and Polα in G_2/M phase occurred with very similar timing. In *poz1Δ* and *rap1Δ* cells, the peak of Trt1^{TERT} recruitment was dramatically delayed compared to Polε and its overall temporal association pattern largely overlapped with Polα (Figure 2.5D).

However, the initial increase in Trt1^{TERT} binding to telomeres occurred with similar timing as Polε in *poz1Δ*, *rap1Δ* or *taz1Δ* cells (Figure 2.7A), and the amount of Trt1^{TERT} binding was already significantly increased in early S-phase (80-100 min) and further elevated during late S/G_2-phases (160-180 min) in these deletion mutants (Figure 2.5B). Thus, the delay in peak binding of Trt1^{TERT} in *poz1Δ* and *rapΔ* cells is caused primarily by the massive increase in Trt1^{TERT} binding during late S/G_2-phases. Likewise, the broad and persistent binding of Trt1^{TERT} in *taz1Δ* cells can be attributed to both a massive increase in early S-phase and persistent binding in late S/G_2-phases. Taken together, I thus concluded that Trt1^{TERT} binding to telomeres occurs around the time when Polε arrives at telomeres, and that its binding is massively increased throughout S-phase in cells that lack Poz1, Rap1 or Taz1, accompanied by delayed (*poz1Δ* and *rap1Δ*) or persistent (*taz1Δ*) binding of Polα.

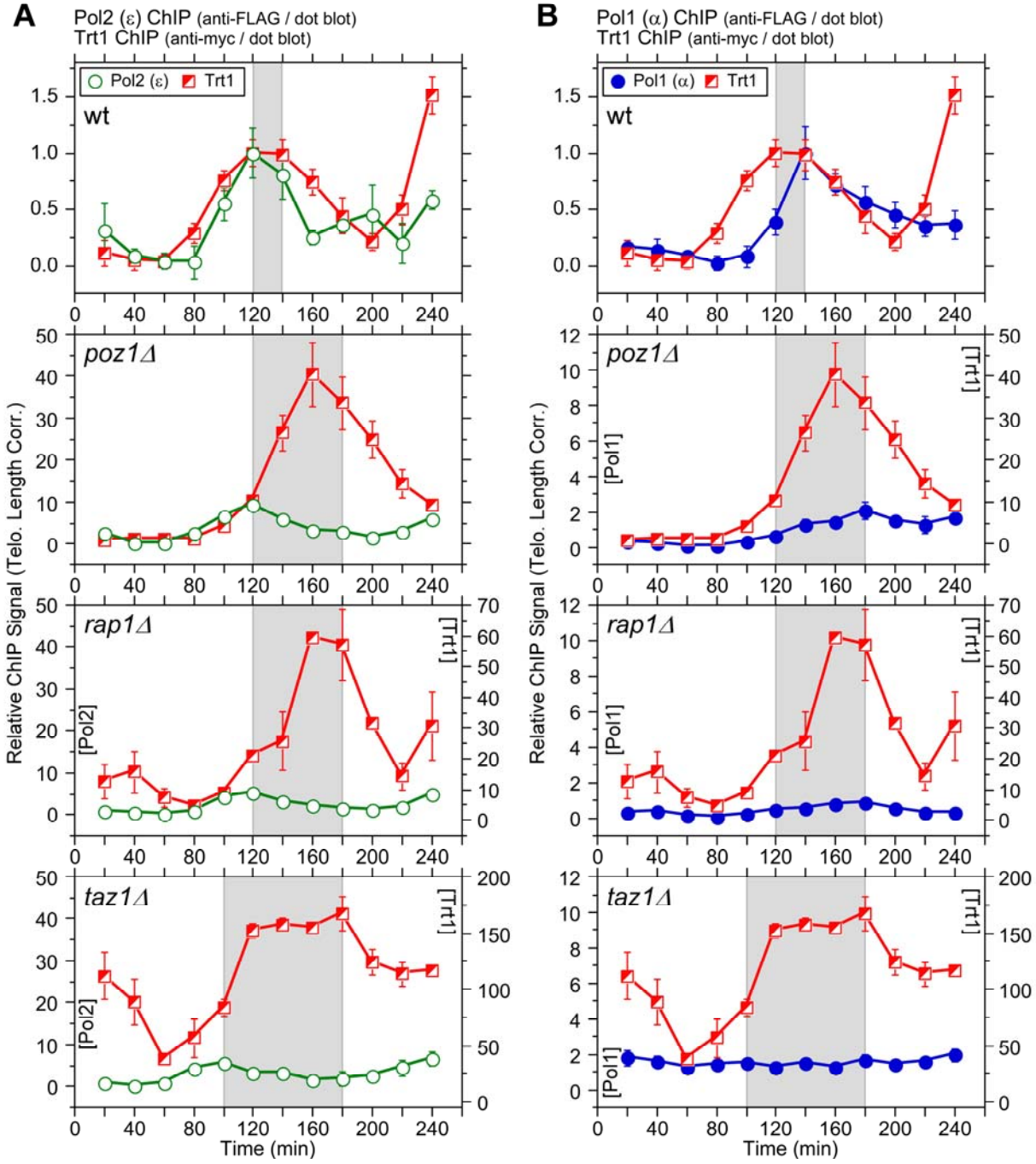

Figure 2.7 Comparison of cell cycle ChIP data among DNA polymerases and Trt1^{TERT}.

Comparison of telomere length corrected ChIP data between Pol2 (ε) and Trt1 (**A**) or Pol1 (α) and Trt1 (**B**) in indicated genomic backgrounds. For explanation of shaded areas in graphs, see Figure 2.5 legend. Error bars correspond to SEM.

2.2.5 Poz1, Rap1 and Taz1 prevent accumulation of the Rad3^{ATR}-Rad26^{ATRIP} complex at telomeres

The differential arrival of leading and lagging strand DNA polymerases could temporarily create extended ssDNA at telomeres that are then replicated by the lagging strand polymerase. Indeed, both the largest subunit of the ssDNA binding complex RPA (Rad11) and the checkpoint kinase regulatory subunit Rad26 (ATRIP ortholog) showed increased binding to telomeres as the leading strand DNA polymerase (Polε) arrives and reduced binding as the lagging strand DNA polymerases (Polα and Polδ) arrive at telomeres (Moser et al., 2009a) (Figure 2.8C wt). Since Polα association is even more delayed in *poz1Δ* and *rap1Δ* cells and severely deregulated in *taz1Δ* cells (Figure 2.5C-D), I predicted that both the Rad3^{ATR}-Rad26^{ATRIP} complex and Rad11^{RPA} to increase in telomere association upon loss of Poz1, Rap1 or Taz1.

Indeed, asynchronous ChIP assays found that Rad3^{ATR}, Rad26^{ATRIP} and Rad11^{RPA} all show a significant increase in binding to telomeres in *poz1Δ*, *rap1Δ* and *taz1Δ* cells (Figures 2.9A and 2.10). The extent of increase was much greater for Trt1^{TERT} and Rad26^{ATRIP} than Rad3^{ATR} and Rad11^{RPA}, but all showed a much greater degree of binding increase to telomeres than shelterin subunits (Tpz1, Ccq1 and Poz1) or Stn1 (Figures 2.9B and 2.11). In contrast to Rad3^{ATR}-Rad26^{ATRIP}, Tel1^{ATM} kinase did not show much increase in telomere association upon elimination of Poz1, Rap1 or Taz1, even though Rad3^{ATR} and Tel1^{ATM} play redundant role(s) in telomere protection and telomerase recruitment (Figure 2.12). These data are consistent with previous conclusions that Rad3^{ATR} plays a much greater role in regulation of telomere length and

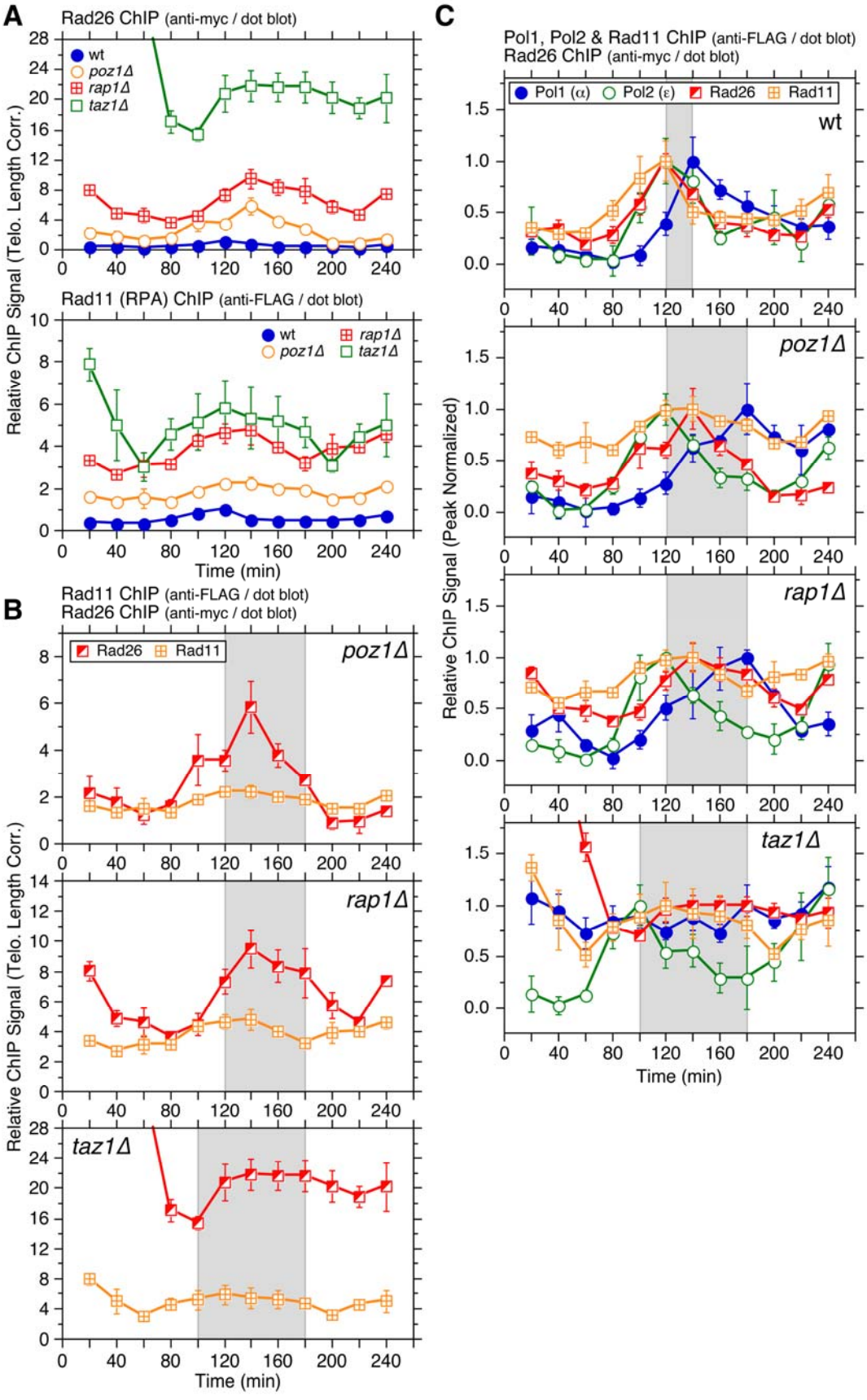
A
Rad26 ChIP (anti-myc / dot blot)
wt
poz1Δ
rap1Δ
taz1Δ
Relative ChIP Signal (Telo. Length Corr.)
Rad11 (RPA) ChIP (anti-FLAG / dot blot)
Time (min)
B
Rad11 ChIP (anti-FLAG / dot blot)
Rad26 ChIP (anti-myc / dot blot)
Rad26
Rad11
C
Pol1, Pol2 & Rad11 ChIP (anti-FLAG / dot blot)
Rad26 ChIP (anti-myc / dot blot)
Pol1 (α)
Pol2 (ε)
Relative ChIP Signal (Peak Normalized)

Figure 2.8 Cell cycle ChIP analysis to monitor association of Rad26^{ATRIP} and Rad11^{RPA} with telomeres.

(**A**) Telomere length adjusted ChIP data for Rad26^{ATRIP} and Rad11^{RPA} in wt, *poz1Δ*, *rap1Δ*, and *taz1Δ* cells. Peak normalized ChIP data, raw ChIP data, and % septated cells to monitor cell cycle progression are shown in Figure 2.13. Anti-myc and anti-FLAG western blot analysis indicated comparable expression levels in different genetic backgrounds for Rad26 and Rad11, respectively (Figure 2.11D). (**B**) Comparison of telomere length adjusted ChIP data for Rad26^{ATRIP} and Rad11^{RPA} in *poz1Δ*, *rap1Δ* or *taz1Δ* cells. (**C**) Comparison of peak normalized ChIP data for Pol1, Pol2, Rad26^{ATRIP}, and Rad11^{RPA}. For (B) and (C), see Figure 2.5 legend for explanation of shaded areas. Error bars correspond to SEM.

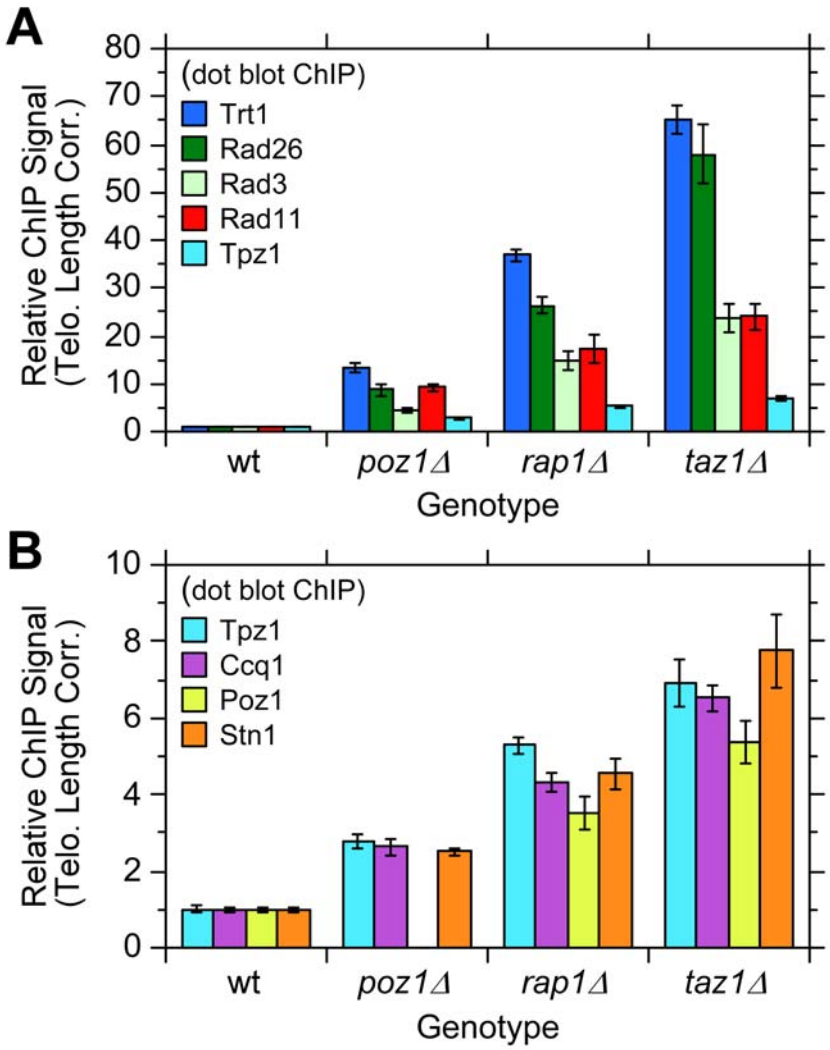

Figure 2.9 Telomere length corrected dot blot-based asynchronous ChIP data for indicated proteins in wt, *poz1Δ*, *rap1Δ* and *taz1Δ* cells.
(**A**) Raw ChIP data from Supplementary Figures 2.10-2.11 for $Trt1^{TERT}$, $Rad26^{ATRIP}$, $Rad3^{ATR}$, $Rad11^{RPA}$ and Tpz1 were corrected for telomere length and normalized to wt cells. Compared to wt cells, *poz1Δ*, *rap1Δ*, and *taz1Δ* cells all showed statistically significant increases in telomere association for $Trt1^{TERT}$ ($p<1.2\times10^{-11}$), $Rad26^{ATRIP}$ ($p<6.4\times10^{-4}$), $Rad3^{ATR}$ ($p<0.047$ for *poz1Δ* while $p<1.8\times10^{-5}$ for *rap1Δ* and *taz1Δ*), $Rad11^{RPA}$ ($p<1.6\times10^{-3}$) and Tpz1 ($p<3.2\times10^{-7}$). (**B**) Raw ChIP data from Supplementary Figure 2.11 for Tpz1, Ccq1, Poz1 and Stn1 were corrected for telomere length and normalized to wt cells. Compared to wt cells, *poz1Δ*, *rap1Δ*, and *taz1Δ* cells all showed statistically significant increases in telomere association for Ccq1 ($p<1.8\times10^{-4}$), Poz1 ($p<1.5\times10^{-5}$) and Stn1 ($p<1.1\times10^{-5}$). Error bars correspond to SEM.

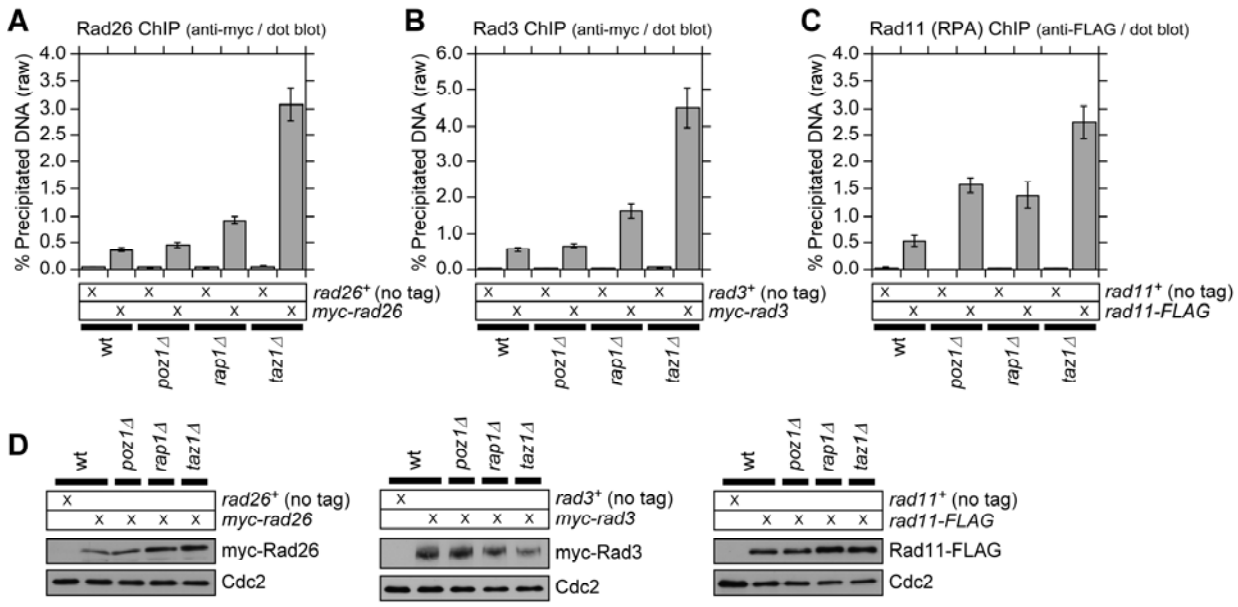

Figure 2.10 Raw % precipitated DNA against input DNA for Rad26^{ATRIP}, Rad3^{ATR} and Rad11^{RPA}.

Raw % precipitated DNA against input DNA for Rad26^{ATRIP} (**A**), Rad3^{ATR} (**B**) and Rad11^{RPA} (**C**) obtained by dot blot-based asynchronous ChIP assays with telomeric DNA probe. Error bars correspond to SEM. (**D**) Anti-myc (Rad26 and Rad3) and anti-FLAG (Rad11) western blot analysis indicated comparable expression levels in different genetic backgrounds. Cdc2 western blot served as a loading control.

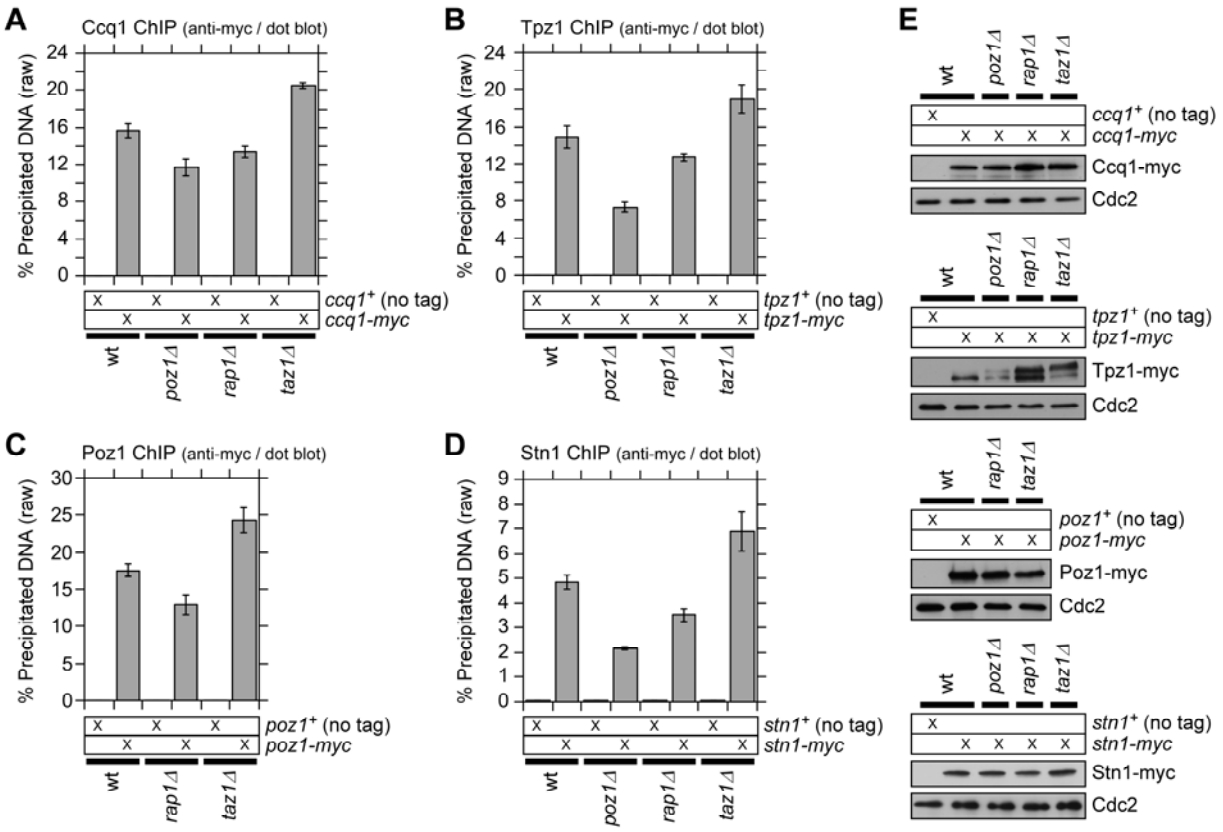

Figure 2.11 Raw % precipitated DNA against input DNA for Ccq1, Tpz1, Poz1 and Stn1.

Raw % precipitated DNA against input DNA for Ccq1 (**A**), Tpz1 (**B**), Poz1 (**C**) and Stn1 (**D**) obtained by dot blot-based asynchronous ChIP assays with telomeric DNA probe. Error bars correspond to SEM. (**E**) Anti-myc western blot analyses indicated comparable expression levels for all proteins in different genetic backgrounds. Cdc2 western blot served as a loading control.

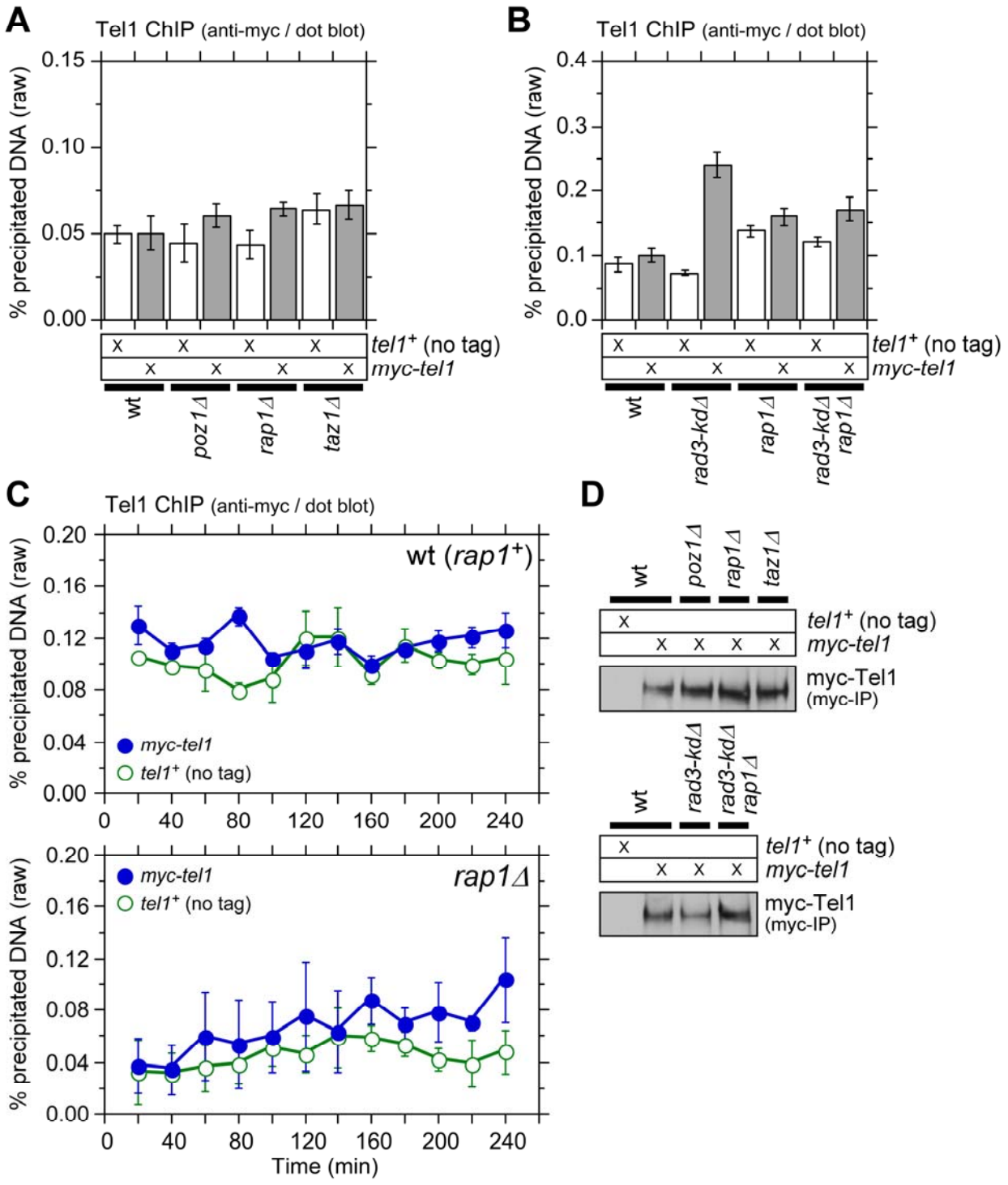
A
Tel1 ChIP (anti-myc / dot blot)
% precipitated DNA (raw)
0.15
0.10
0.05
0.00
tel1+ (no tag)
myc-tel1
wt
poz1Δ
rap1Δ
taz1Δ
B
Tel1 ChIP (anti-myc / dot blot)
% precipitated DNA (raw)
0.4
0.3
0.2
0.1
0.0
tel1+ (no tag)
myc-tel1
wt
rad3-kdΔ
rap1Δ
rad3-kdΔ rap1Δ
C
Tel1 ChIP (anti-myc / dot blot)
% precipitated DNA (raw)
wt (rap1+)
myc-tel1
tel1+ (no tag)
rap1Δ
0.20
0.16
0.12
0.08
0.04
0.00
0
40
80
120
160
200
240
Time (min)
D
wt
poz1Δ
rap1Δ
taz1Δ
tel1+ (no tag)
myc-tel1
myc-Tel1
(myc-IP)
wt
rad3-kdΔ
rad3-kdΔ rap1Δ
tel1+ (no tag)
myc-tel1
myc-Tel1
(myc-IP)

Figure 2.12 Tel1^{ATM} does not show increased binding to telomeres in *poz1Δ*, *rap1Δ* and *taz1Δ* cells.

(**A**, **B**) Raw % precipitated DNA against input DNA for Tel1^{ATM} obtained by dot blot-based asynchronous ChIP assays with telomeric DNA probe. For (**A**), none of the strains showed statistically significant Tel1ATM binding over no tag controls. For (**B**), only *rad3-kdΔ* cells (Subramanian and Nakamura, 2010) showed statistically significant Tel1^{ATM} binding over no tag control ($p=6.0x10^{-4}$). (**C**) Raw data of dot blot-based cell cycle ChIP assays for Tel1^{ATM} in wt or *rap1Δ* cells, performed with *cdc25-22* synchronized cell cultures and telomeric DNA probe. Among all time points, only wt cells at 80 min showed statistically significant Tel1^{ATM} binding over no tag control ($p=4.0x10^{-3}$). Error bars correspond to SEM. (**D**) While myc-Tel1 expressed from its endogenous promoter could not be detected in whole cell extracts, comparable amounts of Tel1^{ATM} were immunoprecipitated (IP) with anti-myc antibody in different genetic backgrounds.

Ccq1 phosphorylation than Tel1^{ATM} in fission yeast (Moser et al., 2011; Moser et al., 2009b; Yamazaki et al., 2012a).

While Rad26^{ATRIP} and Rad11^{RPA} association increased throughout the cell cycle in *poz1*Δ and *rap1*Δ cells compared to wt, the most noticeable change was their increased and persistent binding during the extended time period (80-200 min) between the arrival of Polε and dissociation of Polα (Figures 2.8 and 2.13A-B). While increases in telomere binding during S-phase were more dramatic for Rad26^{ATRIP} than Rad11^{RPA} (Figure 2.8B), both proteins showed significantly higher binding to telomeres in *rap1*Δ than in *poz1*Δ cells (Figure 2.8A), consistent with asynchronous ChIP data (Figure 2.9A) and our previous findings that *rap1*Δ cells show stronger induction of Ccq1 Thr93 phosphorylation and increased binding of Trt1^{TERT} than *poz1*Δ cells (Moser et al., 2011).

For *taz1Δ* cells, both Rad26^{ATRIP} and Rad11^{RPA} showed their strongest binding to telomeres immediately after release from *cdc25-22* induced G_2 arrest (Figures 2.8A and 2.13A-D), suggesting that prolonged arrest in G_2 might cause continued resection of telomeric ends and much higher levels of Rad3^{ATR}-Rad26^{ATRIP} and Rad11^{RPA} accumulation specifically in *taz1Δ* cells. Nevertheless, both Rad26^{ATRIP} and Rad11^{RPA} showed significant reduction in telomere association as cells completed mitosis (~80 min), increased and persistent binding during S/G_2-phase, and slight reduction in binding in late G_2/M-phase (Figures 2.8 and 2.13A-D). Thus, despite the lack of any observable cell cycle regulation for Polα association with telomeres in *taz1Δ* cells, there must be some changes at *taz1Δ* telomeres that allow a slight reduction in association of the Rad3^{ATR}-Rad26^{ATRIP} kinase complex and RPA in late G_2/M-phase.

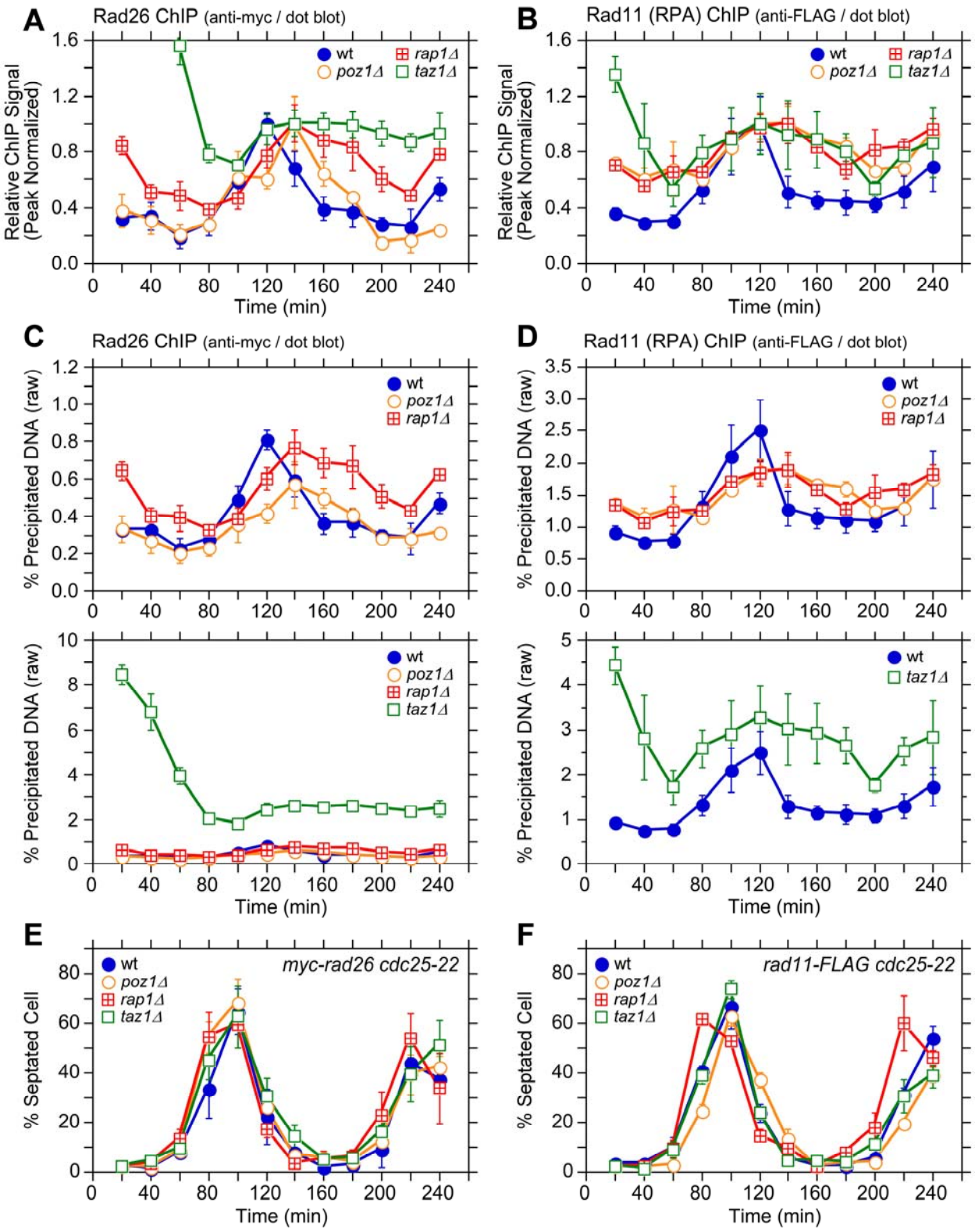
A
Rad26 ChIP (anti-myc / dot blot)
Relative ChIP Signal (Peak Normalized)
wt
poz1Δ
rap1Δ
taz1Δ
Time (min)
B
Rad11 (RPA) ChIP (anti-FLAG / dot blot)
Relative ChIP Signal (Peak Normalized)
Time (min)
C
Rad26 ChIP (anti-myc / dot blot)
% Precipitated DNA (raw)
Time (min)
D
Rad11 (RPA) ChIP (anti-FLAG / dot blot)
% Precipitated DNA (raw)
Time (min)
E
myc-rad26 cdc25-22
% Septated Cell
Time (min)
F
rad11-FLAG cdc25-22
% Septated Cell
Time (min)

Figure 2.13 Cell cycle ChIP assays for Rad26ATRIP and Rad11RPA.
(**A**, **B**) Peak normalized cell cycle ChIP data for Rad26 (**A**) and Rad11 (**B**). (**C**, **D**) Raw data of dot blot-based cell cycle ChIP assays for Rad26 (**C**) and Rad11 (**D**), performed with *cdc25-22* synchronized cell cultures and telomeric DNA probe. (**E**, **F**) % septated cells were measured to monitor cell cycle progression of cdc25-22 synchronized cell cultures for Rad26 (**E**) and Rad11 (**F**) ChIP assays. Error bars correspond to SEM.

2.2.6 Ccq1 Thr93 phosphorylation during cell cycle in wt, *rap1Δ* and *taz1Δ* cells

Phosphorylation of Ccq1 Thr93 by Rad3^{ATR} and Tel1^{ATM} kinases is important for telomerase recruitment in fission yeast (Moser et al., 2011; Yamazaki et al., 2012a). Since Ccq1 is hyper-phosphorylated in *poz1Δ*, *rap1Δ*, or *taz1Δ* cells at Thr93 and additional unidentified phosphorylation sites (Moser et al., 2011), I examined next how Ccq1 phosphorylation is regulated during cell cycle.

While massively increased in *rap1Δ* and *taz1Δ* over wt cells, the overall phosphorylation status of Ccq1, monitored by the presence of a slow mobility band of Ccq1 on SDS-PAGE (marked with *), was constant and did not show any cell cycle regulation in all genetic backgrounds tested (Figure 2.14A). In contrast, Thr93-dependent phosphorylation of Ccq1, detected by phospho-(Ser/Thr) ATM/ATR substrate antibody (Moser et al., 2011), showed cell cycle-regulated changes. In wt cells, Thr93 phosphorylation peaked during late S-phase (100-140 min), but was quickly reduced at later time points and nearly abolished at 200 min before cells entered their next S-phase (Figure 2.14A). Thus, Thr93 phosphorylation was reduced with similar timing as Trt1^{TERT} (Figure 2.5A-B) and Rad26^{ATRIP} (Figure 14A) binding at 160-200 min. In *rap1*Δ and *taz1*Δ cells, Thr93 phosphorylation was increased throughout the entire cell cycle with slight reductions at 60 min and 180-200 min (Figure 2.14A), but did not entirely match the temporal recruitment pattern of Trt1^{TERT} to telomeres, which showed a dramatic increase in binding in late S-phase. Thus, I concluded that there must be other cell cycle-regulated changes besides Ccq1 Thr93 phosphorylation that regulate Trt1^{TERT} recruitment to telomeres.

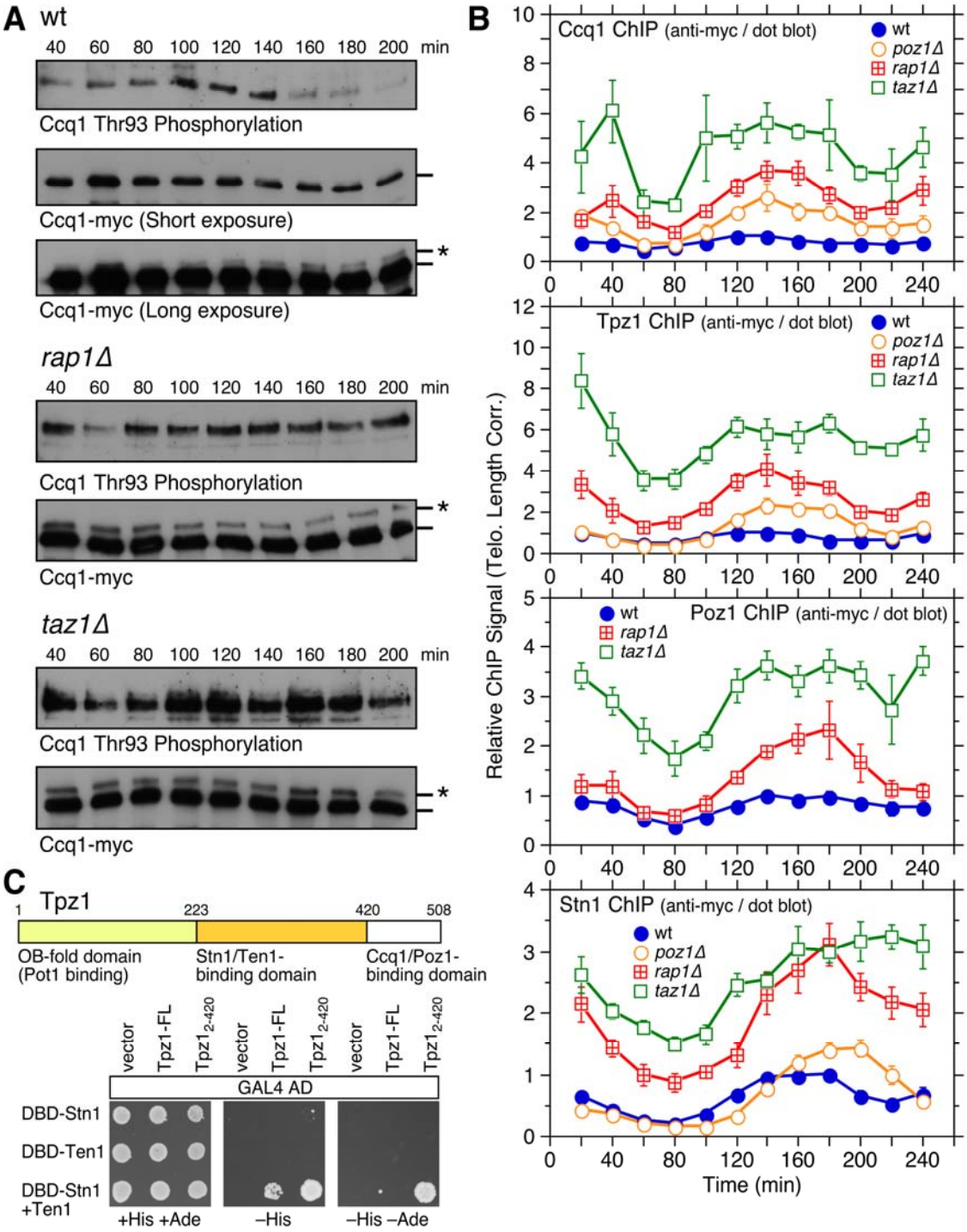
A
wt
40 60 80 100 120 140 160 180 200 min
Ccq1 Thr93 Phosphorylation
Ccq1-myc (Short exposure)
Ccq1-myc (Long exposure)
rap1Δ
Ccq1 Thr93 Phosphorylation
Ccq1-myc
taz1Δ
Ccq1 Thr93 Phosphorylation
Ccq1-myc
B
Ccq1 ChIP (anti-myc / dot blot)
Tpz1 ChIP (anti-myc / dot blot)
Poz1 ChIP (anti-myc / dot blot)
Stn1 ChIP (anti-myc / dot blot)
wt
poz1Δ
rap1Δ
taz1Δ
Relative ChIP Signal (Telo. Length Corr.)
Time (min)
C
Tpz1
1
223
420
508
OB-fold domain (Pot1 binding)
Stn1/Ten1-binding domain
Ccq1/Poz1-binding domain
vector
Tpz1-FL
Tpz1 2-420
GAL4 AD
DBD-Stn1
DBD-Ten1
DBD-Stn1 +Ten1
+His +Ade
–His
–His –Ade

Figure 2.14 Cell cycle regulation of Ccq1 phosphorylation and cell cycle ChIP assays to monitor telomere association of Stn1 and shelterin subunits Ccq1, Tpz1, and Poz1.

(**A**) Western blot analysis of Ccq1 during cell cycle. FLAG-tagged Ccq1 was immunoprecipitated using anti-FLAG antibody, and probed with phospho-(Ser/Thr) ATM/ATR substrate antibody to monitor Ccq1 Thr93 phosphorylation, or probed with anti-FLAG antibody to monitor IP efficiency and existence of slow mobility (marked with *) band corresponding to hyper-phosphorylated Ccq1 (Moser et al., 2011). (**B**) Telomere length adjusted ChIP data for Ccq1, Tpz1, and Stn1 in wt, *poz1Δ*, *rap1Δ*, and *taz1Δ* cells, or for Poz1 in wt, *rap1Δ*, and *taz1Δ* cells. Error bars correspond to SEM. Raw ChIP data and % septated cells to monitor cell cycle progression are shown in Figure 2.15. Anti-myc western blot analyses indicated comparable expression levels in different genetic backgrounds for all proteins (Figure 2.11E). Comparison of peak normalized ChIP data among shelterin subunits and Stn1 are shown in Figures 2.16-2.18. (**C**) Yeast 3-hybrid assay to monitor Tpz1 to Stn1-Ten1 interaction. Co-expression of DBD-Stn1 and Ten1 was necessary to see interaction between Tpz1 and Stn1-Ten1. Additional truncation analysis of Tpz1 (Figure 2.19) established amino acids 224-420 of Tpz1 as the minimum binding-domain to the Stn1-Ten1 complex, while the strongest interaction between Tpz1 and Stn1-Ten1 was observed for C-terminally truncated Tpz1 encoding amino acids 2-420.

2.2.7 Cell cycle-regulated telomere association of shelterin and Stn1 in wt, *poz1Δ*, *rap1Δ*, and *taz1Δ* cells

Previous ChIP analysis had revealed that the shelterin ssDNA-binding subunit Pot1 along with the CST-complex subunit Stn1 show significant late S-phase specific increases in telomere association that matched to the timing of Polα and Trt1^{TERT} recruitment (Moser et al., 2009a). I reasoned that cell cycle-regulated changes in shelterin and CST telomere association could dictate Trt1^{TERT} binding, and thus decided to monitor how loss of Poz1, Rap1 and Taz1 affect cell cycle-regulated association of shelterin and CST. I have limited my analysis to three subunits of shelterin (Ccq1, Tpz1 and Poz1) and Stn1, and decided to exclude Pot1, since I found that addition of an epitope tag to Pot1 significantly altered telomere length of *poz1Δ*, *rap1Δ* and *taz1Δ* cells (data not shown).

Consistent with asynchronous ChIP data (Figure 2.9B), Ccq1, Tpz1, Poz1 and Stn1 all showed gradual increases in overall binding to telomeres in the order of wt, *poz1Δ*, *rap1Δ* and *taz1Δ* when corrected for changes in telomere length (Figure 2.14B). Ccq1 and Tpz1 showed nearly identical temporal recruitment patterns in wt, *poz1Δ*, *rap1Δ,* and *taz1Δ* cells (Figure 2.16), while Poz1 recruitment was delayed compared to Ccq1 and Tpz1, and more closely resembled the pattern found for Stn1 (Figures 2.17 and 2.18).

I was initially surprised by the similarity of the temporal recruitment patterns for Poz1 and Stn1, as we previously failed to detect interaction between shelterin and Stn1-Ten1 by co-immunoprecipitation (Moser et al., 2009a). On the other hand, studies in

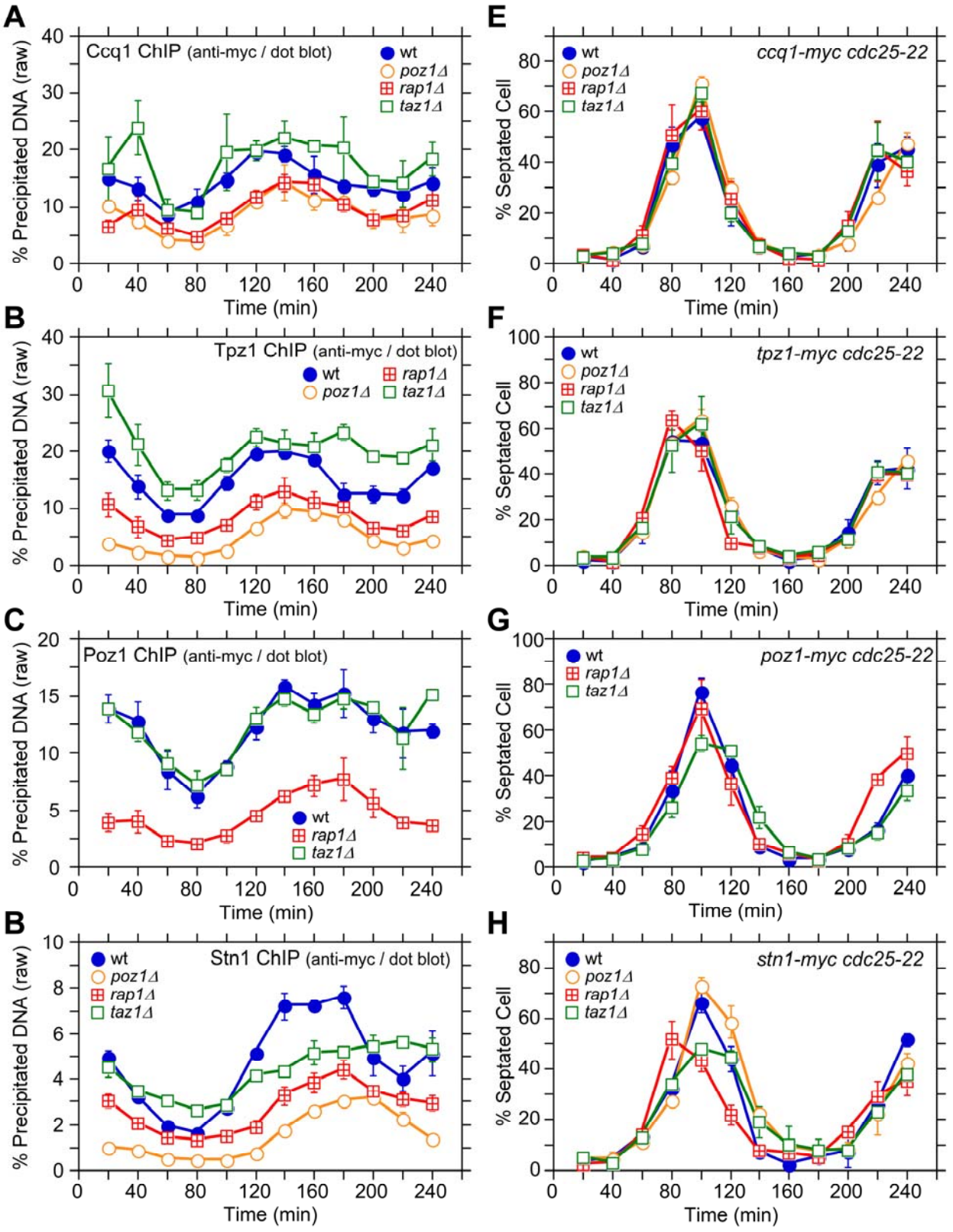
A
Ccq1 ChIP (anti-myc / dot blot)
wt
poz1Δ
rap1Δ
taz1Δ
% Precipitated DNA (raw)
Time (min)
B
Tpz1 ChIP (anti-myc / dot blot)
C
Poz1 ChIP (anti-myc / dot blot)
B
Stn1 ChIP (anti-myc / dot blot)
E
ccq1-myc cdc25-22
% Septated Cell
F
tpz1-myc cdc25-22
G
poz1-myc cdc25-22
H
stn1-myc cdc25-22

Figure 2.15 Cell cycle ChIP assays for shelterin subunits and Stn1.
(**A-D**) Raw data of dot blot-based cell cycle ChIP assays for Ccq1 (**A**), Tpz1 (**B**), Poz1 (**C**) and Stn1 (**D**), performed with *cdc25-22* synchronized cell cultures and telomeric DNA probe. (E-H) % septated cells were measured to monitor cell cycle progression of cdc25-22 synchronized cell cultures for Ccq1 (**E**), Tpz1 (**F**), Poz1 (**G**) and Stn1 (**H**) ChIP assays. Error bars correspond to SEM.

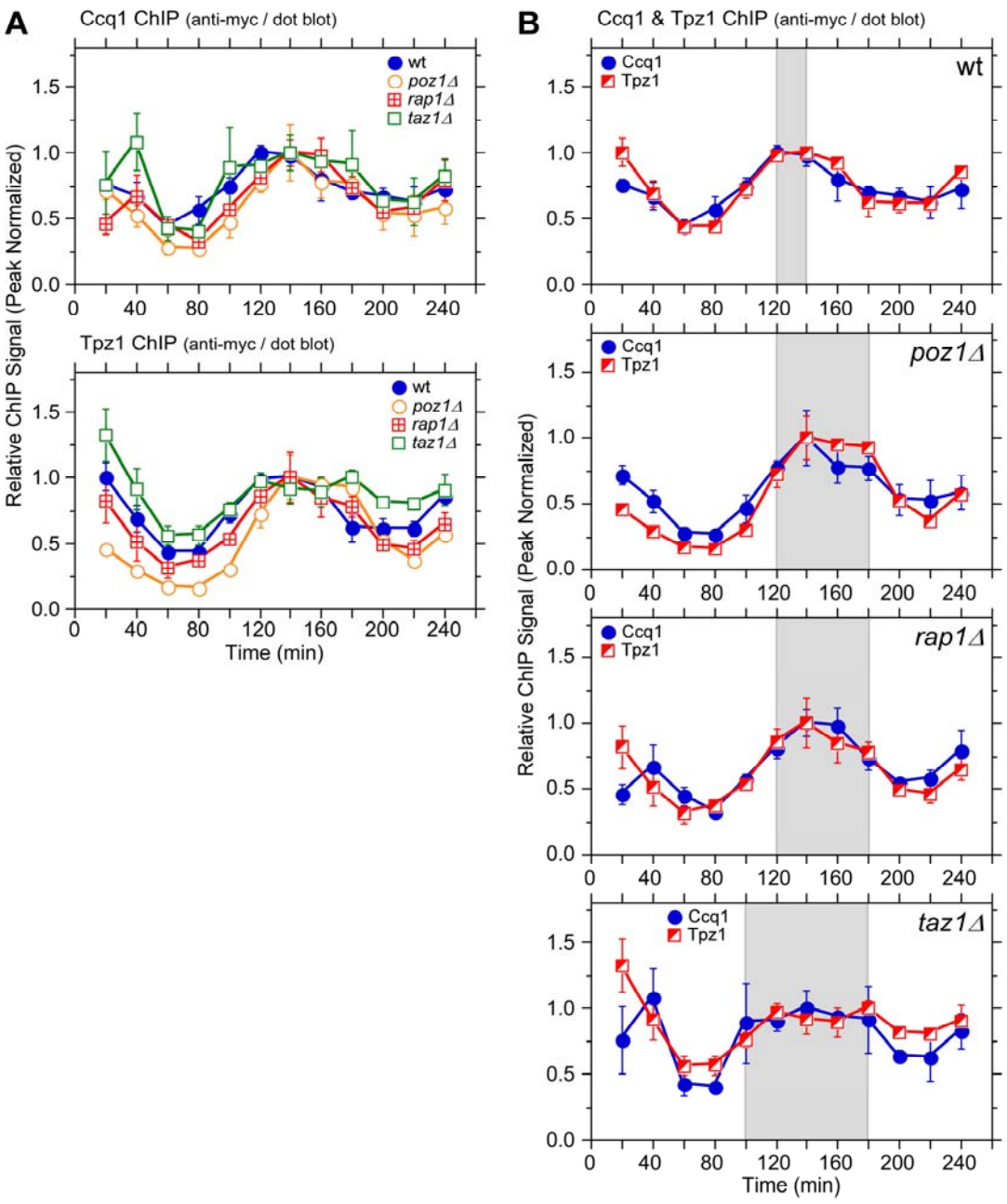

Figure 2.16 Comparison of peak normalized cell cycle ChIP data between Ccq1 and Tpz1.

(**A**) Peak normalized ChIP data for either Ccq1 or Tpz1 in different genetic backgrounds were plotted to compare changes in temporal association with telomeres. (**B**) Comparison of peak normalized ChIP data indicated that temporal changes in telomere association for Ccq1 and Tpz1 are nearly identical in all genetic backgrounds tested. For explanation of shaded areas in graphs, see Figure 2.6 legend. Error bars correspond to SEM.

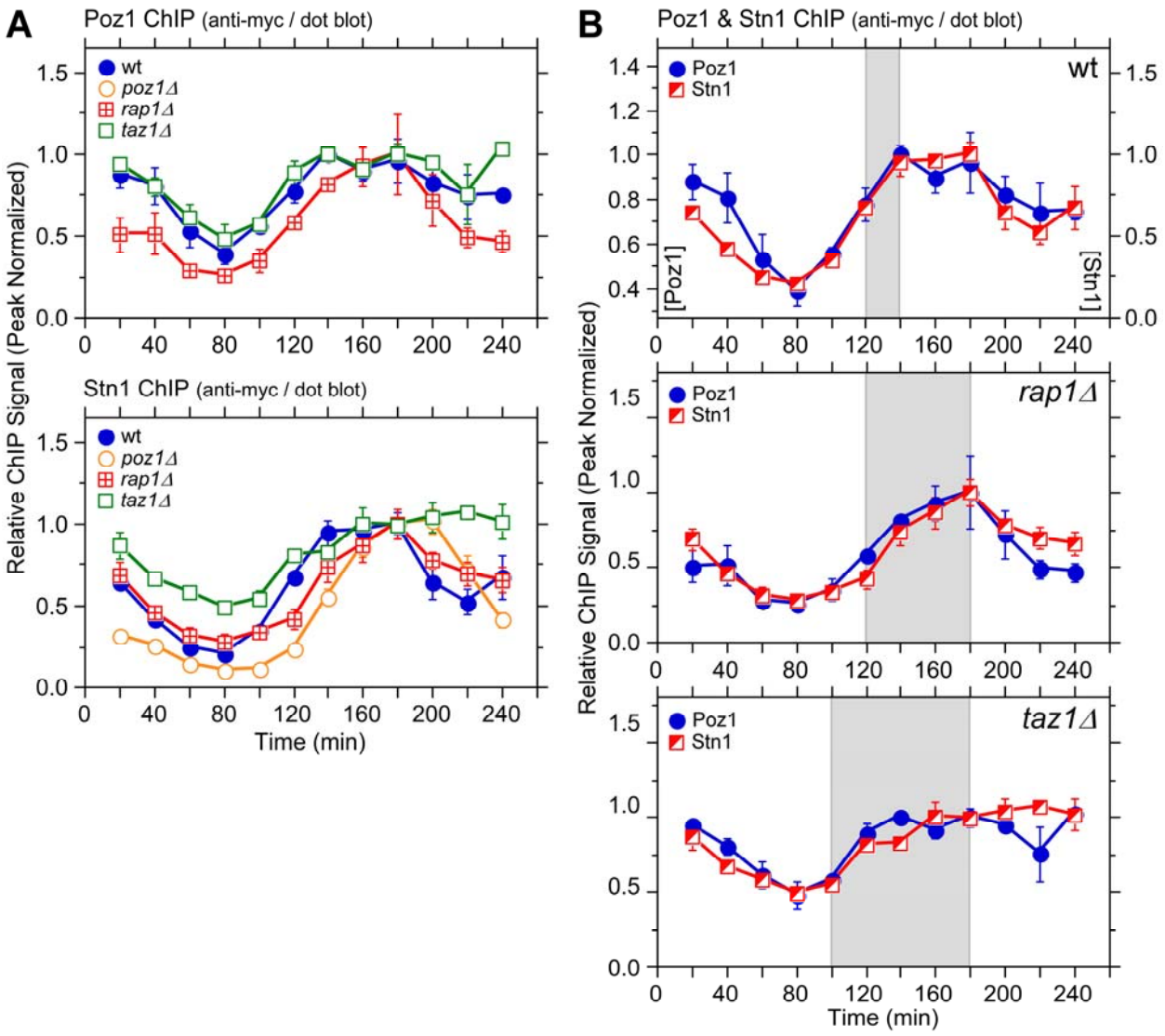

Figure 2.17 Comparison of peak normalized cell cycle ChIP data between Poz1 and Stn1.

(**A**) Peak normalized ChIP data for either Poz1 or Stn1 in different genetic backgrounds were plotted to compare changes in temporal association with telomeres. (**B**) Comparison of peak normalized ChIP data indicated that temporal changes in telomere association for Poz1 and Stn1 are nearly identical in wt, *rap1Δ* and *taz1Δ* cells. For explanation of shaded areas in graphs, see Figure 2.5 legend. Error bars correspond to SEM.

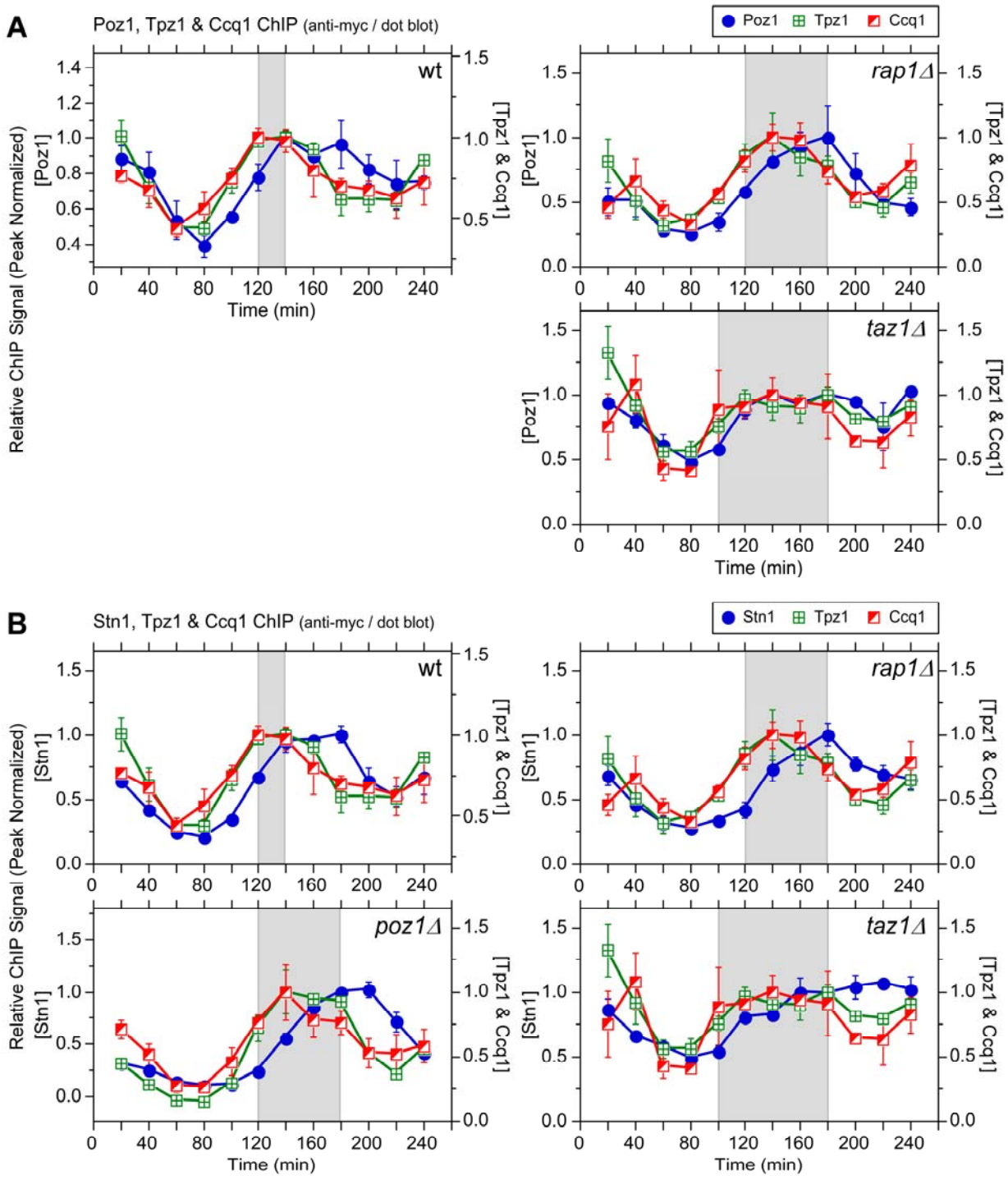
A
Poz1, Tpz1 & Ccq1 ChIP (anti-myc / dot blot)
Poz1
Tpz1
Ccq1
wt
rap1Δ
taz1Δ
Relative ChIP Signal (Peak Normalized)
[Poz1]
[Tpz1 & Ccq1]
Time (min)
B
Stn1, Tpz1 & Ccq1 ChIP (anti-myc / dot blot)
Stn1
Tpz1
Ccq1
wt
rap1Δ
poz1Δ
taz1Δ
Relative ChIP Signal (Peak Normalized)
[Stn1]
[Tpz1 & Ccq1]
Time (min)

Figure 2.18 Comparison of cell cycle ChIP data among Ccq1, Tpz1, Poz1 and Stn1.

(**A**) Comparison of peak normalized ChIP data for Poz1, Tpz1 and Ccq1 in wt, *rap1Δ* and *taz1Δ* cells. For Tpz1 vs. Poz1, Student's t-test found p=0.053 at 120 min (94.7% confidence level) for wt cells, and p=0.058 at 80 min (94.2% confidence level) and p=0.09 at 100 min (91% confidence level) for *rap1Δ* cells. For Ccq1 vs. Poz1, Student's t-test found p=0.045 at 100 min (95.5% confidence level) and p=0.071 at 120 min (92.9% confidence level) for wt cells, and p=0.082 at 100 min (91.8% confidence level) for *rap1Δ* cells. (**B**) Comparison of peak normalized ChIP data for Stn1, Tpz1 and Ccq1 in wt, *poz1Δ*, *rap1Δ* and *taz1Δ* cells. For Tpz1 vs. Stn1, differences were statistically significant at 60-120 min for wt cells ($p<0.03$), at 100, 120, 200 and 220 min for *poz1Δ* cells ($p<0.04$), and at 100, 120, 200 min for *rap1Δ* cells ($p<0.01$). For Ccq1 vs. Stn1, differences were statistically significant at 100, 120 and 180 min for wt cells ($p<0.03$), at 80 and 120 min for *poz1Δ* cells ($p<0.04$), and at 100, 120, 200 min for *rap1Δ* cells ($p<0.02$). For explanation of shaded areas in graphs, see Figure 2.5 legend. Error bars correspond to SEM.

mammalian cells have detected TPP1-CST interaction (Chen et al., 2012; Wan et al., 2009), and 3-hybrid assay also revealed that Tpz1 can interact with Stn1-Ten1 (Figures 2.14C and 2.19). Intriguingly, the Tpz1 interaction with Stn1-Ten1 became stronger when the Ccq1/Poz1 interaction domain of Tpz1 (amino acids 421-508) was deleted (Figure 2.19), suggesting that this domain might negatively regulate the interaction between Tpz1 and Stn1-Ten1. Thus, it is possible that Tpz1-Poz1 interaction might facilitate the timely recruitment of Stn1-Ten1 by reducing the ability of the Tpz1 C-terminal domain to negatively regulate interaction between Tpz1 and Stn1-Ten1.

Comparison with DNA polymerases revealed that Ccq1 and Tpz1 show increases in telomere association along with Polε (80-120 min) and reduction in binding along with Polα (140-220 min) in wt cells (Figure 2.20). The onsets of increased binding in Ccq1 and Tpz1 remained similar (~80 min) in the deletion mutants. However, Ccq1 and Tpz1 binding peaked at 140 min, between the peaks for Polε and Polα in *poz1Δ* and *rap1Δ* cells, while they sustained increased binding longer (120-180 min) in *taz1Δ* (Figures 2.14B and 2.20). Thus, analogous to $Rad26^{ATRIP}$ (Figure 2.8), increased binding of Ccq1 and Tpz1 during S-phase in *poz1Δ*, *rap1Δ* and *taz1Δ* cells may be dictated by increased ssDNA caused by deregulated replication of telomeres.

In contrast, the temporal binding patterns for Stn1 and Poz1 matched closely with the binding pattern for Polα (Figure 2.21A) in all genetic backgrounds tested, except for *taz1Δ*. This is consistent with the notion that Poz1 and Stn1 may closely collaborate in promoting the timely recruitment of Polα to telomeres. I also found that Stn1 in wt, *poz1Δ* and *rap1Δ* cells shows more persistent binding at later time points than Polα (Figure 2.21A), suggesting that Stn1 can sustain increased telomere binding even after

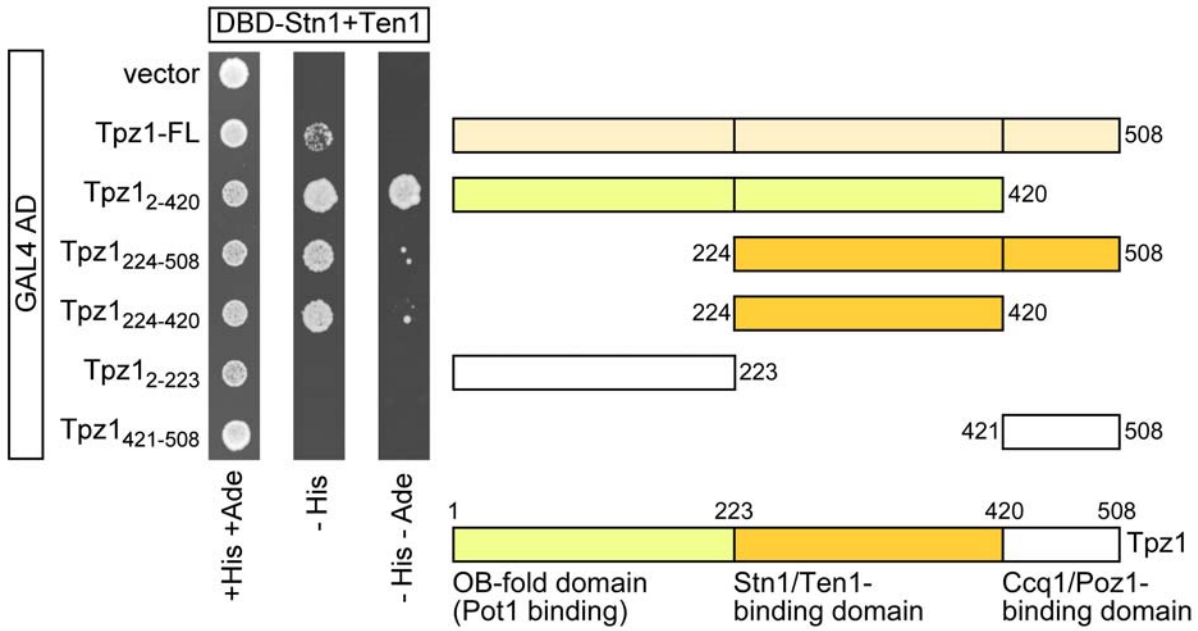

Figure 2.19 Yeast 3-hybrid assay to monitor interaction between Tpz1 and Stn1-Ten1.
Various truncation constructs of Tpz1 were tested for interaction with Stn1 and Ten1. Based on cell growth on –His selection plate, a Tpz1 fragment containing amino acids 224-420 was the smallest Tpz1 construct that retained interaction with Stn1 and Ten1. Based on growth on –His –Ade plate, a Tpz1 fragment containing amino acids 2-420 showed strongest interaction with Stn1 and Ten1.

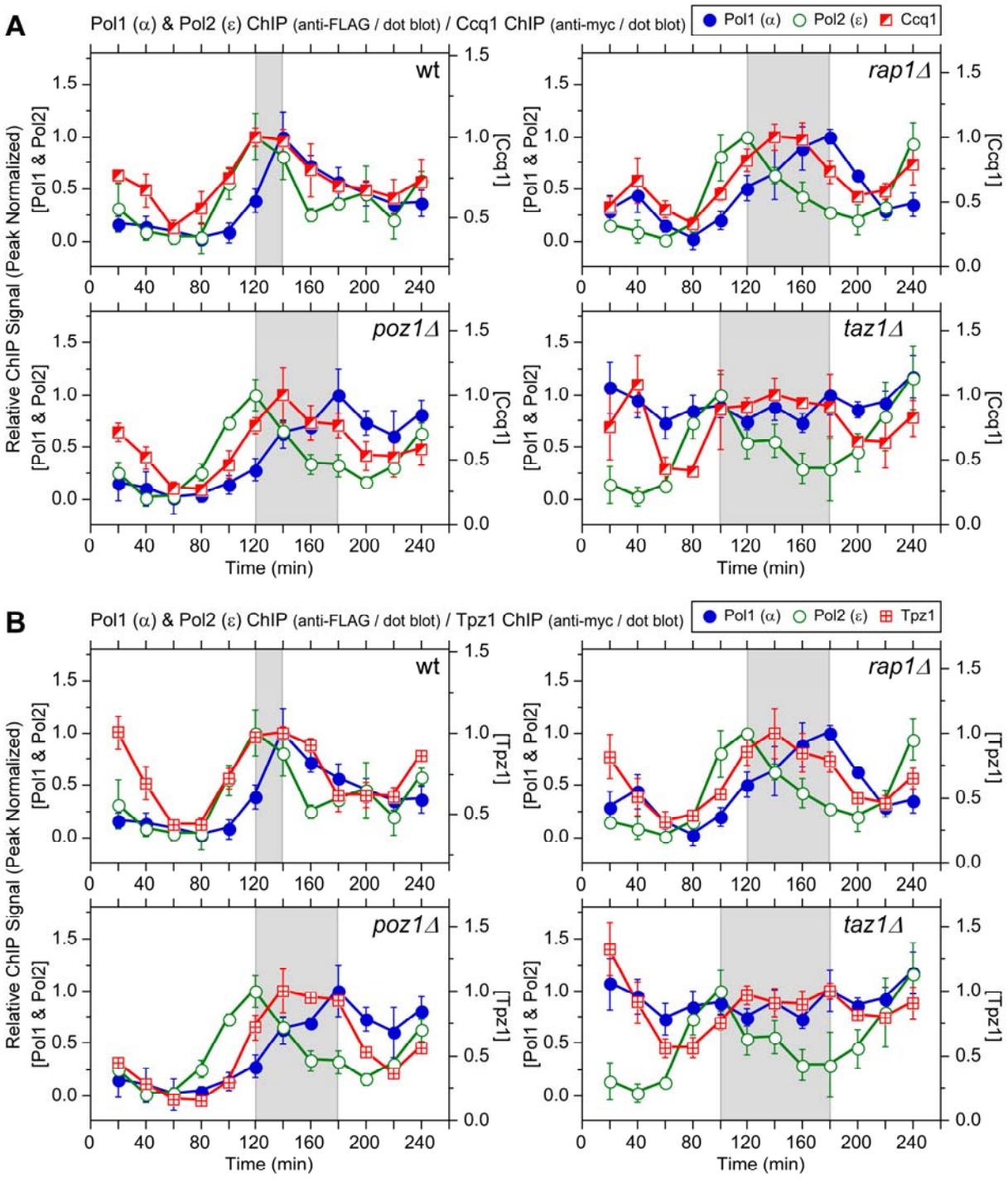

Figure 2.20 Comparison of cell cycle ChIP data among DNA polymerases, Ccq1 and Tpz1.

Comparison of peak normalized ChIP data for Pol1 (α), Pol2 (ε) and Ccq1 (**A**) or Pol1 (α), Pol2 (ε) and Tpz1 (**B**) in wt, *poz1Δ*, *rap1Δ*, and *taz1Δ* cells. For explanation of shaded areas in graphs, see Figure 2.5 legend. Error bars correspond to SEM.

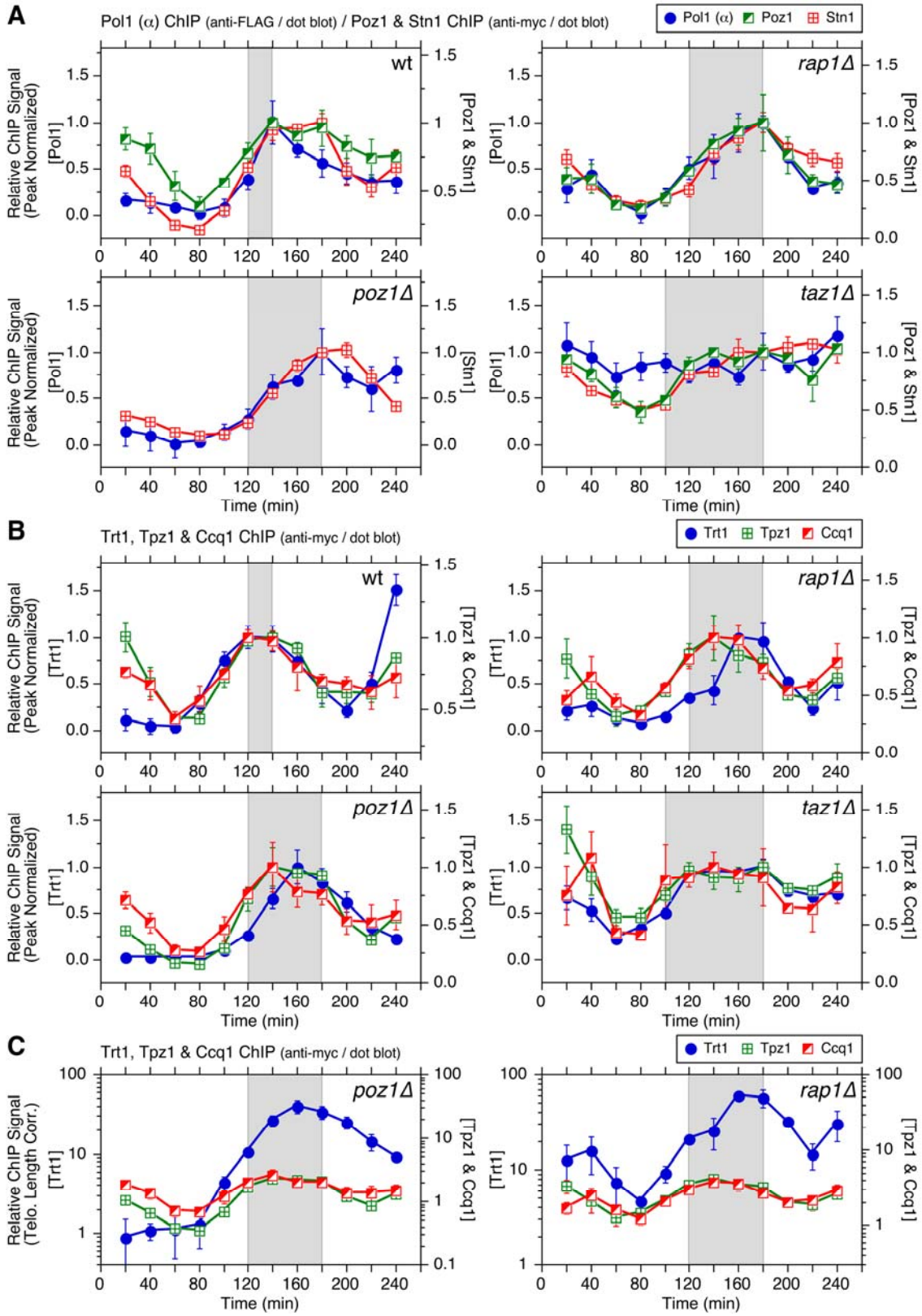
A
Pol1 (α) ChIP (anti-FLAG / dot blot) / Poz1 & Stn1 ChIP (anti-myc / dot blot)
Pol1 (α)
Poz1
Stn1
wt
rap1Δ
poz1Δ
taz1Δ
Relative ChIP Signal (Peak Normalized)
[Pol1]
[Poz1 & Stn1]
[Stn1]
Time (min)
B
Trt1, Tpz1 & Ccq1 ChIP (anti-myc / dot blot)
Trt1
Tpz1
Ccq1
[Trt1]
[Tpz1 & Ccq1]
C
Relative ChIP Signal (Telo. Length Corr.)

Figure 2.21 Comparison of cell cycle ChIP data for Trt1^{TERT}, DNA polymerases, Poz1/Stn1 and Ccq1/Tpz1.

(**A**) Comparison of peak normalized ChIP data for Pol1 (α), Poz1 and Stn1. Comparison for Poz1, Stn1 and Trt1^{TERT} are shown in Figure 2.23. (**B**) Comparison of peak normalized ChIP data for Trt1^{TERT}, Ccq1, and Tpz1. Comparison for Ccq1, Tpz1 and DNA polymerases are shown in Figure 2.20. (**C**) Comparison of telomere length adjusted ChIP data for Trt1^{TERT}, Ccq1 and Tpz1 in *poz1Δ* or *rap1Δ* cells, plotted in log scale. For explanation of shaded areas in graphs, see Figure 2.5 legend. Error bars correspond to SEM.

Polα dissociates from telomeres. Consistently, we have previously observed increased binding of Stn1 to telomeres in S-phase, even when Polα recruitment was inhibited by HU treatment (Moser et al., 2009a).

Ccq1, Tpz1 and Trt1^{TERT} showed nearly identical overall temporal binding patterns in wt and *taz1Δ* cells, consistent with the notion that cell cycle-regulated binding of Tpz1 and Ccq1 plays a major role in controlling Trt1^{TERT} association with telomeres (Figure 2.21B). In contrast, Trt1^{TERT} reached its maximal binding later than Ccq1 and Tpz1 in *poz1Δ* and *rap1Δ* cells (Figure 2.21B). However, this delay is a reflection of the dramatic increase in Trt1^{TERT} binding at 160-200 min in *poz1Δ* and *rap1Δ* cells (Figure 2.5A-B), a time period in which Ccq1 Thr93 phosphorylation is rapidly reduced in wt cells but remained constitutively high in *rap1Δ* or *taz1Δ* cells (Figure 2.14A). Indeed, while huge increases in Trt1^{TERT} binding over Tpz1 or Ccq1 had made it difficult to compare cell cycle-regulated patterns in linear scale plots, plotting data on log scale made it more clear that the initial increase in binding of Trt1^{TERT}, Ccq1 and Tpz1 occurred with similar timing even in *poz1Δ* and *rap1Δ* cells (Figure 2.21C).

Poz1 and Stn1 binding to telomeres was delayed compared to Trt1^{TERT} in wt cells, but all three proteins showed very similar overall temporal binding patterns in deletion mutant cells except for more persistent Stn1 binding at later time points (Figure 2.22A-B). However, since Trt1^{TERT} binding in *poz1Δ*, *rap1Δ* and *taz1Δ* cells increased even in early S-phase, the initial increase in Trt1^{TERT} binding still preceded binding increases of Poz1 and Stn1 in deletion mutant backgrounds (Figure 2.22C). Taken together, my findings are consistent with the notion that the initial increase in binding of Tpz1 and Ccq1 to telomeres in S-phase contributes to Trt1^{TERT} recruitment, and that a

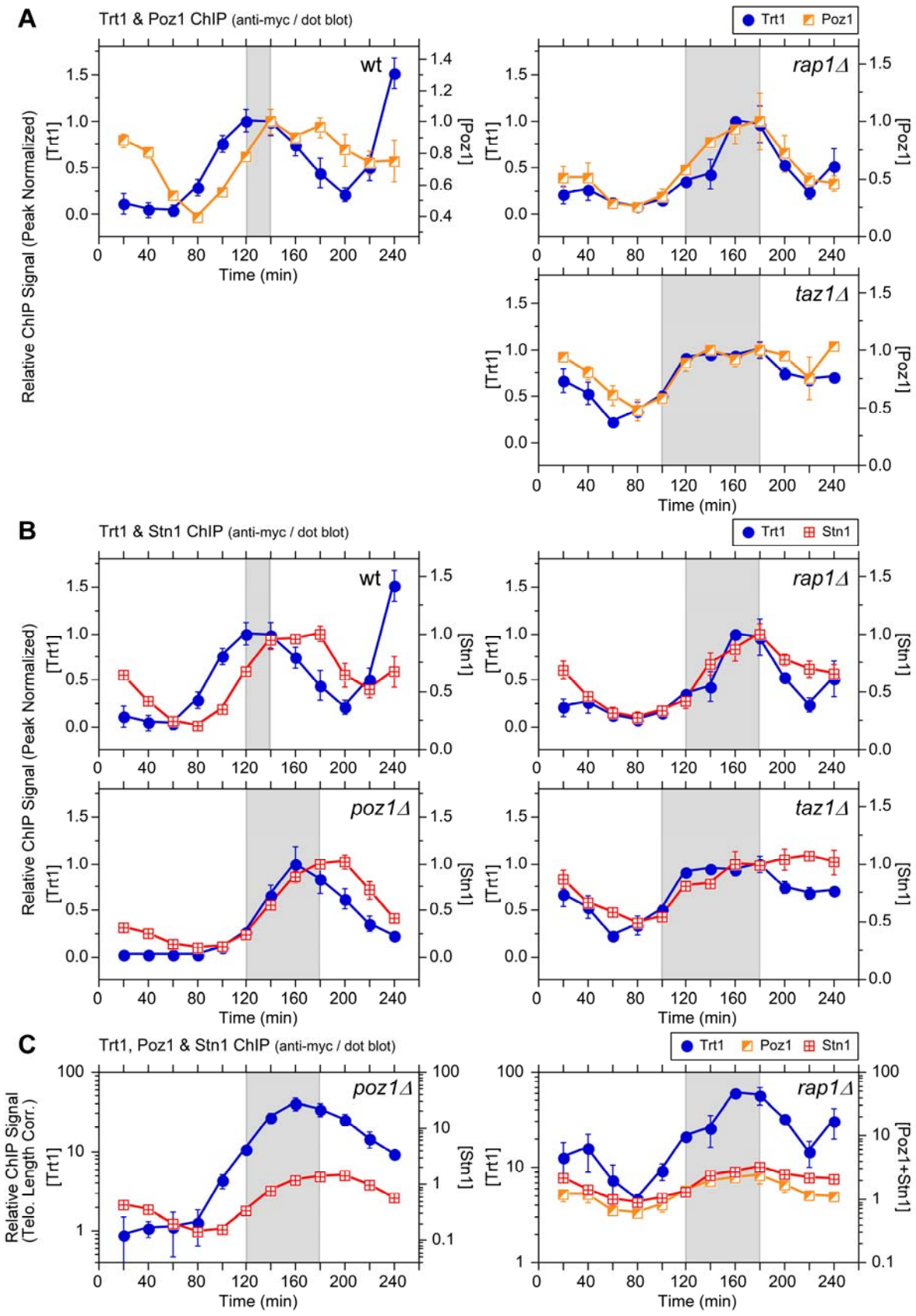
A
Trt1 & Poz1 ChIP (anti-myc / dot blot)
Trt1
Poz1
wt
rap1Δ
taz1Δ
Relative ChIP Signal (Peak Normalized)
[Trt1]
[Poz1]
Time (min)
B
Trt1 & Stn1 ChIP (anti-myc / dot blot)
Trt1
Stn1
wt
rap1Δ
poz1Δ
taz1Δ
Relative ChIP Signal (Peak Normalized)
[Trt1]
[Stn1]
Time (min)
C
Trt1, Poz1 & Stn1 ChIP (anti-myc / dot blot)
Trt1
Poz1
Stn1
poz1Δ
rap1Δ
Relative ChIP Signal
(Telo. Length Corr.)
[Trt1]
[Stn1]
[Poz1+Stn1]
Time (min)

Figure 2.22 Comparison of cell cycle ChIP data among Trt1^{TERT}, Poz1 and Stn1. Comparison of peak normalized ChIP data between Trt1 and Poz1 (**A**) or Trt1 and Stn1 (**B**) for indicated genomic backgrounds. (**C**) Comparison of peak normalized ChIP data among Trt1, Poz1 and Stn1 in *poz1Δ* or *rap1Δ*, plotted on log scale. For explanation of shaded areas in graphs, see Figure 2.5 legend. Error bars correspond to SEM.

subsequent increase in binding of Poz1 and Stn1 contributes to the timely recruitment of Polα, which limits ssDNA and Rad3^{ATR}-Rad26^{ATRIP} accumulation as well as Ccq1 Thr93 phosphorylation and telomerase recruitment.

2.2.8 Contribution of Trt1^{TERT} to regulation of differential temporal binding of DNA Polε and Polα to telomeres

Ccq1 Thr93 phosphorylation is also increased in cells carrying short telomeres (Moser et al., 2011; Yamazaki et al., 2012a). As short telomeres would have less binding sites for Taz1 (Cooper et al., 1997; Tomaska et al., 2004), they may become less effective in excluding the Rad3^{ATR}-Rad26^{ATRIP} complex from telomeres. Consistently, I found that Rad26^{ATRIP} binding is indeed significantly increased in *trt1Δ* cells (Figure 2.23A).

While the notion that telomerase is preferentially recruited to short telomeres, due to reduced binding of Taz1 and increased Ccq1 Thr93 phosphorylation, is an attractive model to explain telomere length homeostasis in fission yeast, there has been a lack of any direct evidence that Trt1^{TERT} binding is indeed increased at short telomeres (Moser et al., 2011). The problem was difficult to address since mutations previously used to induce telomere shortening (*trt1Δ* or *ccq1-T93A*) eliminated telomerase or its recruitment (Moser et al., 2011). We overcame this limitation by monitoring telomere binding of catalytically inactive Trt1^{TERT} (*trt1-D743A*), which causes telomere shortening (Haering et al., 2000). Consistent with the prediction, I found that Trt1-D743A binds stronger than wt Trt1^{TERT} to telomeres in asynchronous cell cultures

(Figure 2.23B and 2.24B), and binds constitutively throughout the cell cycle with increase in binding during S/G_2-phase (Figure 2.23C).

Deletion of Rap1 further increased Trt1-D743A binding (Figure 2.23B-C), especially at the early time points after cell cycle re-entry (20-60min), but did not greatly affect the temporal recruitment pattern of Trt1-D743A for the remainder of the cell cycle. It is not clear why *trt1-D743A rap1Δ* shows increased $Trt1^{TERT}$ binding at early time points, but binding levels were comparable to wt $Trt1^{TERT}$ in *rap1Δ* cells at 20-80 min (Figure 2.23C). In contrast, far more wt $Trt1^{TERT}$ was recruited to telomeres than Trt1-D743A for the remainder of the cell cycle in *rap1Δ* cells, suggesting that the massive increase in telomere association of $Trt1^{TERT}$ in *rap1Δ* cells during late S/G_2-phase is largely dependent on telomerase activity (Figure 2.23C).

Next, I investigated how DNA polymerases were affected in *trt1Δ* or *trt1-D743A* cells. Interestingly, Polε binding to telomeres peaked slightly earlier, and the initial increase in Polα binding also occurred slightly earlier in *trt1Δ* and *trt1-D743A* (~100 min) than wt cells (~120 min) (Figure 2.25A). In contrast, I did not see any major change in Polα recruitment timing at *ars2004* in *trt1Δ* cells (Figure 2.26E). Since *taz1Δ* cells show earlier recruitment of Polε and telomere replication (Tazumi et al., 2012) (Figures 2.4 and 2.6), it is tempting to speculate that reduced binding of Taz1 at short telomeres might be responsible for earlier Polε recruitment (consistent with earlier telomere replication) for cells carrying short telomeres.

While there was no obvious difference between *trt1Δ* and *trt1-D743A* cells in overall temporal recruitment patterns of Polε and Polα (Figure 2.25A), when normalized for telomere length, *trt1-D743A* cells had significantly reduced binding of Polα compared

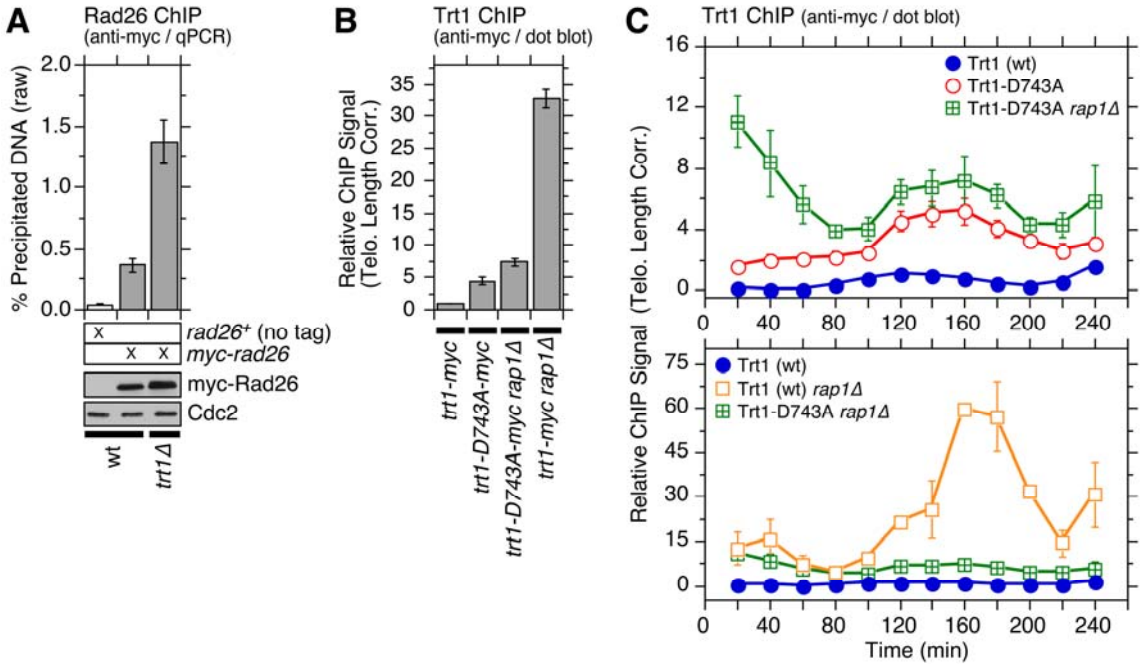

Figure 2.23 Characterization of telomere association for catalytically dead Trt1^{TERT}.

(**A**) Comparison of telomere association of Rad26^{ATRIP} in *wt* and *trt1Δ* cells, monitored by ChIP assay. Rad26^{ATRIP} showed a statistically significant increase in telomere association for *trt1Δ* vs. *trt1*$^{+}$ cells ($p=4.6\times10^{-4}$). Anti-myc western blot found comparable Rad26 expression in wt and *trt1Δ* cells. (**B**) Telomere association of wt or catalytically dead (D743A) Trt1^{TERT} in *rap1*$^{+}$ or *rap1Δ* backgrounds, monitored by ChIP assay (corrected for telomere length). Trt1-D743A showed a statistically significant increase in telomere association compared to wt Trt1^{TERT} ($p=3.2\times10^{-5}$). Raw ChIP data and expression level of Trt1^{TERT}, monitored by anti-myc western blot analysis, are shown in Figure 2.24B. Data for Trt1-D743A ChIP samples, analyzed by qPCR, are also shown in Figure 2.24B. Telomere lengths of strains carrying *trt1Δ* or *trt1-D743A* were also monitored by Southern blot analysis (Figure 2.24A). (**C**) Telomere length corrected cell cycle ChIP assays to monitor association of Trt1^{TERT} with telomeres. Raw and peak normalized ChIP data and % septated cells to monitor cell cycle progression are shown in Figure 2.24C-E. Error bars correspond to SEM.

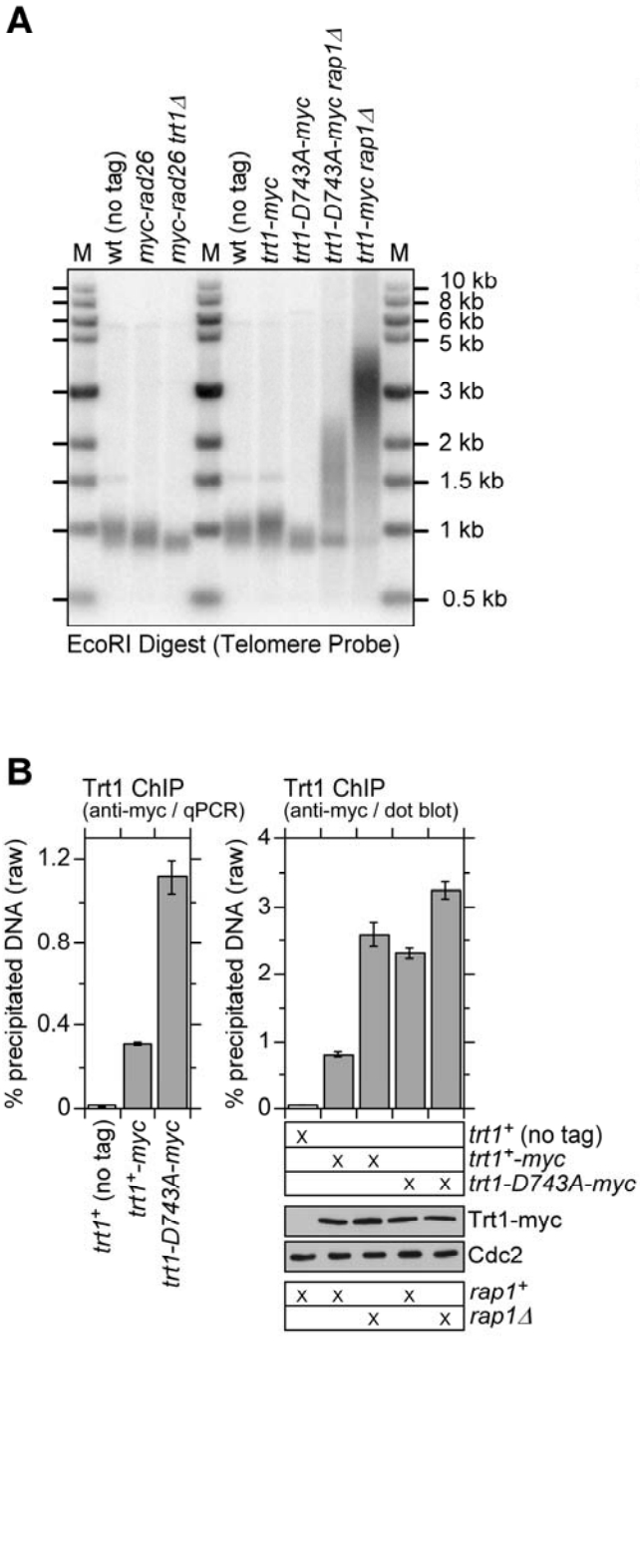
A
M
wt (no tag)
myc-rad26
myc-rad26 trt1Δ
M
wt (no tag)
trt1-myc
trt1-D743A-myc
trt1-D743A-myc rap1Δ
trt1-myc rap1Δ
M
10 kb
8 kb
6 kb
5 kb
3 kb
2 kb
1.5 kb
1 kb
0.5 kb
EcoRI Digest (Telomere Probe)
B
Trt1 ChIP
(anti-myc / qPCR)
% precipitated DNA (raw)
trt1+ (no tag)
trt1+-myc
trt1-D743A-myc
Trt1 ChIP
(anti-myc / dot blot)
% precipitated DNA (raw)
trt1+ (no tag)
trt1+-myc
trt1-D743A-myc
Trt1-myc
Cdc2
rap1+
rap1Δ
C
Trt1 ChIP (anti-myc / dot blot)
Relative ChIP Signal
(Peak Normalized)
Time (min)
D
Trt1 ChIP (anti-myc / dot blot)
trt1-myc (wt)
trt1-D743A-myc
trt1+ (no tag)
% Precipitated DNA (raw)
trt1-D743A-myc
trt1-myc (wt) rap1Δ
trt1-D743A-myc rap1Δ
% Precipitated DNA (raw)
Time (min)
E
trt1-myc (wt)
trt1-D743A-myc
trt1-myc (wt) rap1Δ
trt1-D743A-myc rap1Δ
trt1-myc cdc25-22
% Septated Cell
Time (min)

Figure 2.24 Cell cycle ChIP assays for catalytically dead Trt1-D743A.
(**A**) Telomere length analysis for indicated strains used in ChIP analysis. Genomic DNA was prepared from early generation strains. After digestion with restriction enzyme *EcoRI*, DNA was fractionated on a 1% agarose gel and processed for Southern blot analysis with a telomere probe. (**B**) Raw % precipitated DNA against input DNA for $Trt1^{TERT}$ obtained by real-time quantitative PCR analysis (left) or dot blot-based asynchronous ChIP assays with telomeric DNA probe (right). Trt1-D743A showed a statistically significant increase in telomere association compared to wt $Trt1^{TERT}$ ($p=5.4x10^{-5}$) for PCR-based ChIP assay, independently confirming our conclusion from telomere-length corrected dot blot-based ChIP assay (Figure 2.23B). Anti-myc western blot analysis indicated comparable expression levels of Trt1 in different genetic backgrounds. Cdc2 western blot served as a loading control. (**C**) Peak normalized cell cycle ChIP data for wt or catalytically dead $Trt1^{TERT}$ in *rap1*$^{+}$ or *rap1*Δ cells. (**D**) Raw data of dot blot-based cell cycle ChIP assays for $Trt1^{TERT}$, performed with *cdc25-22* synchronized cell cultures and telomeric DNA probe. (**E**) % septated cells were measured to monitor cell cycle progression of *cdc25-22* synchronized cell cultures for $Trt1^{TERT}$ ChIP assays. Error bars correspond to SEM.

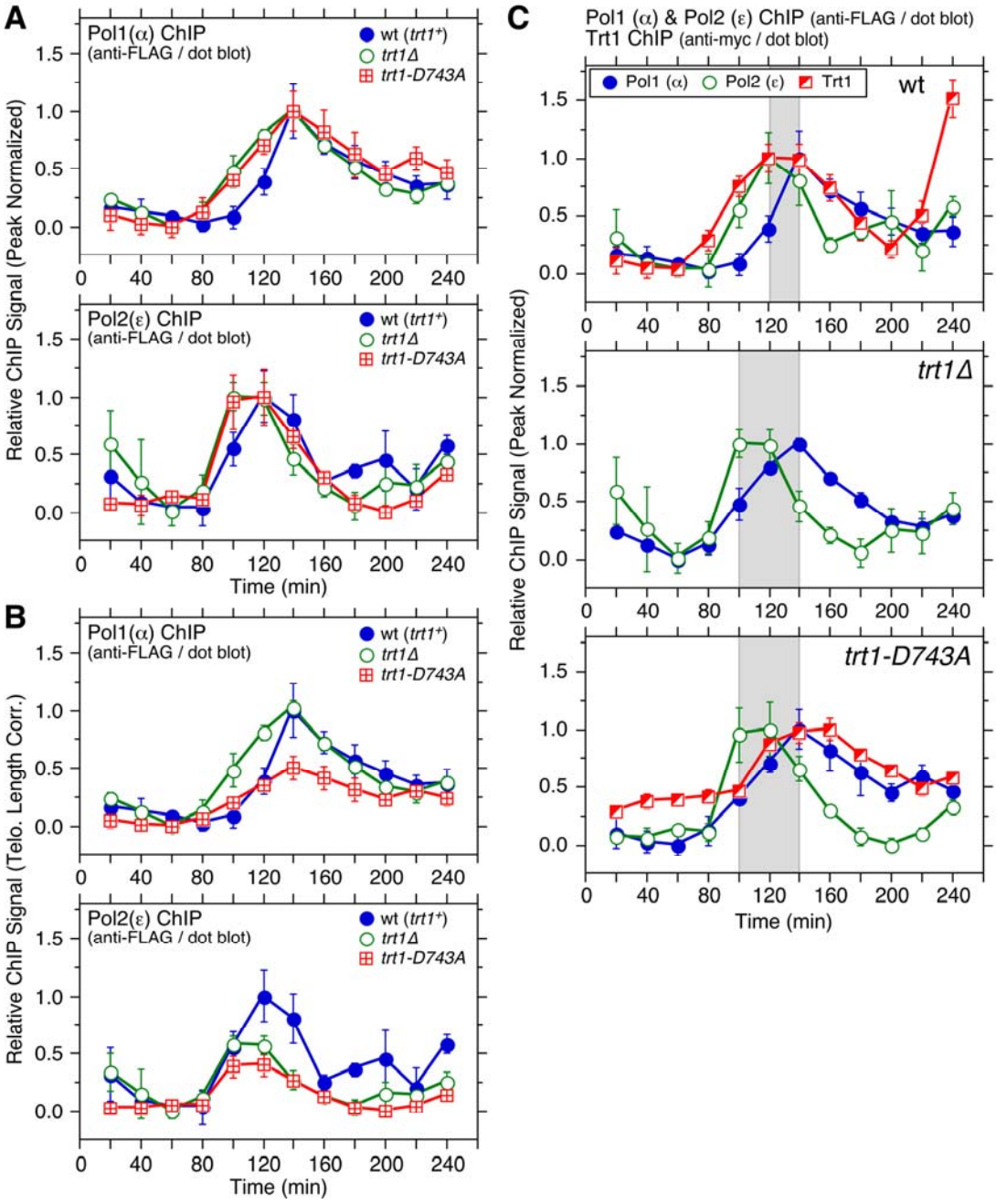
A
Pol1(α) ChIP
(anti-FLAG / dot blot)
wt (trt1+)
trt1Δ
trt1-D743A
Pol2(ε) ChIP
(anti-FLAG / dot blot)
Relative ChIP Signal (Peak Normalized)
Time (min)
B
Pol1(α) ChIP
(anti-FLAG / dot blot)
Pol2(ε) ChIP
(anti-FLAG / dot blot)
Relative ChIP Signal (Telo. Length Corr.)
Time (min)
C
Pol1 (α) & Pol2 (ε) ChIP (anti-FLAG / dot blot)
Trt1 ChIP (anti-myc / dot blot)
Pol1 (α)
Pol2 (ε)
Trt1
wt
trt1Δ
trt1-D743A
Relative ChIP Signal (Peak Normalized)
Time (min)

Figure 2.25 Cell cycle ChIP assays to monitor association of DNA polymerases with telomeres in *trt1Δ* and *trt1-D743A* cells.

(**A, B**) Peak normalized (**A**) or telomere length corrected (**B**) ChIP data for DNA polymerases. Raw ChIP data and % septated cells to monitor cell cycle progression are shown in Figure 2.26A-D. For peak normalized Pol1 (α), Student's t-test found p=0.06 at 100 min (94% confidence level) and p=0.03 at 120 min (97% confidence level) for wt vs. *trt1Δ* cells, and p=0.02 at 100 min (98% confidence level) and p=0.05 at 120 min (95% confidence level) for wt vs. *trt1-D743A* cells. For peak normalized Pol2 (ε), Student's t-test found p=0.07 at 100 min (93% confidence level) for wt vs. *trt1Δ* cells, and p=0.21 at 100 min (79% confidence level) for wt vs. *trt1-D743A* cells. For telomere length corrected Pol1 (α), statistically significant differences were found at 120 ($p=4.1x10^{-4}$), 140 ($p=5.3x10^{-3}$) and 160 min ($4.5x10^{-2}$) for *trt1Δ* vs. *trt1-D743A* cells. Anti-FLAG western blot analysis indicated comparable expression levels in different genetic backgrounds (Figure 2.26F). (**C**) Comparison of peak normalized ChIP data for $Trt1^{TERT}$ and DNA polymerases in *wt*, *trt1Δ*, and *trt1-D743A* cells. (Data for wt is identical to Figure 2.5D, but shown again as a reference.) Statistically significant differences ($p<0.04$) in telomere binding between Pol1 (α) and Pol2 (ε) were found at 100 min and 140-180 min for *trt1Δ* cells, and at 100, 200 and 220 min for *trt1-D743A* cells. Error bars correspond to SEM.

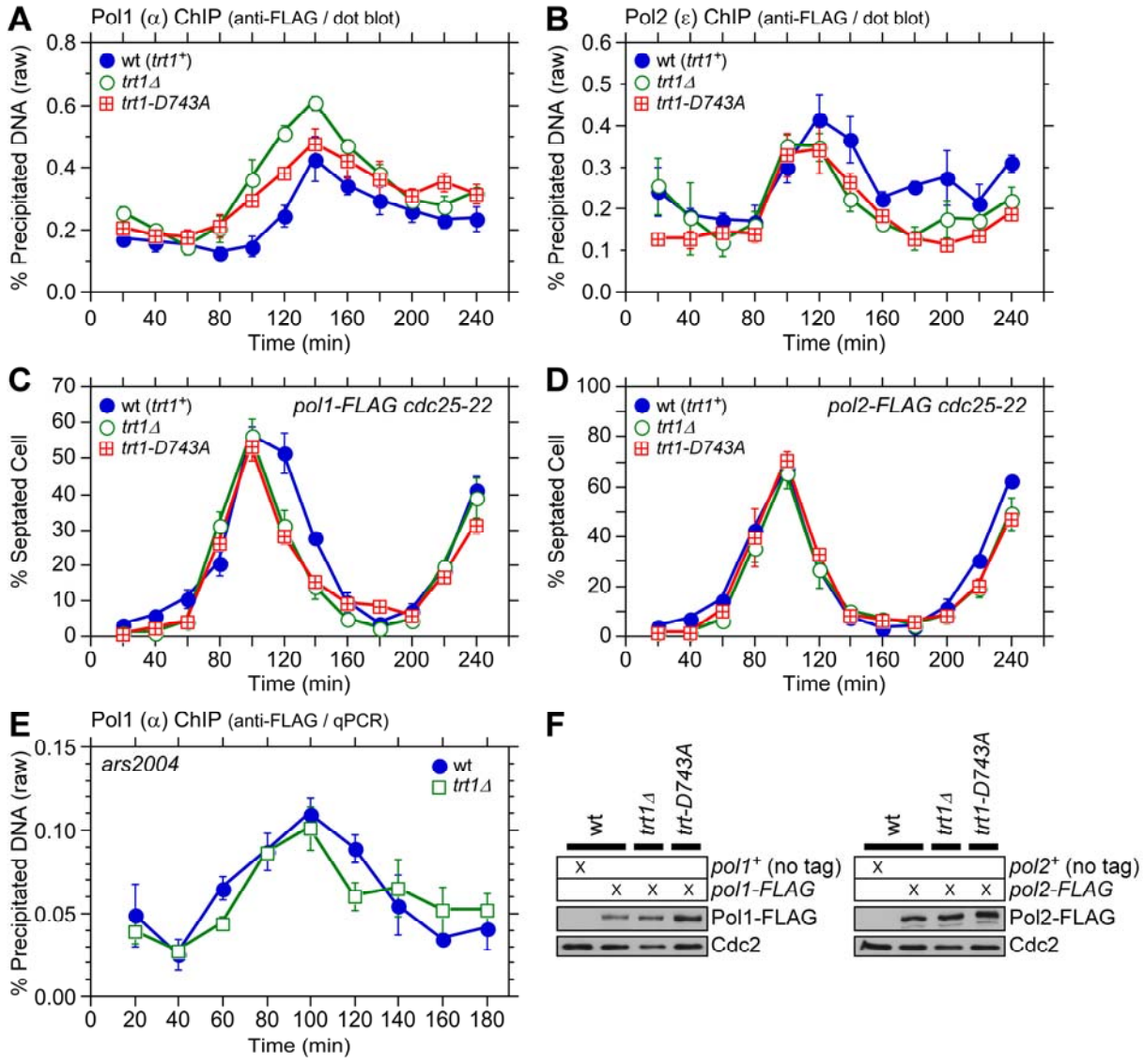

Figure 2.26 Cell cycle ChIP assays for DNA polymerases in *trt1* mutants.
(**A**, **B**) Raw data of dot blot-based cell cycle ChIP assays for Pol1 (α) (**A**) and Pol2 (ε) (**B**), performed with *cdc25-22* synchronized cell cultures and telomeric DNA probe. (**C**, **D**) % septated cells were measured to monitor cell cycle progression of *cdc25-22* synchronized cell cultures for Pol1 (α) (**C**) and Pol2 (ε) (**D**) ChIP assays. (**E**) Pol1 (α) showed similar timing of recruitment to *ars2004* in wt and *trt1Δ* cells. Error bars correspond to SEM. (**F**) Anti-FLAG western blot analysis indicated comparable expression levels in different genetic backgrounds for both Pol1 and Pol2. Cdc2 western blot served as a loading control.

to *trt1Δ* cells, suggesting that the presence of catalytically inactive Trt1^{TERT} may interfere with efficient recruitment of Polα (Figure 2.25B). My data also indicated that Polε still arrives at telomeres significantly earlier than Polα in *trt1Δ* or *trt1-D743A* cells (Figure 2.25C), suggesting that telomerase-dependent telomere extension cannot solely be responsible for the differential arrival of Polε and Polα at telomeres.

By examining the temporal telomere association patterns of DNA polymerases in *rap1Δ trt1Δ* cells, I attempted to investigate if the delay of Polα arrival at telomeres in *rap1Δ* cells (Figure 2.5C-D) is dependent on telomerase. To our surprise, *rap1Δ trt1Δ* cells showed very little cell cycle-regulated Polα recruitment to telomeres (Figure 2.27A), suggesting that Trt1^{TERT} and Rap1 might play redundant roles in coordinating the lagging strand DNA synthesis at telomeres. However, since cells carrying Pol1-FLAG progressed substantially faster through the cell cycle in *trt1Δ rap1Δ* than wt cells (Figure 2.28D), epitope-tagging of Polα may have introduced unintended changes in telomere regulation that caused synergistic genetic interactions specifically in *rap1Δ trt1Δ* cells. In contrast, I did not see much change in the temporal association pattern of Polε or cell cycle progression between wt and *rap1Δ trt1Δ* for cells carrying Pol2-FLAG (Figures 2.27B and 2.28E).

Because studies in other organisms have implicated a connection between Polα and CST in telomere regulation (Casteel et al., 2009; Puglisi et al., 2008; Qi and Zakian, 2000) and cell cycle ChIP data revealed very similar timings of telomere association for Polα and Stn1 (Figure 2.21A), I next examined the cell cycle-regulated association of Stn1 in *rap1Δ trt1Δ* cells. Much like Polα, S phase-induced increase in telomere binding

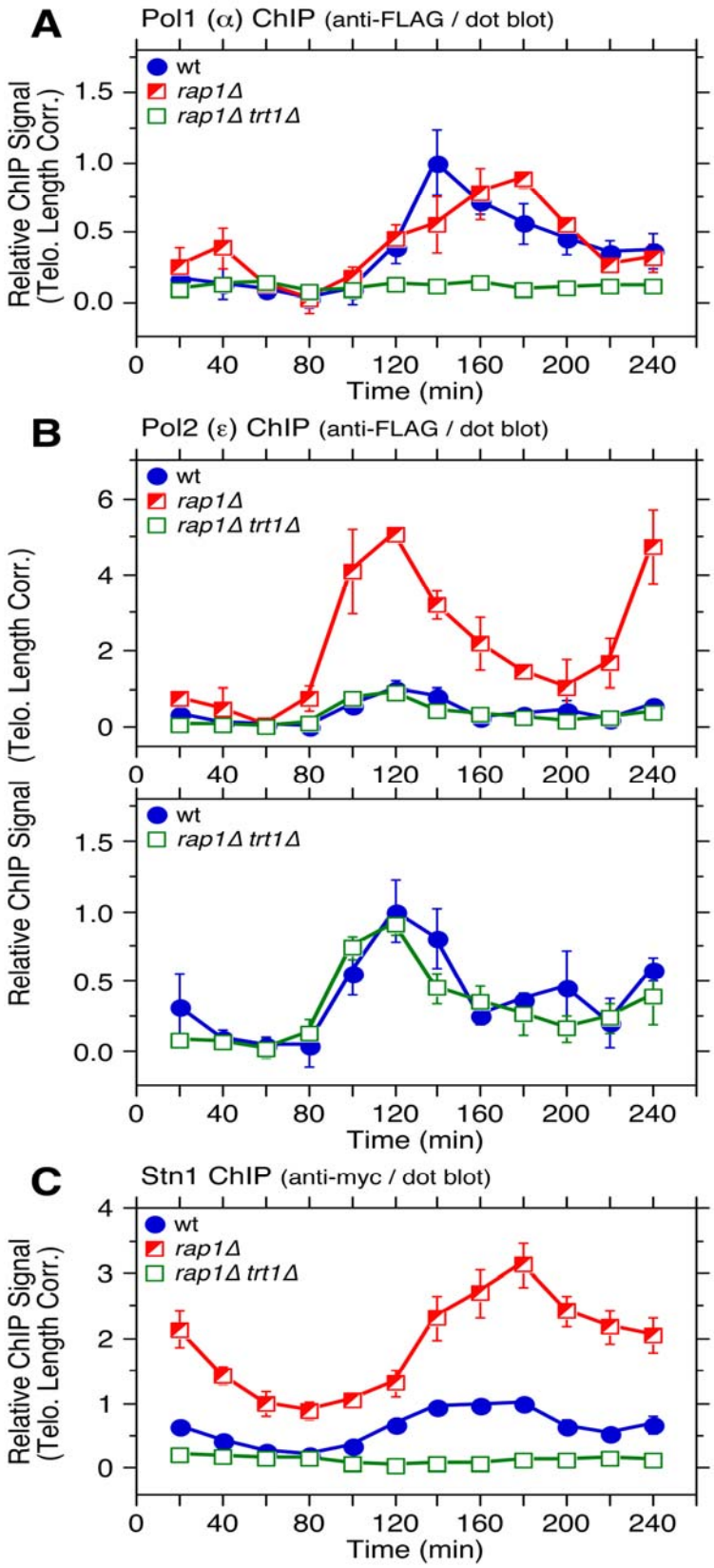
A
Pol1 (α) ChIP (anti-FLAG / dot blot)
wt
rap1Δ
rap1Δ trt1Δ
Relative ChIP Signal (Telo. Length Corr.)
Time (min)
B
Pol2 (ε) ChIP (anti-FLAG / dot blot)
wt
rap1Δ
rap1Δ trt1Δ
Relative ChIP Signal (Telo. Length Corr.)
Time (min)
C
Stn1 ChIP (anti-myc / dot blot)
wt
rap1Δ
rap1Δ trt1Δ
Relative ChIP Signal (Telo. Length Corr.)
Time (min)

Figure 2.27 Cell cycle ChIP assays to monitor association of DNA polymerases and Stn1 with telomeres in *rap1Δ trt1Δ* cells.

(**A-C**) Telomere length adjusted ChIP data for Pol1 (α) (**A**), Pol2 (ε) (**B**), and Stn1 (**C**). Error bars correspond to SEM. Raw ChIP data and % septated cells to monitor cell cycle progression are shown in Figure 2.28A-F. Anti-myc and anti-FLAG western blot analysis indicated comparable expression levels in different genetic backgrounds (Figure 2.28G).

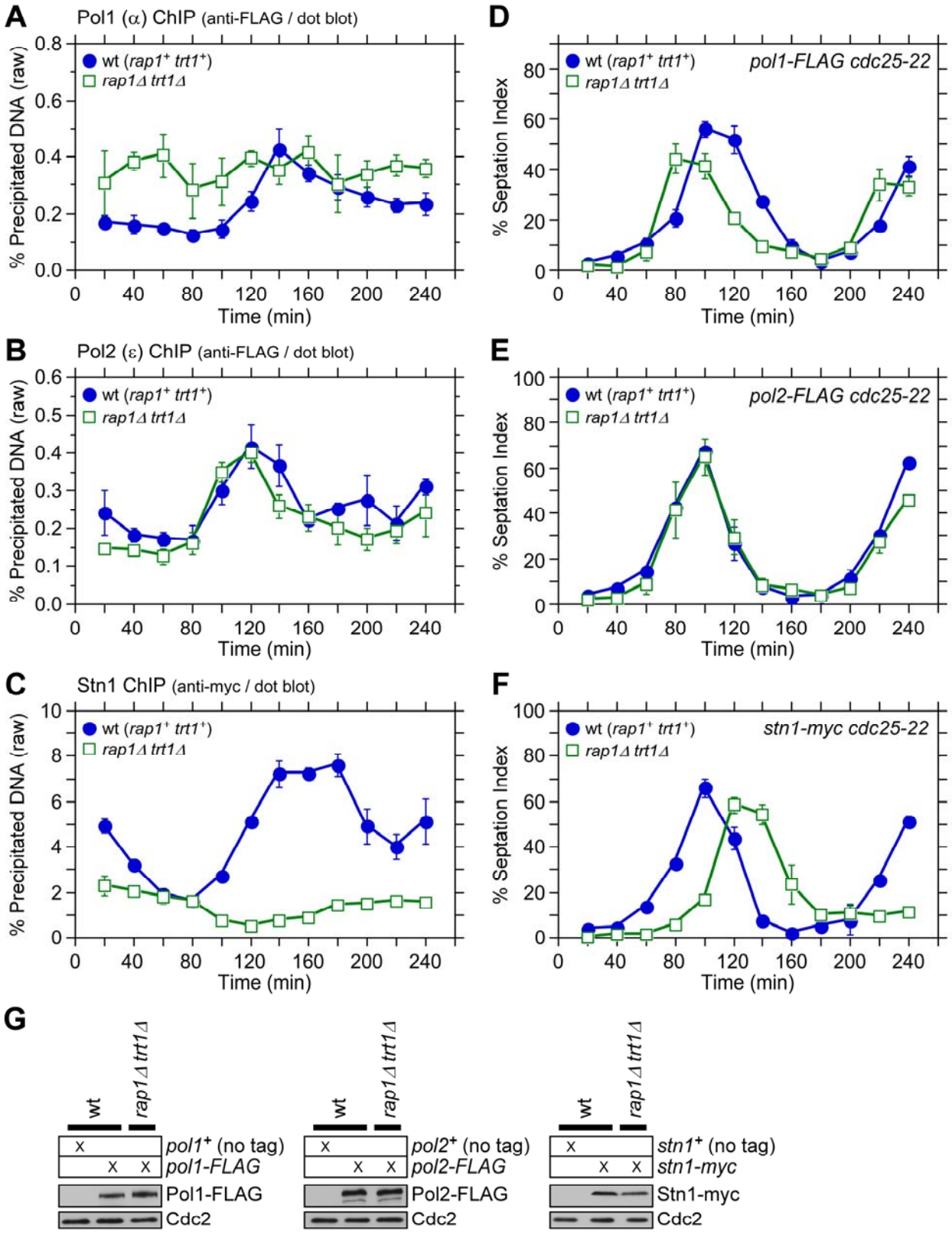
A
Pol1 (α) ChIP (anti-FLAG / dot blot)
% Precipitated DNA (raw)
wt (rap1+ trt1+)
rap1Δ trt1Δ
Time (min)
B
Pol2 (ε) ChIP (anti-FLAG / dot blot)
% Precipitated DNA (raw)
wt (rap1+ trt1+)
rap1Δ trt1Δ
Time (min)
C
Stn1 ChIP (anti-myc / dot blot)
% Precipitated DNA (raw)
wt (rap1+ trt1+)
rap1Δ trt1Δ
Time (min)
D
% Septation Index
wt (rap1+ trt1+)
rap1Δ trt1Δ
pol1-FLAG cdc25-22
Time (min)
E
% Septation Index
wt (rap1+ trt1+)
rap1Δ trt1Δ
pol2-FLAG cdc25-22
Time (min)
F
% Septation Index
wt (rap1+ trt1+)
rap1Δ trt1Δ
stn1-myc cdc25-22
Time (min)
G
wt
rap1Δ trt1Δ
pol1+ (no tag)
pol1-FLAG
Pol1-FLAG
Cdc2
pol2+ (no tag)
pol2-FLAG
Pol2-FLAG
Cdc2
stn1+ (no tag)
stn1-myc
Stn1-myc
Cdc2

Figure 2.28 Cell cycle ChIP assays for DNA polymerases and Stn1 in *rap1Δ trt1Δ* cells.

(**A**-**C**) Raw data of dot blot-based cell cycle ChIP assays for Pol1 (α) (**A**), Pol2 (ε) (**B**) and Stn1 (**C**), performed with *cdc25-22* synchronized cell cultures and telomeric DNA probe. (**D**-**F**) % septated cells were measured to monitor cell cycle progression of *cdc25-22* synchronized cell cultures for Pol1 (D), Pol2 (E) and Stn1 (F) ChIP assays. Error bars correspond to SEM. (**G**) Anti-FLAG (Pol1 and Pol2) and anti-myc (Stn1) western blot analyses indicated comparable expression levels in different genetic backgrounds for both Pol1 (α) and Pol2 (ε). Cdc2 western blot served as a loading control.

of Stn1 was abolished in *rap1Δ trt1Δ* cells (Figure 2.27C). However, I also noticed that Stn1-myc cells progressed through cell cycle slower in *rap1Δ trt1Δ* (Figure 2.28F). Thus, epitope-tagging of Stn1 may have elicited unexplained additional telomere defects in *rap1Δ trt1Δ* cells. In any case, it was striking to find loss of cell cycle-regulated binding for both Polα and Stn1 without affecting Polε association in *rap1Δ trt1Δ* cells, and it might indicate that Rap1 and Trt1 play unexpected redundant roles in maintaining proper cell cycle-regulated localization of both Polα and Stn1-Ten1 to telomeres. It is worth noting that a recent study has found that inhibition of telomerase leads to reduced recruitment of Stn1 to telomeres in late S/G_2-phase in mammalian cells, suggesting that mammalian telomerase also contributes to efficient recruitment of the CST complex to telomeres (Chen et al., 2012).

2.3 Discussion

A static “shelterin” model (de Lange, 2005) has provided a useful framework to understand how various telomere bound factors might be organized together to regulate telomerase action and telomere protection. However, since telomere maintenance regulation is coupled to cell cycle-regulated changes in telomere composition, especially in response to replication of telomeric DNA (Gilson and Geli, 2007; Verdun and Karlseder, 2007), a new model of telomere regulation that takes cell cycle-regulated changes at telomeres into account must be developed.

In fact, since current and previous cell cycle ChIP analyses (Moser et al., 2009a) have shown that individual subunits of shelterin show distinct cell cycle-regulated dynamic telomere association patterns, it is likely that the commonly drawn “closed” configuration of the shelterin complex (Miyoshi et al., 2008) (Figure 2.1G) that fully connects Taz1 to Pot1 via linker proteins Rap1 and Poz1 may never exist, or exist only in a very limited time window during cell cycle. It should also be noted that recent florescence microscopy analysis (Chen et al., 2011) and my new ChIP data (Figure 2.1C) indicate that Rap1 can still be localized to telomeres independently of both Poz1 and Taz1, contrary to a commonly held notion that fission yeast Rap1 recruitment is entirely dependent on Taz1 (Kanoh and Ishikawa, 2001; Miyoshi et al., 2008).

As a first step toward developing a more dynamic telomere regulation model, I determined detailed cell cycle-regulated telomere association patterns for various factors implicated in telomere regulation in fission yeast. Based on results from current and previous studies, I will propose and discuss a new and more dynamic model of

telomere length regulation in fission yeast (Figure 2.29), which hopefully will serve as a useful framework to guide future investigations.

2.3.1 Regulation of replicative DNA polymerases at telomeres by shelterin and Stn1-Ten1

While previous studies have implicated the role of Taz1 and TRF1 in efficient replication of telomeric DNA (Miller et al., 2006; Sfeir et al., 2009), it was very little known how loss of Taz1/TRF1 affects replicative polymerases at telomeres. We found that loss of telomerase inhibitors (Poz1, Rap1 and Taz1) differentially affect leading (Polε) and lagging (Polα) strand DNA polymerases (Figure 2.5C). For *poz1Δ* and *rap1Δ* cells, the peak of Polα binding to telomeres was significantly delayed without affecting Polε, suggesting that Poz1 and Rap1 primarily affect the timely recruitment of the lagging strand DNA polymerase. Consistent with previous studies that observed more severe defects in telomere replication in *taz1Δ* than *rap1Δ* cells (Dehe et al., 2012; Miller and Cooper, 2003; Miller et al., 2005), Polα binding to telomeres was severely deregulated in *taz1Δ* cells. In addition, loss of Taz1 (but not Rap1 or Poz1) caused earlier recruitment of Polε to telomeres, consistent with recent findings that Taz1 and Taz1-interacting protein Rif1 enforce late S-phase replication of telomeres in fission yeast (Hayano et al., 2012; Tazumi et al., 2012). Intriguingly, telomerase deficient cells (*trt1Δ* or *trt1-D743A*), which carry shorter telomeres and thus can accommodate less Taz1, also showed slightly earlier recruitment of Polε to telomeres than wt cells, consistent with earlier replication of telomeres (Figure 2.25).

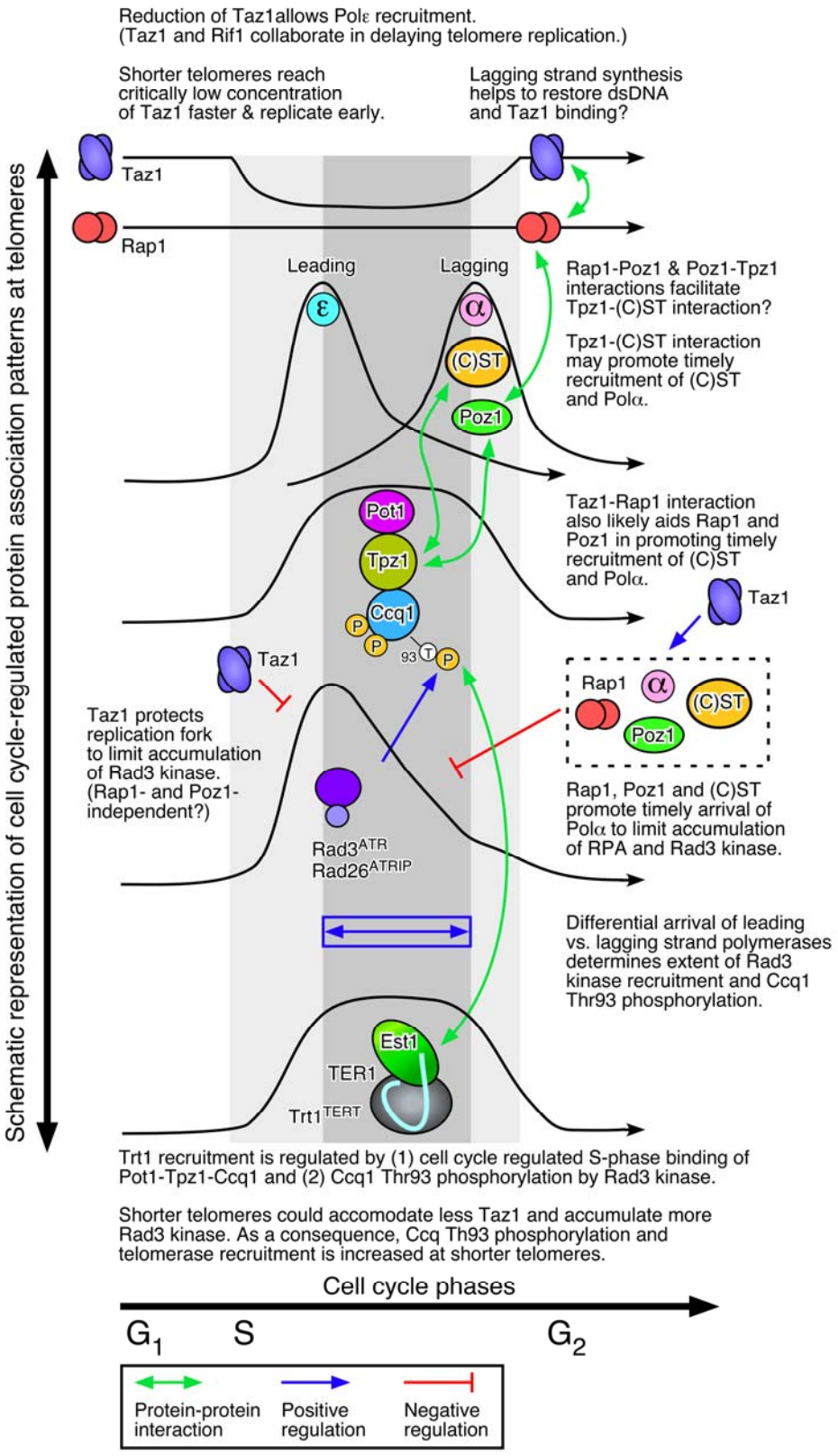

Figure 2.29 A working model of fission yeast telomere length control.

Taken together, I thus propose that (1) Taz1, likely in collaboration with Rif1 but independently of Poz1 and Rap1, enforces late S-phase replication of telomeres, and as a consequence, (2) shorter telomeres in fission yeast are replicated earlier (Figure 2.29). Previously, our laboratory have found that Taz1 binding is reduced by ~2-fold during S-phase (Moser et al., 2009a). Therefore, I speculate that shorter telomeres may be able to reduce Taz1 (and Rif1) density faster to the level compatible with replication, and as a consequence, replicate earlier in S-phase than longer telomeres.

Interestingly, budding yeast cells also replicate shorter telomeres earlier (Bianchi and Shore, 2007a), suggesting that early replication of short telomeres may be evolutionarily conserved. Moreover, even though replication timing of mammalian cells appears to be not strictly dependent on telomere length (Arnoult et al., 2010), TRF1 binding to telomeres is also reduced during S-phase (Verdun et al., 2005) and Rif1, like fission yeast Rif1, contributes to genome-wide regulation of replication timing (Cornacchia et al., 2012; Yamazaki et al., 2012b). It is thus possible that TRF1 might also collaborate with Rif1 in regulating replication timing at telomeres in mammalian cells.

Epistasis analysis of telomere length by Southern blot indicated that Taz1 carries out both Poz1/Rap1-independent and -dependent roles in regulation of telomere length maintenance (Figure 2.1B). Accordingly, I further suggest that Taz1, in collaboration with Rap1 and Poz1, also contributes to replication fork integrity at telomeres by promoting timely and cell cycle-regulated recruitments of the lagging strand DNA polymerases (Polα and Polδ) (Figure 2.29). Completion of the C-strand fill-in synthesis

by lagging strand DNA polymerases would then restore dsDNA and Taz1 binding in late S/G_2 phase, prior to the initiation of mitosis.

Although Rap1 binding to telomeres is not entirely dependent on Taz1, loss of Taz1 significantly reduces Rap1 binding at telomeres (Figure 2.1C), and disruption of the Taz1-Rap1 interaction causes massive elongation of telomeres, much like *rap1Δ* (Chen et al., 2011). Thus, it is easy to imagine how Taz1, through direct interaction with Rap1, would affect Rap1-dependent promotion of lagging strand synthesis at telomeres. Previously identified Rap1-Poz1 and Poz1-Tpz1 interactions (Miyoshi et al., 2008) would also likely be important in regulating the timely recruitments of lagging strand DNA polymerases (Figure 2.1G and Figure 2.29).

In addition, a newly identified interaction between Tpz1 and Stn1-Ten1 (Figure 2.14C) could play a critical role in allowing Rap1 and Poz1 to enforce the timely recruitment of Polα to telomeres, since my ChIP data also implicated a close functional relationship among Poz1, Stn1 and Polα in telomere regulation (Figures 2.21A and 2.27). My findings described in this Chapter are also likely relevant to understand mammalian telomere regulation, since previous studies have found that mammalian TPP1 also interacts with CST (Chen et al., 2012; Wan et al., 2009), and CST collaborates with Polα in regulating C-strand fill-in synthesis at telomeres (Nakaoka et al., 2012; Wang et al., 2012; Wu et al., 2012).

2.3.2 Regulation of Rad3^{ATR} kinase recruitment, Ccq1 Thr93 phosphorylation and telomerase recruitment by shelterin and CST

Since Rad3^{ATR}/Tel1^{ATM}-dependent phosphorylation of Ccq1 at Thr93 promotes Ccq1-Est1 interaction and telomerase recruitment, the mechanism that modulates Thr93 phosphorylation is critical for proper maintenance of telomeres in fission yeast (Moser et al., 2011; Yamazaki et al., 2012a). Poz1, Rap1 and Taz1 negatively regulate Ccq1 Thr93 phosphorylation and telomerase recruitment (Moser et al., 2011), but the underlying mechanism by which these factors limit Thr93 phosphorylation remained unclear.

ChIP data indicated that loss of Poz1, Rap1 and Taz1 causes large increases in telomere associations of RPA and Rad3^{ATR}-Rad26^{ATRIP}, but not Tel1^{ATM} kinase (Figures 2.8, 2.9A and 2.12). Closely matching the extent of increase in Ccq1 Thr93 phosphorylation and Trt1^{TERT} binding (Moser et al., 2009b), RPA and Rad3^{ATR}-Rad26^{ATRIP} showed progressive increase in telomere binding in the order of *poz1Δ*, *rap1Δ* and *taz1Δ* cells, especially during S-phase. Therefore, I suggest that Poz1, Rap1 and Taz1 negatively regulate Rad3^{ATR}-Rad26^{ATRIP} accumulation and Ccq1 Thr93 phosphorylation by controlling the differential arrival of leading and lagging strand polymerases at telomeres (Figure 2.29). Based on cell cycle analysis, I further suggest that S-phase specific Trt1^{TERT} recruitment to telomeres is controlled by both (1) cell cycle-regulated binding of Pot1-Tpz1-Ccq1 and (2) Ccq1 Thr93 phosphorylation. Since Thr93 phosphorylation is quickly lost in wt cells soon after dissociation of Rad26^{ATRIP} from telomeres, it is likely that an unidentified phosphatase is involved in rapidly reducing Thr93 phosphorylation to promote the timely dissociation of Trt1^{TERT} from

telomeres. In *poz1Δ*, *rap1Δ* and *taz1Δ* cells, increased accumulation of Rad3^{ATR} kinase results in constitutive Thr93 phosphorylation, hence persistent and high level binding of Trt1^{TERT} in G_2 phase. I have also shown that catalytically inactive Trt1-D743A has increased and constitutive binding to telomeres (Figure 2.23), consistent with the notion that telomerase is preferentially recruited to short telomeres.

The notion that fission yeast utilizes the differential arrival of leading and lagging strand polymerases to control Rad3^{ATR}-dependent Ccq1 Thr93 phosphorylation and Trt1^{TERT} recruitment can explain why mutations in Polε lead to shorter telomeres while mutations in Polα and Polδ lead to longer telomeres (Dahlen et al., 2003). Since mutations in Polε would likely delay leading but not lagging strand synthesis, cells would have less ssDNA accumulation at telomeres, and as a result, have fewer Rad3^{ATR} and Trt1^{TERT} recruitments to telomeres. Conversely, mutations in Polα and Polδ would lead to increased ssDNA, and more robust recruitments of Rad3^{ATR} and telomerase. Effects on differential strand synthesis at telomeres could also explain why *rif1Δ rap1Δ* cells have longer telomeres than *rap1Δ* cells (Kanoh and Ishikawa, 2001), since the loss of Rif1 is expected to advance the arrival of Polε (Hayano et al., 2012), further expanding the differential strand synthesis over *rap1Δ* cells. Differences in Polα binding (Figure 2.5C) could also explain why *rap1Δ* cells retain S phase-specific G-tail elongation while *taz1Δ* cells show elongated G-tails throughout the cell cycle (Dehe et al., 2012).

Even though budding yeast cells have significantly diverged in telomere protein composition from fission yeast or mammalian cells (Palm and de Lange, 2008), mutations in Polε also cause telomere shortening while mutations in Polα cause telomere lengthening in budding yeast (Adams-Martin et al., 2000; Ohya et al., 2002).

Thus, differential regulation of leading and lagging strand synthesis could have evolutionarily conserved roles in telomerase regulation. Studies in mammalian cells have also found that lagging strand synthesis is significantly delayed (Zhao et al., 2009) and regulated by CST (Wang et al., 2012; Wu et al., 2012). Thus, I believe that findings described in this Chapter are also relevant in understanding how shelterin and CST regulate telomere maintenance in mammalian cells.

2.4 Materials and Methods

2.4.1 Yeast strains, plasmids and primers used in this study

Fission yeast strains used in this study were constructed by standard techniques (Alfa et al., 1993), and they are listed in Table 2.2. For *taz1Δ::ura4*$^+$, *taz1Δ::LEU2*, *rap1Δ::ura4*$^+$, *poz1Δ::natMX6* and *trt1Δ::his3*$^+$, original deletion strains were described previously (Cooper et al., 1997; Kanoh and Ishikawa, 2001; Khair et al., 2009; Nakamura et al., 1997; Nakamura et al., 2002). For *rad3-kdΔ::kanMX4, ura4*$^+$ marker was swapped with kanMX4 by (1) PCR amplifying a *kanMX4* module from a pFA6a-kanMX4 plasmid (Wach et al., 1994) using DNA primers UraKan-T1 and UraKan-B1 (Table 2.3), and (2) transforming *rad3-kdΔ::ura4*$^+$ strain (Bentley et al., 1996; Subramanian and Nakamura, 2010) with the PCR product. For *rap1-myc*, *trt1-myc*, *pol1-FLAG*, *pol2-FLAG*, *myc-rad3*, *myc-rad26*, *myc-tel1*, *rad11-FLAG*, *ccq1-myc*, *ccq1-FLAG*, *tpz1-myc*, *poz1-myc* and *stn1-myc*, original tagged strains were described previously (Moser et al., 2009a; Moser et al., 2009b; Noguchi et al., 2004; Subramanian and Nakamura, 2010; Tomita and Cooper, 2008; Webb and Zakian, 2008). A modified

fission yeast strain with *leu1-32::[hENT1 leu1$^+$]* and *his3-D1 his7-366::[hsv-tk his7$^+$]* that can be used to efficiently incorporate BrdU has been described previously (Hodson et al., 2003). Strains that carry *trt1-D743A::LEU2* allele at endogenous locus were previously described (Subramanian et al., 2008). A heterozygous diploid strain carrying unmarked *trt1-D743A* or *trt1$^+$* was transformed with a PCR product (amplified from a *trt1-G8-13myc::kanMX6* strain using DNA primers trt1-B29 and trt1-T30) to generate cells carrying *trt1-D743A-myc*.

Yeast two/three hybrid assays were performed by mating *Saccharomyces cerevisiae MAT*a (Y2HGold: *MAT*a *trp1-901 leu2-3,-112 ura3-52 his3-200 LYS2::GAL1(UAS)-GAL1(TATA)-HIS3 GAL2(UAS)-GAL2(TATA)-ADE2 gal4Δ gal80Δ URA3::MEL1(UAS)-MEL1(TATA)-AUR1-C MEL1*) strains harboring GAL4-DBD (DNA-binding domain) plasmids with *MAT*α (Y187: *MAT*α *trp1-901 leu2-3,-112 ura3-52 his3-200 ade2-101 gal4Δ gal80Δ met$^-$ URA3::GAL1(UAS)-GAL1(TATA)-LacZ MEL1*) strains harboring GAL4-AD (activation domain) plasmids, as described in the MATCHMAKER system manual (Clontech). Plasmids used in yeast two/three hybrid assays are listed in Table 2.4.

2.4.2 Southern blot, western blot, and ChIP analyses

Pulsed-field gel electrophoresis to analyze telomere fusions in G_1 was performed as previously described (Ferreira and Cooper, 2001; Nakamura et al., 1998). Telomere probe used in Southern blot and dot blot-based ChIP was generated as previously described (Nakamura et al., 1997), and rDNA probe used to determine telomere length correction factor for dot blot-based ChIP analysis was generated using PCR with

primers listed in Table 2.3 (Hayashi et al., 2007; Kanoh et al., 2005). Primers used in real-time PCR-based ChIP assays are also listed in Table 2.3. ChIP samples were analyzed with quantitative real-time PCR or dot blot with telomeric probe as previously described (Moser et al., 2011; Moser et al., 2009a). BrdU incorporation was monitored as previously described (Moser et al., 2009a; Sivakumar et al., 2004). Error bars in all plots represent standard error of the mean (SEM) from multiple independent experiments.

For western blot and ChIP assays, either monoclonal anti-myc (9B11, Cell Signaling) or monoclonal anti-FLAG (M2-F1804, Sigma) antibodies were used. Anti-Cdc2 antibody (y100.4, Abcam) was used in western blot analysis as a loading control. Ccq1 Thr93 phosphorylation was monitored using phospho-(Ser/Thr) ATM/ATR substrate antibody (2851, Cell Signaling) as previously described (Moser et al., 2011). While not specifically raised against a Ccq1 Thr93 phosphopeptide, our previous analysis indicated that the phospho-(Ser/Thr) ATM/ATR substrate antibody can specifically detect a Ccq1 Thr93 phosphopeptide, and detect a band corresponding to immunoprecipitated Ccq1 that is eliminated in *ccq1-T93A* mutant in western blot analysis (Moser et al., 2011). Thus, although I cannot completely eliminate the possibility that this antibody recognizes phosphorylation on other site(s) that might be affected by *ccq1-T93A* mutation, for sake of simplicity, I denoted the signal detected by this antibody as Ccq1 Thr93 phosphorylation in the text.

2.4.3 Establishment of telomere length correction factors

Correction factors for telomere length were established by measuring the hybridization signal intensity of telomere versus rDNA repeats (telomere/rDNA) for *poz1Δ*, *rap1Δ* and *taz1Δ* cells compared to wt cells (Figure 2.2A and Table 2.1), using NaOH denatured genomic DNA samples spotted on Nylon membrane by dot blot apparatus. “Telomere length corrected” ChIP values were then calculated by multiplying the background subtracted % precipitated DNA values (raw % precipitated DNA – no tag control % precipitated DNA) with the correction factors, and normalizing them to wt. For telomere length corrected cell cycle ChIP, values were normalized to the peak binding level of wt cells in late S/G_2-phase. While it may not be a perfect solution, the use of correction factors provided better estimates of changes in protein binding to chromosome ends for cells carrying significantly longer telomeres than wt cells. For telomere length corrected ChIP data, SEM of telomere length corrected ChIP (SEM_Q) was calculated as $SEM_Q = AB\sqrt{(SEM_A/A)^2 + (SEM_B/B)^2}$ (A=background subtracted ChIP; SEM_A=SEM of background subtracted ChIP; B=telomere correction factor; SEM_B=SEM of telomere correction factor).

2.4.4 Statistical Analysis

In order to determine the statistical significance of our data, two-tailed Student's t-tests were performed, and p-values ≤0.05 were considered as statistically significant differences.

Table 2.1 Telomere length correction factors (telomere/rDNA) for dot blot-based ChIP

Tagged protein	Genetic background	Correction factor[a]	Tagged protein	Genetic background	Correction factor[a]
Trt1-myc	wt	1.000±0.011 (n=23)	Rad11-FLAG	wt	1.000±0.026 (n=17)
	poz1Δ	7.523±0.235 (n=22)		*poz1Δ*	2.950±0.063 (n=17)
	rap1Δ	7.576±0.133 (n=23)		*rap1Δ*	6.281±0.152 (n=17)
	taz1Δ	6.507±0.085 (n=22)		*taz1Δ*	4.407±0.093 (n=15)
	trt1-D743A	1.277±0.158 (n=9)			
	trt1-D743A rap1Δ	2.409±0.190 (n=7)			
Pol1-FLAG	wt	1.000±0.013 (n=18)	Tpz1-myc	wt	1.000±0.014 (n=18)
	poz1Δ	2.474±0.044 (n=18)		*poz1Δ*	5.671±0.107 (n=18)
	rap1Δ	1.802±0.032 (n=18)		*rap1Δ*	6.229±0.154 (n=18)
	taz1Δ	1.001±0.027 (n=18)		*taz1Δ*	5.420±0.194 (n=18)
	trt1Δ	0.669±0.035 (n=9)			
	trt1-D743A	0.508±0.049 (n=9)			
	rap1Δ trt1Δ	0.146±0.009 (n=9)			
Pol2-FLAG	wt	1.000±0.020 (n=18)	Ccq1-myc	wt	1.000±0.020 (n=36)
	poz1Δ	5.389±0.146 (n=18)		*poz1Δ*	3.544±0.140 (n=33)
	rap1Δ	6.362±0.151 (n=15)		*rap1Δ*	5.061±0.216 (n=35)
	taz1Δ	5.008±0.087 (n=15)		*taz1Δ*	4.975±0.258 (n=35)
	trt1Δ	0.632±0.015 (n=9)			
	trt1-D743A	0.450±0.014 (n=9)			
	rap1Δ trt1Δ	0.832±0.016 (n=9)			
myc-Rad3	wt	1.000±0.019 (n=9)	Poz1-myc	wt	1.000±0.025 (n=26)
	poz1Δ	3.730±0.097 (n=9)		*rap1Δ*	4.773±0.311 (n=24)
	rap1Δ	4.790±0.114 (n=9)		*taz1Δ*	3.892±0.282 (n=27)
	taz1Δ	2.750±0.101 (n=9)			
myc-Rad26	wt	1.000±0.017 (n=18)	Stn1-myc	wt	1.000±0.021 (n=25)
	poz1Δ	6.842±0.132 (n=18)		*poz1Δ*	3.624±0.237 (n=27)
	rap1Δ	9.516±0.165 (n=18)		*rap1Δ*	5.416±0.364 (n=27)
	taz1Δ	6.105±0.124 (n=16)		*taz1Δ*	4.497±0.260 (n=26)
				rap1Δ trt1Δ	0.666±0.013 (n=9)

[a]Mean ± standard error of the mean. Values are normalized to wt cells with indicated tagged proteins. Number of samples used to determine correction factors are also indicated as (n=#).

Table 2.2 Fission yeast strains used in this study

Figure		Strain	Full Genotype[a]
2.1A-F	wt	TN2411	*h⁻ his3-D1*
	poz1Δ	YTC8489	*h⁻ ade6-M216 his3-D1 poz1Δ::natMX6*
	rap1Δ	YTC9370	*h⁺ his3-D1 rap1Δ::ura4⁺*
	taz1Δ	YTC9369	*h⁺ ade6-M216 his3-D1 taz1Δ::ura4⁺*
	poz1Δ rap1Δ	YTC9371	*h⁺ his3-D1 poz1Δ::natMX6 rap1Δ::ura4⁺*
	poz1Δ taz1Δ	YTC9372	*h⁺ ade6-M216 his3-D1 poz1Δ::natMX6 taz1Δ::ura4⁺*
	rap1Δ taz1Δ	YTC9373	*h⁺ ade6-M210 his3-D1 rap1Δ::ura4⁺ taz1Δ::LEU2*
	poz1Δ rap1Δ taz1Δ	YTC9374	*h⁺ his3-D1 poz1Δ::natMX6 rap1Δ::ura4⁺ taz1Δ::LEU2*
2.1C	*rap1⁺* (no tag)	TN2411	*h⁻ his3-D1*
	rap1-myc	YTC9493	*h⁺ ade6-M210 rap1⁺-7myc::kanMX*
	rap1-myc poz1Δ	YTC9929	*h⁻ ade6-M210 his3-D1 rap1⁺-7myc::kanMX poz1Δ::natMX6*
	rap1-myc taz1Δ	YTC9934	*h⁺ ade6-M210 rap1⁺-7myc::kanMX taz1Δ::ura4⁺*
	rap1-myc poz1Δ taz1Δ	YTC10060	*h⁻ ade6-M210 his3-D1 rap1⁺-7myc::kanMX poz1Δ::natMX6 taz1Δ::ura4⁺*
2.1F	*trt1⁺* (no tag)	SS5264	*h⁻ his3-D1 cdc25-22*
	trt1-myc	TN7708	*h⁻ his3-D1 trt1⁺-G₈-13myc::kanMX6 cdc25-22*
	trt1-myc poz1Δ	YTC8558	*h⁻ his3-D1 trt1⁺-G₈-13myc::kanMX6 poz1Δ::natMX6 cdc25-22*
	trt1-myc rap1Δ	YTC8969	*h⁻ his3-D1 trt1⁺-G₈-13myc::kanMX6 rap1Δ::ura4⁺ cdc25-22*
	trt1-myc taz1Δ	TN8601	*h⁻ his3-D1 trt1⁺-G₈-13myc::kanMX6 taz1Δ::ura4⁺ cdc25-22*
	trt1-myc poz1Δ taz1Δ	YTC9404	*h⁻ his3-D1 trt1⁺-G₈-13myc::kanMX6 poz1Δ::natMX6 taz1Δ::ura4⁺ cdc25-22*
	trt1-myc rap1Δ taz1Δ	YTC9411	*h⁻ ade6-M210 his3-D1 trt1⁺-G₈-13myc::kanMX6 rap1Δ::ura4⁺ taz1Δ::LEU2 cdc25-22*
	trt1-myc poz1Δ rap1Δ	YTC9453	*h⁻ his3-D1 trt1⁺-G₈-13myc::kanMX6 poz1Δ::natMX6 rap1Δ::ura4⁺ cdc25-22*
	trt1-myc poz1Δ rap1Δ taz1Δ	YTC9452	*h⁻ his3-D1 trt1⁺-G₈-13myc::kanMX6 poz1Δ::natMX6 rap1Δ::ura4⁺ taz1Δ::LEU2 cdc25-22*
2.2, 2.5, 2.6, 2.7, 2.8C, 2.20, 2.21, 2.22, 2.25C	*trt1-myc*	TN7708	*h⁻ his3-D1 trt1⁺-G₈-13myc::kanMX6 cdc25-22*
	trt1-myc poz1Δ	YTC8558	*h⁻ his3-D1 trt1⁺-G₈-13myc::kanMX6 poz1Δ::natMX6 cdc25-22*
	trt1-myc rap1Δ	YTC8969	*h⁻ his3-D1 trt1⁺-G₈-13myc::kanMX6 rap1Δ::ura4⁺ cdc25-22*
	trt1-myc taz1Δ	TN8601	*h⁻ his3-D1 trt1⁺-G₈-13myc::kanMX6 taz1Δ::ura4⁺ cdc25-22*
	pol1-FLAG	TN4781	*h⁻ his3-D1 pol1⁺-5FLAG::kanMX cdc25-22*
	pol1-FLAG poz1Δ	YTC8705	*h⁻ his3-D1 pol1⁺-5FLAG::kanMX poz1Δ::natMX6 cdc25-22*
	pol1-FLAG rap1Δ	YTC9589	*h⁻ his3-D1 pol1⁺-5FLAG::kanMX rap1Δ::ura4⁺ cdc25-22*
	pol1-FLAG taz1Δ	YTC9375	*h⁻ his3-D1 pol1⁺-5FLAG::kanMX taz1Δ::ura4⁺ cdc25-22*
	pol2-FLAG	TN4782	*h⁺ ade6-M210 his3-D1 pol2⁺-5FLAG::kanMX cdc25-22*
	pol2-FLAG poz1Δ	YTC8693	*h⁻ ade6-M210 his3-D1 pol2⁺-5FLAG::kanMX poz1Δ::natMX6 cdc25-22*
	pol2-FLAG rap1Δ	YTC9423	*h⁻ ade6-M210 his3-D1 pol2⁺-5FLAG::kanMX rap1Δ::ura4⁺ cdc25-22*
	pol2-FLAG taz1Δ	YTC9280	*h⁻ ade6-M210 his3-D1 pol2⁺-5FLAG::kanMX taz1Δ::ura4⁺ cdc25-22*
	wt (no tag)	SS5264	*h⁻ his3-D1 cdc25-22*
	poz1Δ (no tag)	YTC8929	*h⁻ his3-D1 poz1Δ::natMX6 cdc25-22*
	rap1Δ (no tag)	YTC8938	*h⁺ his3-D1 rap1Δ::ura4⁺ cdc25-22*
	taz1Δ (no tag)	YTC8933	*h⁻ his3-D1 taz1Δ::ura4⁺ cdc25-22*
2.8, 2.13	*myc-rad26*	TN7840	*h⁻ his3-D1 9myc-rad26⁺::hphMX6 cdc25-22*
	myc-rad26 poz1Δ	YTC10349	*h⁻ his3-D1 9myc-rad26⁺::hphMX6 poz1Δ::natMX6 cdc25-22*
	myc-rad26 rap1Δ	YTC10338	*h⁻ his3-D1 9myc-rad26⁺::hphMX6 rap1Δ::ura4⁺ cdc25-22*
	myc-rad26 taz1Δ	YTC10420	*h⁺ his3-D1 9myc-rad26⁺::hphMX6 taz1Δ::ura4⁺ cdc25-22*
	rad11-FLAG	BAM5875	*h⁺ his3-D1 rad11⁺-5FLAG::kanMX cdc25-22*
	rad11-FLAG poz1Δ	YTC10334	*h⁺ his3-D1 rad11⁺-5FLAG::kanMX poz1Δ::natMX6 cdc25-22*
	rad11-FLAG rap1Δ	YTC10341	*h⁺ his3-D1 rad11⁺-5FLAG::kanMX rap1Δ::ura4⁺ cdc25-22*

	rad11-FLAG taz1Δ	YTC10319	*h⁻ his3-D1 rad11⁺-5FLAG::kanMX taz1Δ::ura4⁺ cdc25-22*
2.14A	*ccq1-FLAG*	TN6847	*h⁻ his3-D1 ccq1⁺-5FLAG::kanMX6 cdc25-22*
	ccq1-FLAG rap1Δ	YTC10947	*h⁻ ccq1⁺-5FLAG::kanMX6 rap1Δ::ura4⁺ cdc25-22*
	ccq1-FLAG taz1Δ	YTC10950	*h⁺ his3-D1 ccq1⁺-5FLAG::kanMX6 taz1Δ::ura4⁺ cdc25-22*
2.14B,	*ccq1-myc*	TN7456	*h⁻ his3-D1 ccq1⁺-13myc::kanMX6 cdc25-22*
2.15-2.18,	*ccq1-myc poz1Δ*	YTC8709	*h⁻ his3-D1 ccq1⁺-13myc::kanMX6 poz1Δ::natMX6 cdc25-22*
2.20-2.22	*ccq1-myc rap1Δ*	YTC9384	*h⁺ his3-D1 ccq1⁺-13myc::kanMX6 rap1Δ::ura4⁺ cdc25-22*
	ccq1-myc taz1Δ	YTC9292	*h⁻ his3-D1 ccq1⁺-13myc::kanMX6 taz1Δ::ura4⁺ cdc25-22*
	tpz1-myc	TN7467	*h⁻ his3-D1 tpz1⁺-13myc::kanMX6 cdc25-22*
	tpz1-myc poz1Δ	YTC9362	*h⁻ his3-D1 tpz1⁺-13myc::kanMX6 poz1Δ::natMX6 cdc25-22*
	tpz1-myc rap1Δ	YTC9307	*h⁻ his3-D1 tpz1⁺-13myc::kanMX6 rap1Δ::ura4⁺ cdc25-22*
	tpz1-myc taz1Δ	YTC9327	*h⁻ his3-D1 tpz1⁺-13myc::kanMX6 taz1Δ::ura4⁺ cdc25-22*
	poz1-myc	TN6843	*h⁻ his3-D1 poz1⁺-13myc::kanMX6 cdc25-22*
	poz1-myc rap1Δ	YTC9314	*h⁻ his3-D1 poz1⁺-13myc::kanMX6 rap1Δ::ura4⁺ cdc25-22*
	poz1-myc taz1Δ	YTC9285	*h⁻ his3-D1 poz1⁺-13myc::kanMX6 taz1Δ::ura4⁺ cdc25-22*
	stn1-myc	TN6886	*h⁻ his3-D1 stn1⁺-13myc::kanMX6 cdc25-22*
	stn1-myc poz1Δ	YTC8717	*h⁻ his3-D1 stn1⁺-13myc::kanMX6 poz1Δ::natMX6 cdc25-22*
	stn1-myc rap1Δ	YTC9299	*h⁻ his3-D1 stn1⁺-13myc::kanMX6 rap1Δ::ura4⁺ cdc25-22*
	stn1-myc taz1Δ	YTC9414	*h⁺ his3-D1 stn1⁺-13myc::kanMX6 taz1Δ::ura4⁺ cdc25-22*
2.23A,	*rad26⁺* (no tag)	TN2411	*h⁻ his3-D1*
2.24A	*myc-rad26*	LS7680	*h⁻ his3-D1 9myc-rad26⁺::hphMX6*
	myc-rad26 trt1Δ	YTC12785	*h⁻ ade6-M216 his3-D1 9myc-rad26⁺::hphMX6 trt1Δ::his3⁺*
2.23B-C,	*trt1⁺* (no tag)	SS5264	*h⁻ his3-D1 cdc25-22*
2.24,	*trt1-myc*	TN7708	*h⁻ his3-D1 trt1⁺-G₈-13myc::kanMX6 cdc25-22*
2.25C	*trt1-myc rap1Δ*	YTC8969	*h⁻ his3-D1 trt1⁺-G₈-13myc::kanMX6 rap1Δ::ura4⁺ cdc25-22*
	trt1-D743A-myc	YTC12787	*h⁻ ade6-M210 his3-D1 trt1-D743A-G₈-13myc::kanMX6 cdc25-22*
	trt1-D743A-myc rap1Δ	YTC12788	*h⁻ ade6-M210 his3-D1 trt1-D743A-G₈-13myc::kanMX6 rap1Δ::ura4⁺ cdc25-22*
2.25-2.26	*pol1-FLAG trt1⁺*	TN4781	*h⁻ his3-D1 pol1⁺-5FLAG::kanMX cdc25-22*
	pol1-FLAG trt1Δ	TN8388[b]	*h⁻ ade6-M210 his3-D1 pol1⁺-5FLAG::kanMX trt1Δ::his3⁺ cdc25-22 //pNR210-trt1⁺(ade6⁺; P_{adh}::tk; trt1⁺)*
	pol1-FLAG trt1-D743A	YTC10066[b]	*h⁻ ade6-M210 his3-D1 pol1⁺-5FLAG::kanMX trt1-D743A::LEU2 cdc25-22 //pNR210-trt1⁺ (ade6⁺; P_{adh}::tk; trt1⁺)*
	pol2-FLAG trt1⁺	TN4782	*h⁺ ade6-M210 his3-D1 pol2⁺-5FLAG::kanMX cdc25-22*
	pol2-FLAG trt1Δ	TN8393[b]	*h⁻ ade6-M210 his3-D1 pol2⁺-5FLAG::kanMX trt1Δ::his3⁺ cdc25-22 //pNR210-trt1⁺ (ade6⁺; P_{adh}::tk; trt1⁺)*
	pol2-FLAG trt1-D743A	YTC10064[b]	*h⁻ ade6-M210 his3-D1 pol2⁺-5FLAG::kanMX trt1-D743A::LEU2 cdc25-22 //pNR210-trt1⁺ (ade6⁺; P_{adh}::tk; trt1⁺)*
2.27-2.28	*pol1-FLAG*	TN4781	*h⁻ his3-D1 pol1⁺-5FLAG::kanMX cdc25-22*
	pol1-FLAG rap1Δ	YTC9589	*h⁻ his3-D1 pol1⁺-5FLAG::kanMX rap1Δ::ura4⁺ cdc25-22*
	pol1-FLAG rap1Δ trt1Δ	BAM10118[b]	*h⁻ ade6-M210 his3-D1 pol1⁺-5FLAG::kanMX rap1Δ::ura4⁺ trt1Δ::his3⁺ cdc25-22 //pNR210-trt1⁺ (ade6⁺; P_{adh}::tk; trt1⁺)*
	pol2-FLAG	TN4782	*h⁺ ade6-M210 his3-D1 pol2⁺-5FLAG::kanMX cdc25-22*
	pol2-FLAG rap1Δ	YTC9423	*h⁻ ade6-M210 his3-D1 pol2⁺-5FLAG::kanMX rap1Δ::ura4⁺ cdc25-22*
	pol2-FLAG rap1Δ trt1Δ	BAM10114[b]	*h- ade6-M210 his3-D1 pol2⁺-5FLAG::kanMX rap1Δ::ura4⁺ trt1Δ::his3⁺ cdc25-22 //pNR210-trt1⁺ (ade6⁺; P_{adh}::tk; trt1⁺)*
	stn1-myc	TN6886	*h⁻ his3-D1 stn1⁺-13myc::kanMX6 cdc25-22*
	stn1-myc rap1Δ	YTC9299	*h⁻ his3-D1 stn1⁺-13myc::kanMX6 rap1Δ::ura4⁺ cdc25-22*
	stn1-myc rap1Δ trt1Δ	YTC13543[b]	*h- ade6-M210 his3-D1 stn1⁺-13myc::kanMX6 rap1Δ::ura4⁺ trt1Δ::his3⁺ cdc25-22 //pNR210-trt1⁺ (ade6⁺; P_{adh}::tk; trt1⁺)*
	wt (no tag)	SS5264	*h⁻ his3-D1 cdc25-22*

2.4	wt	TN4777	*h⁻ leu1-32::[hENT1 leu1⁺] his3-D1 his7-366::[hsv-tk his7+] cdc25-22*
	poz1Δ	YTC9777	*h⁻ leu1-32::[hENT1 leu1⁺] his3-D1 his7-366::[hsv-tk his7⁺] poz1Δ::natMX6 cdc25-22*
	rap1Δ	YTC6430	*h⁻ leu1-32::[hENT1 leu1⁺] his3-D1 his7-366::[hsv-tk his7⁺] rap1Δ::ura4⁺ cdc25-22*
	taz1Δ	YTC6479	*h⁻ leu1-32::[hENT1 leu1⁺] his3-D1 his7-366::[hsv-tk his7⁺] taz1Δ::ura4⁺ cdc25-22*
2.9-2.11	*trt1-myc*	TN7708	*h⁻ his3-D1 trt1⁺-G₈-13myc::kanMX6 cdc25-22*
	trt1-myc poz1Δ	YTC8558	*h⁻ his3-D1 trt1⁺-G₈-13myc::kanMX6 poz1Δ::natMX6 cdc25-22*
	trt1-myc rap1Δ	YTC8969	*h⁻ his3-D1 trt1⁺-G₈-13myc::kanMX6 rap1Δ::ura4⁺ cdc25-22*
	trt1-myc taz1Δ	TN8601	*h⁻ his3-D1 trt1⁺-G₈-13myc::kanMX6 taz1Δ::ura4⁺ cdc25-22*
	myc-rad26	TN7840	*h⁻ his3-D1 9myc-rad26⁺::hphMX6 cdc25-22*
	myc-rad26 poz1Δ	YTC10349	*h⁻ his3-D1 9myc-rad26⁺::hphMX6 poz1Δ::natMX6 cdc25-22*
	myc-rad26 rap1Δ	YTC10338	*h⁻ his3-D1 9myc-rad26⁺::hphMX6 rap1Δ::ura4⁺ cdc25-22*
	myc-rad26 taz1Δ	YTC10420	*h⁺ his3-D1 9myc-rad26⁺::hphMX6 taz1Δ::ura4⁺ cdc25-22*
	myc-rad3	YTC13163	*h⁺ his3-D1 9myc-rad3⁺ cdc25-22*
	myc-rad3 poz1Δ	YTC13047	*h⁺ his3-D1 9myc-rad3⁺ poz1Δ::natMX6 cdc25-22*
	myc-rad3 rap1Δ	YTC13053	*h⁺ his3-D1 9myc-rad3⁺ rap1Δ::ura4⁺ cdc25-22*
	myc-rad3 taz1Δ	YTC13057	*h⁺ his3-D1 9myc-rad3⁺ taz1Δ::ura4⁺ cdc25-22*
	rad11-FLAG	BAM5875	*h⁺ his3-D1 rad11⁺-5FLAG::kanMX cdc25-22*
	rad11-FLAG poz1Δ	YTC10334	*h⁺ his3-D1 rad11⁺-5FLAG::kanMX poz1Δ::natMX6 cdc25-22*
	rad11-FLAG rap1Δ	YTC10341	*h⁺ his3-D1 rad11⁺-5FLAG::kanMX rap1Δ::ura4⁺ cdc25-22*
	rad11-FLAG taz1Δ	YTC10319	*h⁻ his3-D1 rad11⁺-5FLAG::kanMX taz1Δ::ura4⁺ cdc25-22*
	tpz1-myc	TN7467	*h⁻ his3-D1 tpz1⁺-13myc::kanMX6 cdc25-22*
	tpz1-myc poz1Δ	YTC9362	*h⁻ his3-D1 tpz1⁺-13myc::kanMX6 poz1Δ::natMX6 cdc25-22*
	tpz1-myc rap1Δ	YTC9307	*h⁻ his3-D1 tpz1⁺-13myc::kanMX6 rap1Δ::ura4⁺ cdc25-22*
	tpz1-myc taz1Δ	YTC9327	*h⁻ his3-D1 tpz1⁺-13myc::kanMX6 taz1Δ::ura4⁺ cdc25-22*
	ccq1-myc	TN7456	*h⁻ his3-D1 ccq1⁺-13myc::kanMX6 cdc25-22*
	ccq1-myc poz1Δ	YTC8709	*h⁻ his3-D1 ccq1⁺-13myc::kanMX6 poz1Δ::natMX6 cdc25-22*
	ccq1-myc rap1Δ	YTC9384	*h⁺ his3-D1 ccq1⁺-13myc::kanMX6 rap1Δ::ura4⁺ cdc25-22*
	ccq1-myc taz1Δ	YTC9292	*h⁻ his3-D1 ccq1⁺-13myc::kanMX6 taz1Δ::ura4⁺ cdc25-22*
	poz1-myc	TN6843	*h⁻ his3-D1 poz1⁺-13myc::kanMX6 cdc25-22*
	poz1-myc rap1Δ	YTC9314	*h⁻ his3-D1 poz1⁺-13myc::kanMX6 rap1Δ::ura4⁺ cdc25-22*
	poz1-myc taz1Δ	YTC9285	*h⁻ his3-D1 poz1⁺-13myc::kanMX6 taz1Δ::ura4⁺ cdc25-22*
	stn1-myc	TN6886	*h⁻ his3-D1 stn1⁺-13myc::kanMX6 cdc25-22*
	stn1-myc poz1Δ	YTC8717	*h⁻ his3-D1 stn1⁺-13myc::kanMX6 poz1Δ::natMX6 cdc25-22*
	stn1-myc rap1Δ	YTC9299	*h⁻ his3-D1 stn1⁺-13myc::kanMX6 rap1Δ::ura4⁺ cdc25-22*
	stn1-myc taz1Δ	YTC9414	*h⁺ his3-D1 stn1⁺-13myc::kanMX6 taz1Δ::ura4⁺ cdc25-22*
	wt (no tag)	SS5264	*h⁻ his3-D1 cdc25-22*
	poz1Δ (no tag)	YTC8929	*h⁻ his3-D1 poz1Δ::natMX6 cdc25-22*
	rap1Δ (no tag)	YTC8938	*h⁺ his3-D1 rap1Δ::ura4⁺ cdc25-22*
	taz1Δ (no tag)	YTC8933	*h⁻ his3-D1 taz1Δ::ura4⁺ cdc25-22*
2.12A, C, 2.12D	*tel1⁺* (no tag)	SS5264	*h⁻ his3-D1 cdc25-22*
	myc-tel1	YTC13049	*h⁺ ade6-704 his3-D1 9myc-tel1⁺ cdc25-22*
	myc-tel1	LS8284	*h⁻ ade6-704 his3-D1 9myc-tel1⁺*
	poz1Δ (no tag)	YTC8930	*h⁺ his3-D1 poz1Δ::natMX6 cdc25-22*
	myc-tel1 poz1Δ	YTC10940	*h⁻ ade6-704 his3-D1 9myc-tel1⁺ poz1Δ::natMX6 cdc25-22*
	rap1Δ (no tag)	YTC8938	*h⁺ his3-D1 rap1Δ::ura4⁺ cdc25-22*
	myc-tel1 rap1Δ	YTC10935	*h⁺ ade6-704 his3-D1 9myc-tel1⁺ rap1Δ::ura4⁺ cdc25-22*
	taz1Δ (no tag)	YTC8933	*h⁻ his3-D1 taz1Δ::ura4⁺ cdc25-22*
	myc-tel1 taz1Δ	YTC10932	*h⁺ ade6-704 his3-D1 9myc-tel1⁺ taz1Δ::ura4⁺ cdc25-22*

2.12B, D	*tel1*$^+$ (no tag)	TN2411	*h*$^-$ *his3-D1*
	myc-tel1	LS8284	*h*$^-$ *ade6-704 his3-D1 9myc-tel1*$^+$
	rap1Δ (no tag)	TN5346	*h*$^+$ *his3-D1 rap1Δ::ura4*$^+$
	myc-tel1 rap1Δ	YTC10938	*h*$^-$ *his3-D1 9myc-tel1*$^+$ *rap1Δ::ura4*$^+$
	rad3-kdΔ (no tag)	TN1678	*h*$^-$ *ade6-M216 his3-D1 rad3-kdΔ::kanMX4*
	myc-tel1 rad3-kdΔ	YTC12932	*h*$^-$ *ade6-704 his3-D1 9myc-tel1*$^+$ *rad3-kdΔ::kanMX4*
	rad3-kdΔ rap1Δ (no tag)	YTC13045	*h*$^+$ *ade6*$^-$ *his3-D1 rad3-kdΔ::kanMX4 rap1Δ::ura4*$^+$
	myc-tel1 rad3-kdΔ rap1Δ	YTC12931	*h*$^+$ *ade6-704 his3-D1 9myc-tel1*$^+$ *rad3-kdΔ::kanMX4 rap1Δ::ura4*$^+$

[a]All strains are *leu1-32 ura4-D18*, except for strains expressing hENT1, which are *leu1-32::[hENT1 leu1*$^+$*] ura4-D18.*

[b]Early generation strains that have just lost *trt1*$^+$ plasmid (*pNR210-trt1*$^+$) were used to ensure that ChIP assays monitored *trt1Δ* or *trt1-D743A* cells carrying longest telomeres as possible.

Table 2.3 DNA primers used in this study

Primer Name	Primer Sequence (5' to 3')	Description
jk380	TATTTCTTTATTCAACTTACCGCACTTC	Used as real-time PCR primers for telomere ChIP (Kanoh et al., 2005).
jk381	CAGTAGTGCAGTGTATTATGATAATTAAAATGG	
ars2004-66-F	CGGATCCGTAATCCCAACAA	Used as real-time PCR primers for *ars2004* ChIP (Hayashi et al., 2007).
ars2004-66-R	TTTGCTTACATTTTCGGGAACTTA	
BAM140	TTTTCAGGGTCGGTAGAGTCAGAG	Used to PCR amplify a region near *ars3001* within rDNA repeats. The PCR product was used as template to generate rDNA region probe to establish telomere correction factors.
BAM141	CCTCCTTACTTCTCCTTATTCCACG	
trt1-B29	CTTATTCTAAATGAAAGGAGATTAGC	Used to PCR amplify *trt1-G$_8$-13myc::kanMX6* construct to generate cells carrying *trt1-D743A-G$_8$-13myc::kanMX6* allele.
trt1-T30	TAGGCTAGGATACTCTATGTGTATGAGAGC	
UraKan-T1	CCCACTGGCTATATGTATGCATTTGTGTTAAAA AAGTTTGTATAGATTATTTAATCTACTCAGCATT CTTTCTCTAACGCGCCAGATCTGTTTAGCTTGC	Used to swap marker from *ura4*$^+$ to *kanMX4*. 5' end anneals to *ura4*$^+$ and 3' end (underlined) anneals to *kanMX4* module in pFA6a-kanMX4 plasmid.
UraKan-B1	GATATTGACGAAACTTTTTGACATCTAATTTATT CTGTTCCAACACCAATGTTTATAACCAAGTTTT ATCTTGTTTGGGCGGCGTTAGTATCGAATCGA C	

Table 2.4 Plasmids used in this study

Plasmid (Lab stock #)	Genes	Description
pTELO (254)	Fission yeast telomere fragment; *ampR*	Carries a telomeric repeat fragment (*ApaI-SacI*) used in generating a telomere probe for Southern blot analysis (Nakamura et al., 1997).
pNR210-trt1^{+} (290)	*ade6*$^{+}$; *trt1*$^{+}$; P_{adh}*::tk*; *ampR*	Trt1 plasmid used to maintain telomeres. It also expresses *tk* (herpes simplex virus thymidine kinase) gene to allow counter selection of the plasmid on media containing 5FdUR (Sivakumar et al., 2004).
pFA6a-kanMX4 (4)	*kanMX4*; *ampR*	Used as a PCR template for *kanMX4* (Wach et al., 1994) to swap marker to generate *rad3-kd∆::kanMX4* strain.
pTM580 (461)	Full length *GAD-tpz1*; *LEU2*; *ampR*	pGAD-GH-Tpz1 full length plasmid from Isikawa lab (Miyoshi et al., 2008).
pGAD-GH-tpz1$_{2\text{-}420}$ (838)	*GAD-tpz1*$_{2\text{-}420}$; *LEU2*; *ampR*	Expresses truncated GAL4 AD-Tpz1 (2-420).
pGAD-GH-tpz1$_{224\text{-}508}$ (814)	*GAD-tpz1*$_{224\text{-}508}$; *LEU2*; *ampR*	Expresses truncated GAL4 AD-Tpz1 (224-508).
pGAD-GH-tpz1$_{224\text{-}420}$ (818)	*GAD-tpz1*$_{224\text{-}420}$; *LEU2*; *ampR*	Expresses truncated GAL4 AD-Tpz1 (224-420).
pGAD-GH-tpz1$_{2\text{-}223}$ (812)	*GAD-tpz1*$_{2\text{-}223}$; *LEU2*; *ampR*	Expresses truncated GAL4 AD-Tpz1 (2-223).
pGAD-GH-tpz1$_{421\text{-}508}$ (816)	*GAD-tpz1*$_{421\text{-}508}$; *LEU2*; *ampR*	Expresses truncated GAL4 AD-Tpz1 (421-508).
pGBKT7-stn1 (476)	*DBD-stn1*; *TRP1*; *kanR*	Expresses GAL4 DNA BD-Stn1.
pGBKT7-ten1 (474)	*DBD-ten1*; *TRP1*; *kanR*	Expresses GAL4 DNA BD-Ten1.
pGBKT7-stn1+ten1 (570)	*DBD-stn1*; *ten1*; *TRP1*; *kanR*	Expresses GAL4 DNA BD-Stn1 and wt Ten1. (Not fused to either GAL4 DNA BD or GAL4 AD.)

3. Identification of Tpz1 phosphorylation sites and their possible roles in fission yeast telomere length regulation

3.1 Introduction

As described in earlier Chapters, our laboratory has recently reported that deletion of the shelterin complex subunits Taz1, Rap1 and Poz1 (involved in negative regulation of telomere extension by telomerase) causes hyper-phosphorylation of Ccq1 by DNA damage checkpoint kinases $Rad3^{ATR}$ and $Tel1^{ATM}$, and that Ccq1 phosphorylation on Thr93 is critical for Est1-Ccq1 interaction and telomerase recruitment (Chang et al., 2013; Moser et al., 2011). In this chapter, I show that Tpz1, much like Ccq1, undergoes $Rad3^{ATR}$/$Tel1^{ATM}$ -dependent hyper-phosphorylation upon loss of Taz1, Rap1 or Poz1. Furthermore, I show that telomere shortening also induces Tpz1 hyper-phosphorylation. To identify Tpz1 phosphorylation sites and examine potential roles of Tpz1 phosphorylation in fission yeast telomere regulation, I purified Tpz1 proteins and carried out mass spectrometry analysis of Tpz1 in collaboration with John Yates' group at The Scripps Research Institute. Our analyses have identified 28 novel *in vivo* phosphorylation sites of Tpz1. Moreover, we found that some of those sites are still phosphorylated in cells lacking both $Rad3^{ATR}$ and $Tel1^{ATM}$ kinases, strongly implicating involvement of other unidentified kinase(s) in Tpz1 phosphorylation. Mutational analyses of selected Tpz1 phosphorylation sites have identified phosphorylation sites that contribute in telomere length regulation and/or phosphorylation-dependent mobility shift of Tpz1 on SDS PAGE by $Rad3^{ATR}$/$Tel1^{ATM}$ or other kinase(s). These initial characterizations should be useful in fully understanding

how Tpz1 and Ccq1 phosphorylation might collaborate in achieving optimal fission yeast telomere length regulation in the future.

3.2 Results

3.2.1 Tpz1 is hyper-phosphorylated in cells lacking telomerase inhibitors (Poz1, Rap1 or Taz1) and in cells carrying short telomeres.

Much like Ccq1, I found that mobility of Tpz1 protein on SDS-PAGE is significantly reduced in *poz1Δ*, rap1*Δ* or *taz1Δ* cells (Figure 3.1A). Mirroring the extent of Tpz1 mobility shift, Tpz1 association with telomerase RNA *TER1* was also increased (Figure 3.2C). Thus, I wondered whether post-translational modification of Tpz1 might also contribute to telomerase recruitment in fission yeast. I suspected that the Tpz1 mobility shift might be caused by phosphorylation, and thus treated wild type, *poz1Δ*, *rap1Δ* or *taz1Δ* cell lysates with λ phosphatase. Indeed, increased slow mobility bands for Tpz1 in *poz1Δ*, *rap1Δ* and *taz1Δ* cells were phosphatase-sensitive (Figure 3.1B), indicating that Tpz1 is hyper-phosphorylated in the absence of Poz1, Rap1 or Taz1. Furthermore, I also found that phosphatase treatment causes Tpz1 proteins in the wild type cells to move faster on SDS-PAGE, indicating that Tpz1 protein is phosphorylated not only in mutant cells, but also in the wild type cells (Figure 3.1B).

In budding yeast, it was found that short telomeres induce preferential telomere extension and increased binding of telomerase, and replicate earlier than other telomeres (Bianchi and Shore, 2007a, b; Sabourin et al., 2007). $Tel1^{ATM}$ kinase is specifically recruited to these short telomeres, indicating a phosphorylation event might

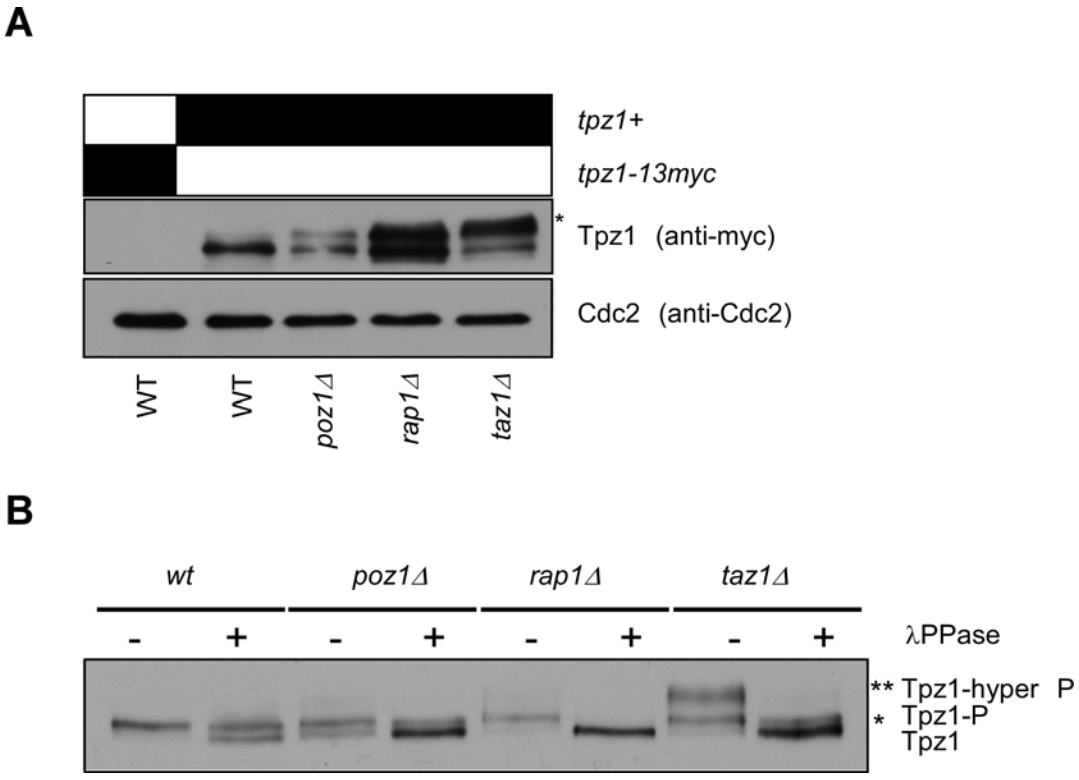

Figure 3.1 Tpz1 hyperphosphorylation in *poz1Δ*, *rap1Δ* and *taz1Δ* cells.
(**A**) Anti-myc western blot analysis detected the mobility changes of Tpz1(*), implying the potential post translational modification of Tpz1 in *poz1Δ*, *rap1Δ* and *taz1Δ* cells. (**B**) λ phosphatase treatment of Tpz1 protein showed that slow-moving signals collapsed down to fast-moving signals, suggesting that Tpz1 was phosphorylated in *poz1Δ*, *rap1Δ*, and *taz1Δ* cells, as well as in *wt* cells.

play a role in promoting telomere extension. In fission yeast, short telomeres (in *ccq1-T93A*, *est1Δ* or *trt1Δ* cells) also appear to replicate earlier (Chang et al., 2013), and Rad3^{ATR}/Tel1^{ATM}-dependent Ccq1 hyper-phosphorylation and telomerase recruitment also increases in cells with short telomeres due to increased recruitment of the Rad3^{ATR}-Rad26^{ATRIP} kinase complex (Chang et al., 2013; Moser et al., 2011). Thus, I suspected that Tpz1 might also undergo hyper-phosphorylation in cells carrying short telomeres. Indeed, I observed that Tpz1 protein is hyper-phosphorylated in *ccq1-T93A* or *trt1Δ* cells (Figure 3.2A-B). Thus, it appears that phosphorylation status of Ccq1 and Tpz1 is under similar regulation, potentially suggesting that Tpz1 phosphorylation might also play critical role(s) in telomere length regulation, much like Ccq1 phosphorylation.

3.2.2 Ccq1 is required for hyper-phosphorylation of Tpz1.

Ccq1 is essential for recruitment of the telomerase complex (Trt1^{TERT}, Est1 and telomerase RNA *TER1*) to telomeres (Miyoshi et al., 2008; Moser et al., 2011; Moser et al., 2009b; Tomita and Cooper, 2008; Webb and Zakian, 2012; Yamazaki et al., 2012a), and *ccq1Δ* cells suffer from checkpoint activation and telomere shortening due to lack of telomere protection and proper telomere extension by telomerase (Tomita and Cooper, 2008). In *ccq1Δ* and *rap1Δ ccq1Δ* cells, Tpz1 interaction with telomerase RNA (TER1) is almost completely eliminated, indicating that telomerase-Tpz1 interaction depends on Ccq1 in both wild type and *rap1Δ* cells (Moser et al., 2009b) (Fig. 3.2C). It has been shown that Rad3^{ATR}/Tel1^{ATM}-dependent Ccq1 Thr93 phosphorylation (strongly induced

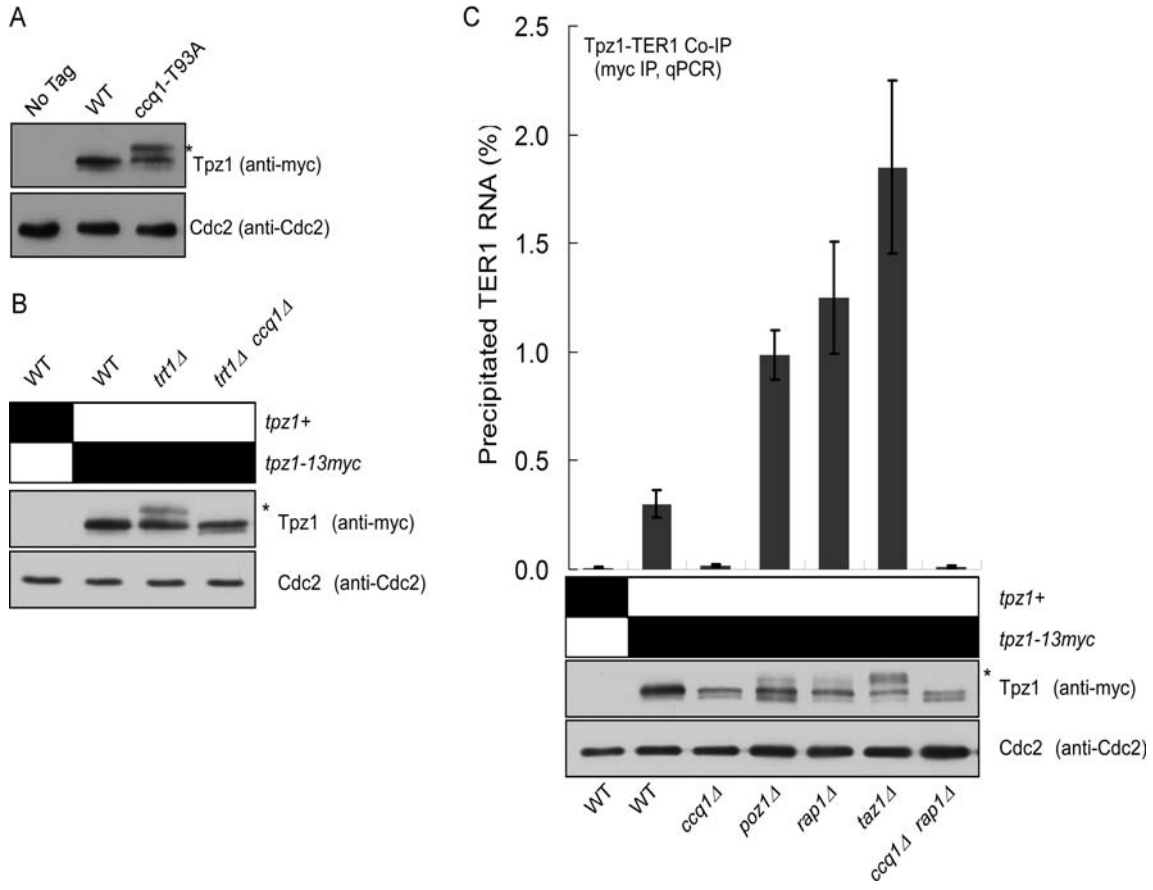

Figure 3.2 Ccq1 serves as an adaptor of Tpz1 hyperphosphorylation.
(**A-B**) Tpz1 protein hyperphosphorylation was seen in the Ccq1 phosphorylation deficient mutant in (**A**) and *trt1* deletion in (**B**) as assayed by western blot analysis. Additional deletion of Ccq1 protein eliminated Tpz1 hyperphosphorylation in trt1 deletion cells by Tpz1-TER1 RNA co-IP. (**C**) Similar assays also were used in long telomere cells (*rap1Δ*). *rap1Δ ccq1Δ* deletion abolished both Tpz1 hyperphosphorylation and Tpz1-TER1 RNA interaction in C. Both data in (B) and (C) illustrates that Ccq1 could serve as an adapter for Tpz1 phosphorylation, possibly by $Rad3^{ATR}$ and $Tel1^{ATM}$ kinases, as well as telomerase association of Tpz1 western blots were performed with anti-myc antibody for Tpz1 protein and anit-Cdc2 antibody for Cdc2 as the loading control. Tpz1-TER1 RNA co-IP was described in Methods section.

in *rap1Δ* cells) promotes Ccq1-Est1 interaction to facilitate telomerase recruitment (Moser et al., 2011).

Since changes in the extent of phosphorylation for Ccq1 and Tpz1 closely mirrored one another, I wondered if Ccq1 might contribute to the regulation of Tpz1 phosphorylation status. Thus, I deleted Ccq1 protein in either *rap1Δ* or *trt1Δ* cells, and then monitored Tpz1 phosphorylation status by western blot analysis. Indeed, hyper-phosphorylation of Tpz1 was abolished in *ccq1Δ rap1Δ* or *ccq1Δ trt1Δ* cells (Figure 3.2B-C), suggesting that Ccq1 is crucial for Tpz1 hyper-phosphorylation. Thus, I concluded that Ccq1 not only mediates telomerase recruitment at telomeres but also serves as an adaptor that facilitates Tpz1 hyper-phosphorylation.

3.2.3 Rad3^{ATR} and Tel1^{ATM} kinases contribute to Tpz1 hyper-phosphorylation.

Previous studies have shown that Ccq1 is hyper-phosphorylated by Rad3^{ATR} and Tel1^{ATM} kinases in cells lacking negative regulators of telomerase (Poz1, Rap1 or Taz1) (Chang et al., 2013; Moser et al., 2011). Therefore, I investigated whether Rad3^{ATR}/Tel1^{ATM} kinases are also responsible for Tpz1 phosphorylation by examining Tpz1 phosphorylation status in *rap1Δ* cells that lacked Rad3^{ATR} alone, Tel1^{ATM} alone or both kinases. I found that slow mobility bands of Tpz1 on SDS-PAGE are significantly reduced in *rad3Δ rap1Δ* cells and nearly eliminated in *rad3Δ tel1Δ rap1Δ* cells, but hardly affected in *tel1Δ rap1Δ* cells (Figure 3.3A). These data thus indicated that Tpz1 is mainly phosphorylated by Rad3^{ATR} kinase in wild type cells, but Tel1^{ATM} kinase can contribute to Tpz1 phosphorylation in the absence of Rad3^{ATR} kinase. I have also found that Tpz1 hyper-phosphorylation bands induced in *poz1Δ* or *taz1Δ* cells are

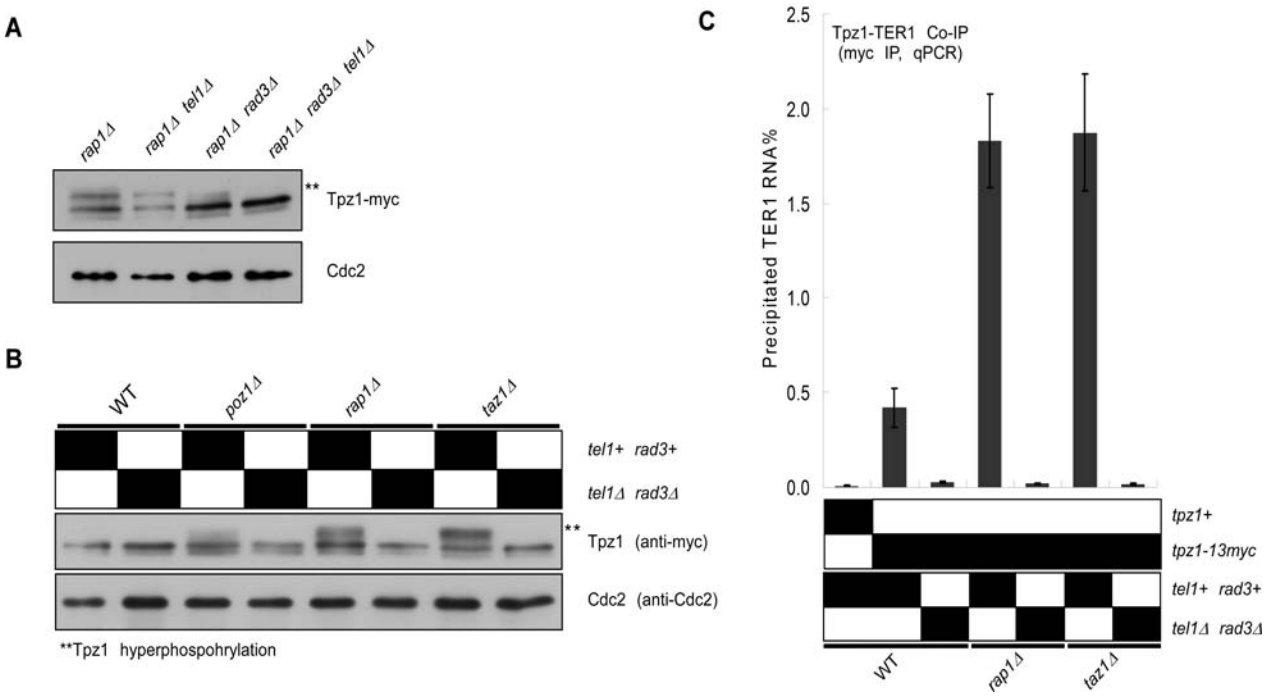

Figure 3.3 Tpz1 is a phosphorylation target of PIKK kinase Rad3^{ATR} and Tel1^{ATM} kinases in the cells.

(**A**) *rap1Δ*-induced hyperphosphorylation was largely reduced by additional deletion of Rad3^{ATR} protein alone or both Rad3^{ATR} and Tel1^{ATM} proteins. (**B**) Hyper-phosphorylation of Tpz1 protein in *poz1Δ*, *rap1Δ*, or *taz1Δ* was abolished with additional *rad3 tel1* double deletion. (**C**) Tpz1-TER1 RNA interaction was disrupted in *rap1Δ rad3Δ tel1Δ* and *taz1Δ rad3Δ tel1Δ* cells. Both data showed the importance of both Rad3^{ATR} and Tel1^{ATM} proteins for Tpz1 hyper-phosphorylation and TER1 RNA association of Tpz1. Western blots were performed with anti-myc antibody for Tpz1 protein and anit-Cdc2 antibody for Cdc2 as the loading control. Tpz1-TER1 RNA co-IP was described in Methods section.

eliminated in *rad3Δ tel1Δ* background (Figure 3.3B). Furthermore, I found that the enhanced Tpz1-*TER1* RNA interaction observed in *rap1Δ* or *taz1Δ* cells is completely abolished in *rad3Δ tel1Δ* cells (Figure 3.3C). These data thus raised a possibility that $Rad3^{ATR}$/$Tel1^{ATM}$-dependent phosphorylation of Tpz1 might also contribute to telomerase recruitment.

3.2.4 Mutations on putative $Rad3^{ATR}$/$Tel1^{ATM}$ phosphorylation sites alone do not affect telomere length.

To investigate the potential functional significance of $Rad3^{ATR}$/$Tel1^{ATM}$-dependent phosphorylation of Tpz1 in telomere maintenance, I introduced Alanine mutations for Serine or Threonine residues within all six SQ/TQ sites (preferred phosphorylation sites for $Rad3^{ATR}$/$Tel1^{ATM}$ kinases) found in Tpz1: Ser63, Ser97, Ser164, Ser309, Ser340, and Thr354 (Figure 3.4A). To test which of these residues contribute to the observed Tpz1 mobility shifts on SDS-PAGE, I also examined Tpz1 mobility on SDS-PAGE in *rap1*Δ cells that carried mutations at N-terminal three (3AQ-N), C-terminal three (3AQ-C), C-terminal four (4AQ) or all six (6AQ) SQ/TQ sites (Figure 3.4A). I found that Tpz1 hyper-phosphorylation bands are significantly reduced but not completely eliminated in *tpz1-6AQ*, *tpz1-4AQ* and *tpz1-3AQ-C* mutants. On the other hand, I did not observe much change in Tpz1 mobility for *tpz1*-3AQ-N mutant cells (Figure 3.4B). These data thus suggested that only C-terminal four SQ/TQ sites (S164, S309, S340, and T354) primarily contribute to the observed SDS-PAGE mobility shift of Tpz1 in *rap1*Δ cells.

Next, I tested whether phosphorylation of SQ/TQ sites might be important in telomere length regulation by monitoring telomere length changes for various SQ/TQ

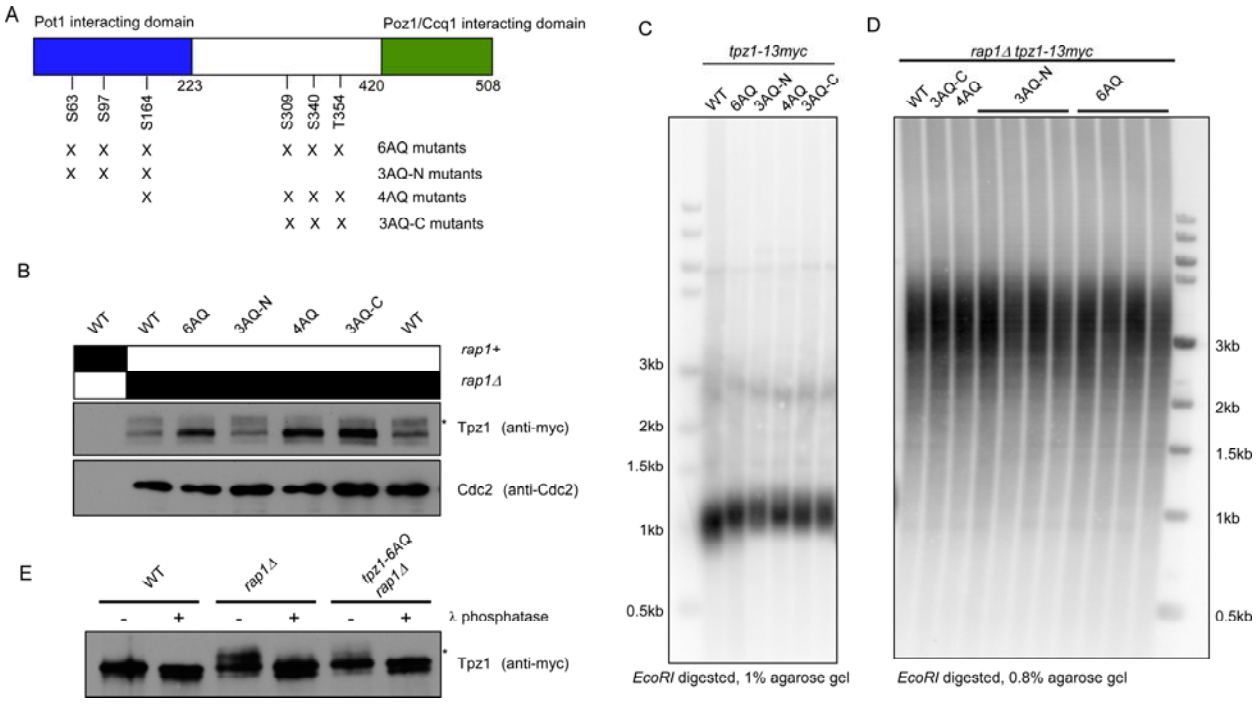

Figure 3.4 Mutations on putative target sites of Rad3^{ATR} and Tel1^{ATM} kinases do not affect telomere length.

(**A**) Schematic diagram of 6 predicted ATM/ATR target sites (SQ or TQ) on Tpz1. (**B-D**) Site-directed mutagenesis on Ser or Thr residue to Ala of Tpz1 SQ/TQ sites in *wt* and *rap1Δ* cells. Tpz1 hyperphosphorylation was mostly eliminated in Tpz1-6AQ, -4AQ and -3AQ-C mutant cells, detected by western Blot analysis in B. However, 6AQ, -4AQ and -3AQ-C mutation did not change telomerase dependent telomere elongation in *rap1* deletion cells by Southern blot of telomere length in C. (**E**) λ phosphatase treatment of Tpz1 protein in Tpz1-6AQ rap1Δ cells, showed residual slow-moving signal was phosphatase sensitive. Both data in (C) and (D) suggested that other *in vivo* targets of Tpz1 phosphorylation might also contribute to hyperphosphorylation status and telomere phenotypes. Western blots were performed with anti-myc antibody for Tpz1 protein and anit-Cdc2 antibody for Cdc2 as the loading control. Southern blot of telomere length was described in Methods section.

site mutants by Southern blot analysis. Unfortunately, I found that various *tpz1* AQ mutations including *tpz1-6AQ* do not lead to changes in telomere length in either wild type (*rap1*$^{+}$) or *rap1Δ* cells (Figure 3.4C-D), suggesting that potential phosphorylation events at these six SQ/TQ sites on their own do not play a significant role in telomere length regulation. However, since Tpz1-6AQ protein in *rap1Δ* cells retained residual slow mobility bands that are sensitive to phosphatase treatment, it is possible that phosphorylation of Tpz1 on sites other than six SQ/TQ sites might play important role(s) in regulation of telomere length.

3.2.5 Identification of Tpz1 phosphorylation sites by mass spectrometry

As described in the previous section, I established that Tpz1 is already phosphorylated in wild type cells but becomes hyper-phosphorylated by Rad3^{ATR}/Tel1^{ATM} kinases upon elimination of negative regulators of telomerase. However, *tpz1-6AQ* mutant allele, which mutated all six preferred Rad3^{ATR}/Tel1^{ATM} phosphorylation sites within Tpz1, did not fully eliminate hyper-phosphorylation bands observed in *rap1Δ* cells, or alter telomere length. These findings thus raised a possibility that additional phosphorylation sites (which could be phosphorylated by Rad3^{ATR}/Tel1^{ATM} or other unidentified kinases) might play critical roles in telomere length regulation by Tpz1. Thus, in order to better evaluate the functional significance of Tpz1 phosphorylation in telomere maintenance, I decided to identify Tpz1 phosphorylation sites *in vivo* by mass spectrometry analysis.

To identify Rad3^{ATR}/Tel1^{ATM}-dependent and -independent Tpz1 phosphorylation sites that are already phosphorylated in wild type cells or phosphorylated in the absence

of telomerase inhibitors, I decided to purify Tpz1 proteins from the wild type, *rap1Δ*, *taz1Δ*, or *rad3Δ tel1Δ* cells. Initially, I attempted to carry out one-step FLAG-tag purifications with strains that express endogenous-levels of Tpz1 from its own locus. However, I was unable to obtain sufficient quantity of Tpz1 protein necessary to identify Tpz1 phosphorylation sites since Tpz1 is a low abundance protein (data not shown). Therefore, in order to obtain sufficient quantities of purified Tpz1 for phosphorylation site identification, I decided to utilize strains that can over-express Tpz1-3FLAG protein under the control of an inducible *nmt1* promoter (add reference for the original nmt1 plasmid paper).

The presence of Tpz1-3FLAG protein during purification steps was monitored by western blot analysis, and as shown in Fig. 3.5A and 3.5C. Using anti-FLAG M2 beads, I was able to pull-down and elute significant quantities of Tpz1 in the purification process. However, I did notice that some of slower mobility Tpz1 bands on SDS PAGE that likely correspond to hyper-phosphorylated Tpz1 was reduced in “Bound” and “Eluted” portions, potentially indicating loss of phosphorylation and/or protein degradation during the purification process.

I have also carried out one-step FLAG purification for a strain that over-expresses untagged Tpz1 under the control of the nmt1 promoter as a negative control for mass spectrometry analysis. Silver staining of purified samples on SDS-PAGE gels showed major ~80 kDa bands, enriched only in samples purified from cells over-expressing Tpz1-3FLAG (Figure 3.5B, 3.5D; wild type, *rap1Δ*, *taz1Δ*, *rad3Δ tel1Δ*). These enriched bands were identified as Tpz1 since it closely matched in size to bands detected by FLAG western blot analysis of Tpz1-3FLAG protein. In addition to Tpz1

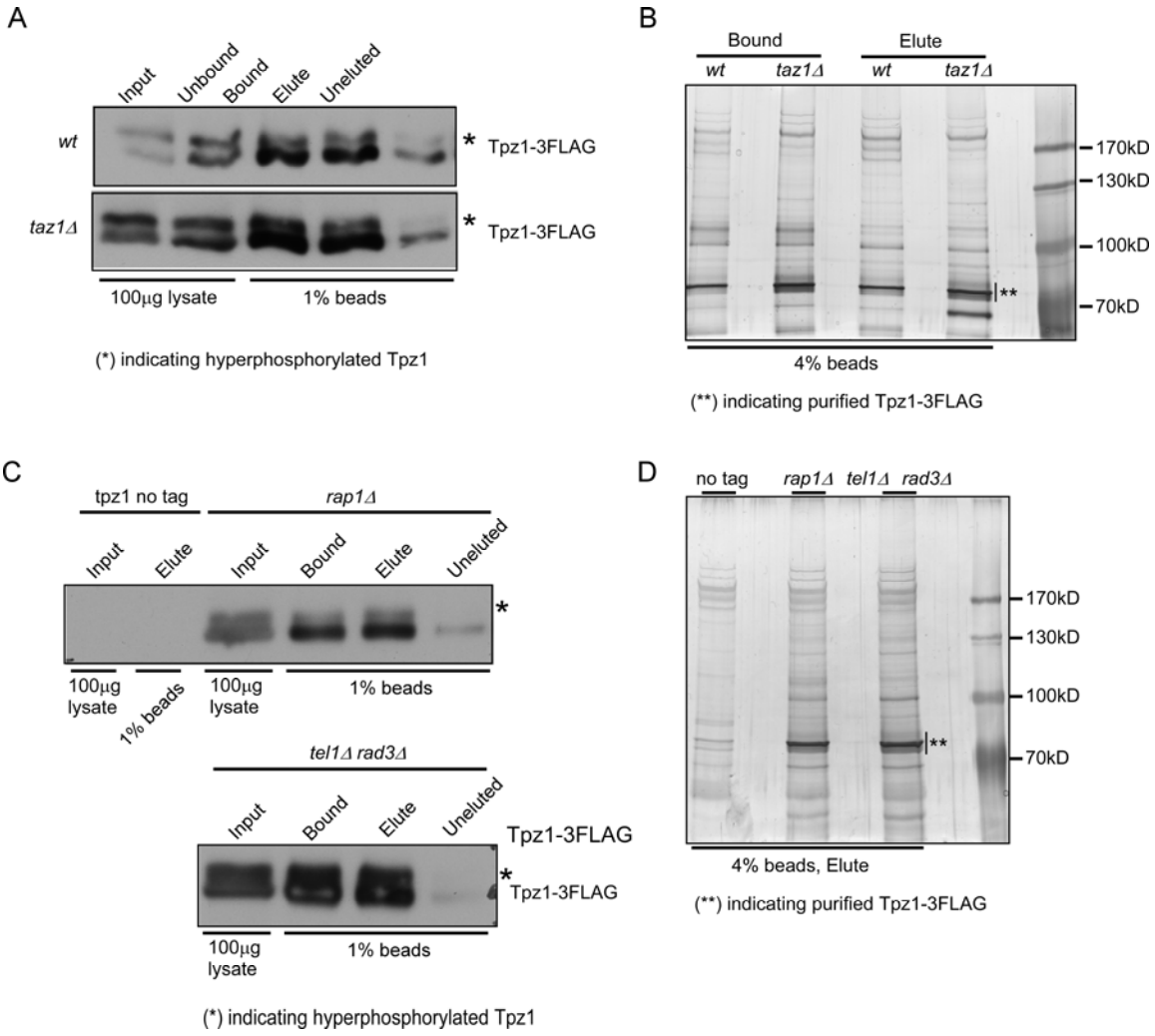

Figure 3.5 Purification of overexpressed Tpz1 from *wt*, *rap1Δ*, *taz1Δ*, and *rad3Δ tel1Δ* cells.

Overexpressed Tpz1 was purified by one-step purification with Sigma M2 beads and analyzed by western blot (**A**, **C**) and Silver staining (**B**, **D**). Hyperphosphorylation (*) was detected in wt, taz1Δ, rap1Δ and rad3Δ tel1Δ cells (A, C), and unique enriched bands were found on Silver staining SDS-PAGE gels for Tpz1-3FLAG overexpressed strains. Western blots were performed with anti-myc antibody for Tpz1 protein and Silver staining procedure was described in Methods section.

bands, there were additional co-purifying bands that were only found in cells over-expressing FLAG-tagged Tpz1. These bands might represent proteins that associate with Tpz1-containing complex(es) *in vivo*. Therefore, I sent purified samples to our collaborator Dr. Aaron Aslanian in John Yates' laboratory at The Scripps Research Institute for mass spectrometry analyses to identify Tpz1 phosphorylation sites and Tpz1 interaction partners.

Dr. Aslanian was able to successfully identify 28 phosphorylation sites for Tpz1 among wild type, *rad3Δ tel1Δ*, *rap1Δ* and *taz1Δ* cells (Figure 3.6A). In addition, he was able to detect other shelterin subunits Pot1, Ccq1, Poz1 and Rap1 (data not shown). To our surprise, most of the Tpz1 phosphorylation sites (23 sites) were already found in the wild type cells, and we only saw a few sites that were phosphorylated only in either *rap1Δ* or *taz1Δ* cells. Since over-expression of Tpz1 caused telomere elongation and hyper-phosphorylation bands were already detectable in wild type background (Fig. 3.5), it appears that we were able to detect phosphorylation of Tpz1 at sites that are normally only phosphorylated in cells lacking telomerase inhibitors for endogenous levels of Tpz1 due to over-expression of Tpz1. In fact, we actually found more phosphorylation sites from the wild type sample than samples prepared from *rap1Δ* or *taz1Δ* cells, possibly due to variations in the quality of the purified samples that might have affected our ability to identify phosphorylation sites, or due to actual differences in phosphorylation patterns. Further studies are thus clearly needed to fully determine potential differences in phosphorylation patterns of endogenous Tpz1 among wild type, *rap1Δ* and *taz1Δ* cells. Nevertheless, we also found additional phosphorylation sites in *rap1Δ* (Ser164 and Ser318) and *taz1Δ* cells (Ser309, Thr378, and Thr419) that were not

identified in wild type cells. Two of these phosphorylation sites (Ser164 and Ser309) occurred within the SQ motif, the site predicted to be phosphorylated by Rad3^{ATR}/Tel1^{ATM} kinases. Comparison of the data between wild type and *rad3Δ tel1Δ* samples has also identified 10 phosphorylation sites that were commonly found in both backgrounds, confirming the notion that Tpz1 can be phosphorylated *in vivo* by unidentified kinase(s) other than Rad3^{ATR}/Tel1^{ATM} kinases. While I cannot completely exclude the possibility that variations in sample preparation might have caused identification of fewer phosphorylation sites in *rad3Δ tel1Δ* cells, 13 phosphorylation sites that were found only in wild type but not in *rad3Δ tel1Δ* samples (including Ser164 and Ser309 within the SQ motif) might represent Rad3^{ATR}/Tel1^{ATM}-dependent phosphorylation sites (Fig. 3.6).

3.2.6 Mutational analyses of Tpz1 phosphorylation sites identified by mass spectrometry.

Previous studies have defined functional motifs of Tpz1 by the protein-protein interaction relationship with other shelterin components: the amino-terminal domain (amino acids 2-223) for Pot1 binding, the central domain (amino acids 224-420) for Stn1 binding, and the carboxyl-terminus (amino acids 412-508) for Poz1/Ccq1 binding (Chang et al., 2013; Miyoshi et al., 2008). Most of newly identified Tpz1 phosphorylation sites mapped to the central region of Tpz1 rich in Serine and Threonine residues (amino acids 309-412), while four sites mapped to Pot1 binding domain and only a single site (Ser490) to the Poz1/Ccq1 binding domain (Fig. 3.6B and 3.7).

A

Motif	phospho sites	*wt*	*rad3Δ tel1Δ*	*rap1Δ*	*taz1Δ*
Pot1 binding 1-223	S138	*			
	S162	*			
	S164 (SQ)	*		S164 (SQ)	
	S194	*			
Stn1/Ten1 biding 224-420	S234	*			
	T238	*			
	S287				
	T294				
	T298				
	S309 (SQ)	*			S309 (SQ)
	S318	*		S318	
	S327	*			
	T328	*			
	S333	*			
	S334	*			
	S340 (SQ)	*			
	T354 (TQ)	*			
	S360				
	S375				
	T378	*			T378
	T379	*			
	S383	*			
	T393				
	T397	*			
	S404	*			
	S407	*			
	S410	*			
	T412	*			
	T419				T419
Ccq1/Poz1 biding 421-508	S490				
phosphorylation site		23	10	10	19

B

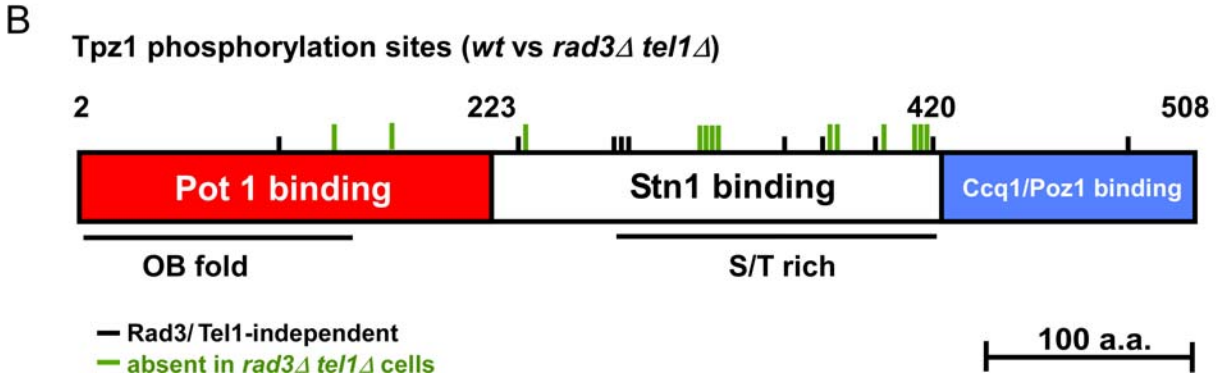

Figure 3.6 Identification of Tpz1 phosphorylation sites by Mass Spectrometry analysis.
(**A**) *In vivo* phosphorylation sites of Tpz1 were discovered by Mass Spectrometry analyses (ASscore>13 by statistic software DTASelect). (*) labeled sites were subject to Alanine mutation, whereas the phosphorylated sites in red with (AScore>1000) stayed unchanged. Unique *in vivo* phosphorylation targets identified from *rap1Δ* and *taz1Δ* cells were labeled in yellow. (**B**) Comparison of Tpz1 phosphorylation targets in *wt* and *rad3 tel1* deletion cells. 10 common sites were found in both cells, and 13 sites disappeared in *rad3 tel1* deletion cells, supporting the notion that Tpz1 could be phosphorylated by kinases other than $Rad3^{ATR}$ and $Tel1^{ATM}$ kinases.

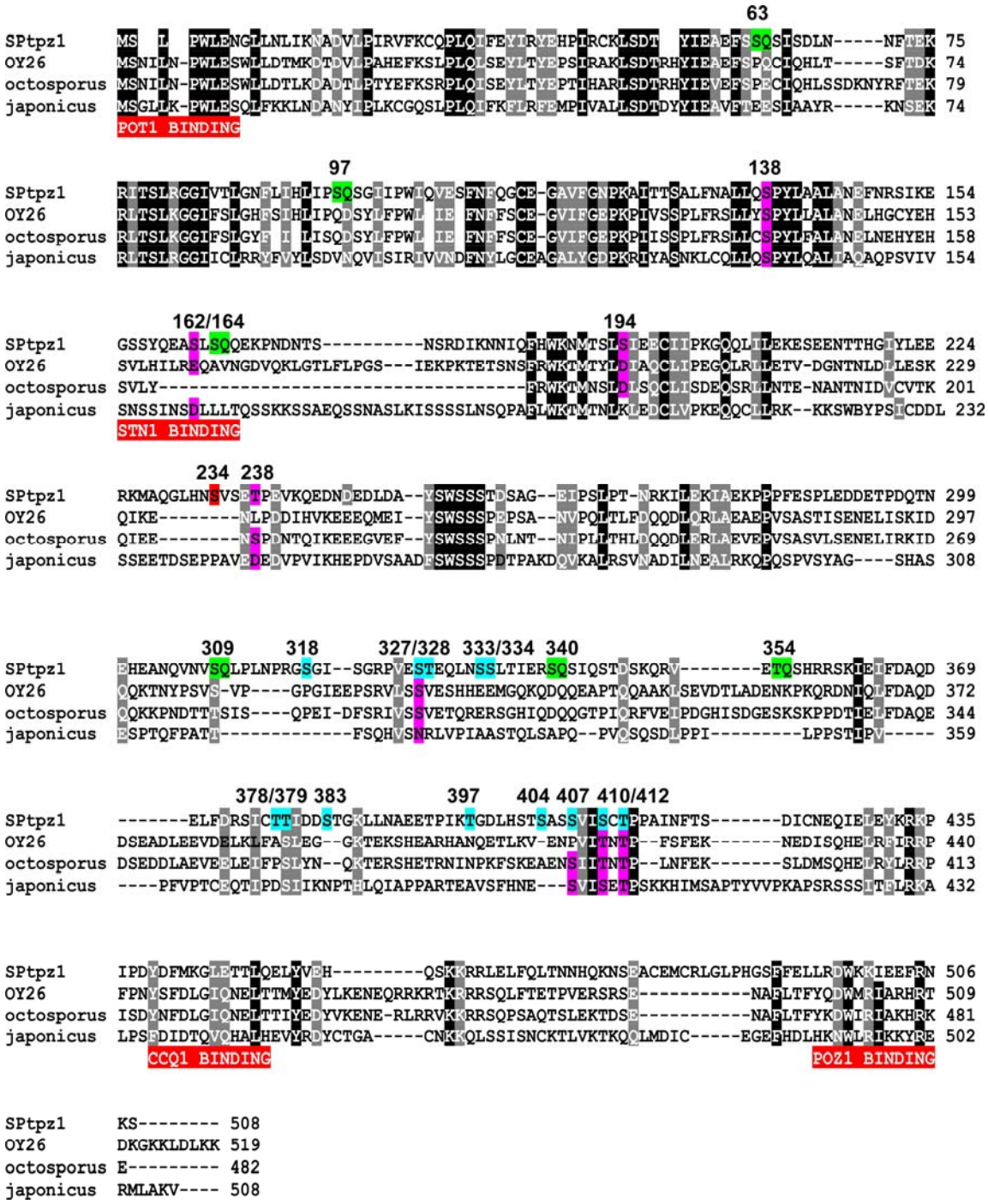

Figure 3.7 Sequence alignments of fission yeast clade- *Schizosaccharomyces pombe*, *S. octosporus*, *S. cryophilus* (OY26), and *S. japonicus*.
Putative Rad3^{ATR} and Tel1^{ATM} target sites (SQ/TQ) were labeled in green. Highly conserved phosphorylated residues and sites in the Ser/Thr rich region were labeled in pink and light blue individually.

I decided to focus mutational analysis of phosphorylation sites for sites that are better conserved among four closely related *Schizosacchromyces* fission yeast clade-*S. pombe*, *S. octosporus*, *S. cryophilus*, and *S. japonicus* (Fig. 3.7): Ser138, Ser162, Ser194, Thr238 and Ser318. In addition, I chose to mutate phosphorylation sites located within the S/T rich region: Ser327, Thr328, Ser333, Ser334, Thr378, Thr379, Ser383, Thr397, Ser404, Ser407, Ser410, and Thr412 (Figure 3.8A). While only Ser164 and Ser309 were verified as *in vivo* targets of Tpz1 phosphorylation by mass spectrometry, SQ/TQ site mutagenesis analysis described in the earlier section (Figure 3.4B) found similar reduction in hyper-phosphorylation bands of Tpz1 in *rap1Δ* cells for *tpz1-6AQ* and *tpz1-4AQ* alleles. Therefore, we also included four SQ/TQ sites (Ser164, Ser309, Ser340 and Thr354) in my mutational analysis of Tpz1.

Initially, I mutated phosphorylation sites individually or in a group in the wild type cells. (See Fig. 3.8A for a schematic view of mutated residues for combination mutants,) Western blot analysis of these mutants showed that *S138A* induced Tpz1 hyper-phosphorylation. While most of other mutations did not change the mobility of Tpz1 protein on SDS-PAGE, *tpz1-S/T-N* (S/T-rich N-terminal domain), *tpz1-S/T-C* (S/T-rich C-terminal domain), *tpz1-S/T-N+C* (S/T-rich N-terminal and C-terminal domains) and *tpz1-S410A/T412A* mutants showed differential effects on Tpz1 phosphorylation status (Figure 3.8B). Telomere length analysis by Southern blot revealed that S138A mutant carries long telomeres (Figure 3.8C). By contrast, T238A, S234A/T238A, S/T-N, S/T-C, S/T-N+C and S410A/T412A mutants caused slight telomere shortening (Figures 3.8C-D). The extent of shortening was greater for S/T-N, S/T-C, S/T-N+C and S410A/T412A mutants than T238A and S234A/T238A mutants (Figures 3.8C-D). For S162A/S164A.

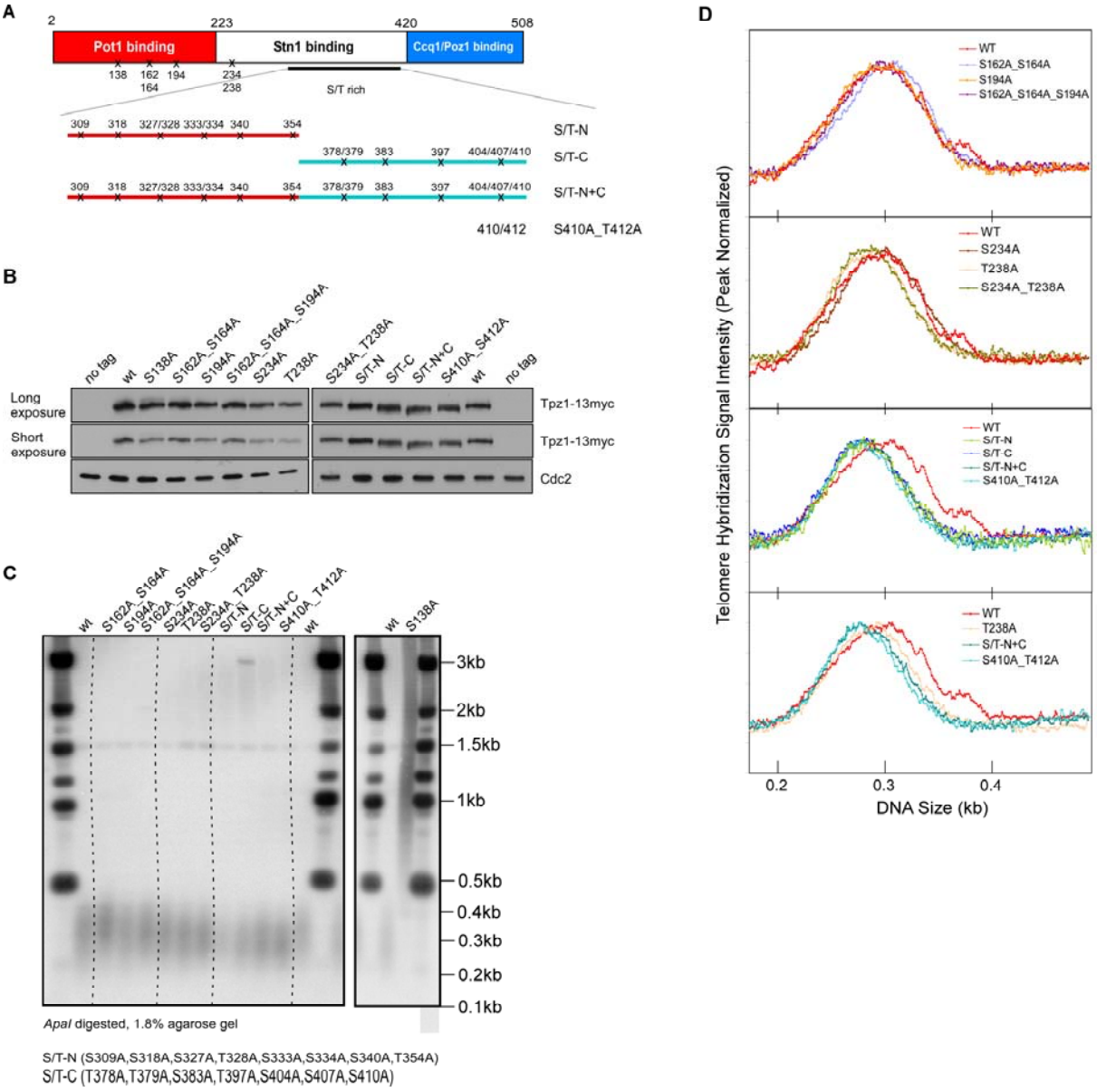

Figure 3.8 Mutagenesis analyses of *in vivo* phosphorylation targets on Tpz1 in wild type cells.

(**A**) Schematic diagram of mutations on Tpz1 phosphorylation sites. (**B-C**) Western blot of Tpz1 protein showed mobility shifts of Tpz1 in S/T-C, S/T-N+C and S410A_T412A cells in (**B**), as well as telomere shortening by Southern blot of telomere length in (**C**), implying that Tpz1 phosphorylation is important for telomere maintenance in wild type cells. Western blots were performed with anti-myc antibody for Tpz1 protein and anit-Cdc2 antibody for Cdc2 as the loading control. Southern blot of telomere length was described in Methods section.

S194A, S162A/S164A/S194A and S234A mutants, I did not detect changes in telomere length compared to wild type cells. These data suggested that Ser138 phosphorylation might be involve in negative regulation of telomere extension, while phosphorylation on T238 and S/T-rich domain residues might positively contribute to the regulation of telomere maintenance.

For S/T-N, S/T-C, S/T-N+C and S410A/T412A mutant cells, I further tested if these mutants might also contribute to regulation of telomere length in *rap1Δ* background. Western blot analysis of Tpz1 protein showed that *S/T-N* and *S/T-N+C* completely eliminated Tpz1 hyper-phosphorylation, whereas Tpz1 proteins in other mutant cells still retained hyper-phosphorylation (Figure 3.9A), suggesting that mutated sites in S/T-N region (Figure 3.8A), including three SQ/TQ sites and phosphorylation targets absent in *rad3Δ tel1Δ* cells, are responsible for appearance of slow mobility bands on SDS-PAGE. These mutations did not affect telomerase dependent telomere elongation in *rap1Δ* cells, even though mutations in *S/T-N* and *S/T-N+C* cells did abolish Tpz1 hyper-phosphorylation. Thus, it appears that phosphorylation sites lost in *S/T-N* or *S/T-C* became dispensable for telomere maintenance in *rap1Δ* cells. While further studies are necessary to provide more mechanistic understanding on how phosphorylation sites mutated in S138, S/T-N, S/T-C, and S410/T412 affect telomere maintenance, my initial mutational analyses have thus successfully identified Tpz1 phosphorylation sites that contribute to telomere length regulation in fission yeast.

A

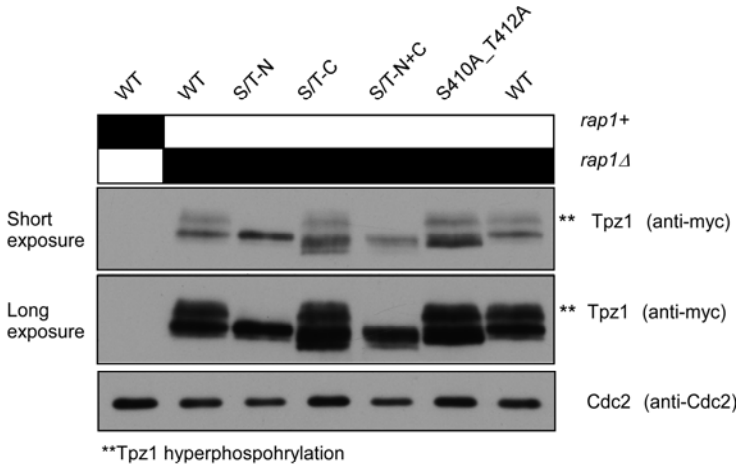

**Tpz1 hyperphospohrylation

B

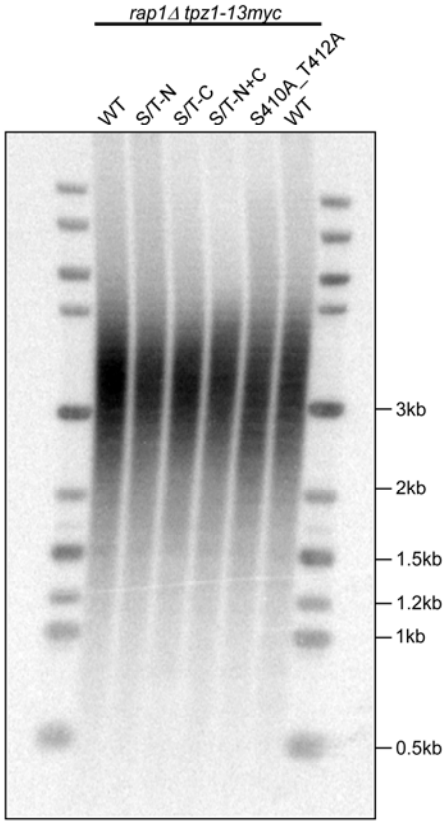

ApaI digested, 0.8% agarose gel

Figure 3.9 Mutagenesis analyses of *in vivo* phosphorylation on Tpz1 in *rap1Δ*. (**A**) In the western blot analysis, both S/T-N and S/T-N+C mutations eliminated *rap1Δ*-induced hyperphosphorylation of Tpz1, indicating that residues mutated in S/T-N were responsible for Tpz1 hyperphosphorylation in *rap1Δ* cells. Although Some Tpz1 proteins were hyperphosphorylated in S/T-C and S410A_S412A cells, a portion of Tpz1 proteins still had mobility shifts, which was seen in the wild type cells in Fig. 3.9B. (**B**) Southern blot analysis of Tpz1 phosphorylation deficient mutants in *rap1Δ* cells did not show any change of telomere length, suggesting that either the essential phosphorylation responsible for telomere extension remained in these mutants, or redundant pathways regulated by Rap1 protein can still promote telomere extension. Western blots were performed with anti-myc antibody for Tpz1 protein and anit-Cdc2 antibody for Cdc2 as the loading control. Southern blot of telomere length was described in Methods section.

3.3 Discussion

Post-translational modifications of telomeric protein, such as phosphorylation, ubiquitylation and SUMOylation, have been found to play roles in regulation of telomere maintenance, with roles of phosphorylation examined most extensively (Hang et al., 2011; Li et al., 2009; Rai et al., 2011; Tseng et al., 2009). For example, phosphorylation of budding yeast Cdc13 Thr308 has been shown to promote Cdc13-Est1 interaction to facilitate telomerase recruitment to telomeres. Similarly, $Rad3^{ATR}$/$Tel1^{ATM}$-dependent phosphorylation of Ccq1 Thr93 promotes Ccq1-Est1 interaction to facilitate telomerase recruitment to telomeres in fission yeast (Moser et al., 2011; Yamazaki et al., 2012a).

In this chapter, I demonstrated that Tpz1 undergoes both $Rad3^{ATR}$/$Tel1^{ATM}$-dependent and -independent phosphorylation at multiple sites, and began to address the functional significance of phosphorylation at those sites by mutational analyses. I also demonstrated that Ccq1, a direct interaction partner of Tpz1, not only mediates Tpz1-telomerase association, but also served as an adapter that facilitates $Rad3^{ATR}$/$Tel1^{ATM}$-dependent phosphorylation of Tpz1. *In vivo* phosphorylation sites were found in different genetic backgrounds (*wt*, *rap1Δ*, *taz1Δ* and *rad3Δ tel1Δ*) by mass spectrometry analyses, and phosphorylation site mutants that affect Tpz1 mobility on SDS-PAGE and telomere length homeostasis were identified. Therefore, data presented in this Chapter support the notion that phosphorylation of Tpz1 contributes to regulation of telomere length homeostasis in fission yeast.

3.3.1 Phosphorylation of Tpz1 regulates telomere length homeostasis

Using mass spectrometry analyses, we were able to identify 28 novel *in vivo* phosphorylation sites from different genetic backgrounds (*wt*, *rap1Δ*, *taz1Δ* and *rad3Δ tel1Δ*). Furthermore, we were able to show that at least 10 of those phosphorylation sites are phosphorylated independently of $Rad3^{ATR}$/$Tel1^{ATM}$ kinases. Among $Rad3^{ATR}$/$Tel1^{ATM}$-independent phosphorylation site, phosphorylation at Ser138 appears to be especially critical for telomere length regulation, since the *tpz1-S138A* mutation caused a dramatic increase in telomere length (Fig. 3.8C). Thus, future analysis of *tpz1-S138A* cells may reveal how phosphorylation of this site might uncover important insights into how Tpz1 S138 phosphorylation contributes to telomere length regulation.

Since telomerase recruitment to telomeres peaks in late S phase (Moser et al., 2009a), it would also be intriguing to further investigate roles of cell cycle-regulated kinases, such as cyclin-dependent kinase, in Tpz1 phosphorylation. Five potentially unique phosphorylation sites were detected in *rap1Δ* and *taz1Δ* cells, including two SQ sites that are predicted to be preferred phosphorylation sites for $Rad3^{ATR}$ and $Tel1^{ATM}$ kinases. Despite the fact that over-expressed Tpz1 did induce the mobility shift and caused slight telomere elongation, it is thus likely that Tpz1 phosphorylation sites identified in this Chapter could serve as valuable information for the future investigation to better understand how phosphorylation of Tpz1 contributes to telomere maintenance in fission yeast.

Mutagenesis studies of Tpz1 phosphorylation sites found that *tpz1-3AQ-C* mutant (S309A, S340A, T354A) cells do not completely lose *rap1Δ*-induced hyper-phosphorylation of Tpz1 (Figure 3.4B). However, mutations on additional

phosphorylation sites (S318A, S327A, T328A, S333A, S334A) included in *tpz1-S/T-N* allele completely eliminated the residual slow mobility band shift (Figure 3.9A). Consistent with the notion that Rad3^{ATR} and Tel1^{ATM} kinases either directly or indirectly promote phosphorylation of Ser318, Ser327, Ser328, Ser333 and Ser334, we did not detect phosphorylation of these sites in *rad3Δ tel1Δ* cells. Previous studies have confirmed that Rad3^{ATR} and Tel1^{ATM} kinases promote telomere extension through phosphorylation on Ccq1 Thr93 (Moser et al., 2011). Therefore, I hoped that mutating Rad3^{ATR}/Tel1^{ATM} -dependent phosphorylation site in the Tpz1 S/T-N region may cause telomere shortening comparable to ccq1-T93A mutation in *wt* or *rap1Δ* cells. However, mutations in the S/T-N region caused only slight on telomere shortening, suggesting that these phosphorylation sites are not as critical as Ccq1-T93 phosphorylation for telomere length regulation.

On the other hand, even though mutations of phosphorylation sites included in the *tpz1-S/T-C* allele (T378A, T379A, S383A, S397A, S404A, S407A, S410A and T412A) did not eliminate Tpz1 mobility shift in *rap1Δ* cells (Fig. 3.9A-B), the *tpz1-S/T-C* mutation caused Tpz1 to migrate faster on SDS-PAGE and caused slight telomere shortening in wild type (i.e. *rap1*$^{+}$ background) cells (Figure 3.8-C). Since phosphorylation of sites mutated in *tpz1-S/T-C* allele were not detected in *rad3Δ tel1Δ* cells (Fig. 3.9A-B), phosphorylation at those sites may also be facilitated either directly or indirectly by Rad3^{ATR} and Tel1^{ATM} kinases. Thus, these findings suggest that phosphorylation of sites within the C-terminal half of the S/T-rich domain may positively contribute to telomere extension or prevent telomere shortening by caused by the end-replication problem or degradation of telomeres. However, since telomere shortening

observed in *tpz1-S/T-C* mutant cells are very subtle and elimination of Rap1 completely suppressed telomere shortening phenotype of *tpz1-S/T-C* cells, Tpz1 phosphorylation within the S/T-C domain appear to only play a minor role in telomere length regulation or function redundantly with other mechanism that ensure telomere extension in fission yeast.

Further investigation should be performed to narrow down the residues that contribute to the observed mobility shift and telomere length change. We should also elucidate whether mutations on *in vivo* Tpz1 phosphorylation sites will affect its interaction with other shelterin complex components, which is reported to promote (Tpz1-Ccq1 and Tpz1-Pot1 interaction) or prevent (Tpz1-Poz1 interaction) telomerase recruitment (Jun et al., 2013). Additionally, characterization of Ccq1 Thr93 phosphorylation status and telomere association of telomerase for various Tpz1 phosphorylation site mutants that affected telomere length will likely provide mechanistic insights into how phosphorylation of Tpz1 contributes in telomere maintenance. While I have completed mutational analysis for majority of Tpz1 phosphorylation sites identified, we should also investigate remaining Tpz1 phosphorylation sites that have not yet been mutated.

3.3.2 Tpz1/TPP1 phosphorylation may represent a conserved mechanism to regulate telomere

Previous studies have shown that mammalian POT1 and TRF2 protect DNA damage responses at telomeres by limiting activation of ATM and ATR kinases (Denchi and de Lange, 2007). In Chapter 2, I have shown that removal of Poz1, Rap1 or Taz1

leads to increased telomere association of Rad3^{ATR} kinase, indicating that negative regulation of ATM/ATR kinases at telomere by the shelterin complex appears to be evolutionarily conserved. Recently, it was shown that Ccq1 Thr93 phosphorylation by Rad3^{ATR}/Tel1^{ATM} kinases is important for Ccq1-Est1 interaction and telomerase recruitment to telomeres, and Ccq1 Thr93 phosphorylation is negatively regulated by Poz1, Rap1 and Taz1 proteins (Moser et al., 2011; Yamazaki et al., 2012a). In this Chapter, I showed that Rad3^{ATR}and Tel1^{ATM} kinases also phosphorylate Tpz1, and the extent of Tpz1 phosphorylation after removal of Poz1, Rap1 or Taz1 closely mirror the extent of telomerase association with telomeres.

For mammalian cells, TPP1 (Tpz1 homolog) is found to directly interact with telomerase catalytic subunit TERT and stimulate telomerase processivity (repetitive addition of telomeric repeats), while CDK1 kinase-dependent phosphorylation at TPP1 Ser111 is involved in telomere extension (Zhang et al., 2013). Although there is currently no evidence demonstrating direct Tpz1-Trt1^{TERT} interaction for fission yeast, analogous to TPP1-TERT interaction in mammalian cells, we and others have shown that Tpz1 can co-immunoprecipitate with telomerase RNA *TER1* and Tpz1-telomerase interaction is dependent on Ccq1 (Miyoshi et al., 2008). Since Ccq1 is essential for Rad3^{ATR}/ Tel1^{ATM}-dependent Tpz1 hyper-phosphorylation, it is possible that Ccq1 contributes to telomerase recruitment not only by Ccq1 Thr93-dependent mechanism, but also by Tpz1 phosphorylation-dependent mechanism. While mammalian ortholog of Ccq1 has not been identified, it is possible that the mammalian shelterin complex might also utilize Ccq1-like protein to facilitate TPP1 phosphorylation. Alternatively, other subunits of the mammalian shelterin complex, such as TIN2 might fulfill the role of Ccq1

in promoting TPP1 phosphorylation, since studies have identified TIN2 mutations that cause telomere shorting and reduced recruitment of telomerase to telomeres (Canudas et al., 2011; Yang et al., 2011). Therefore, future investigations into the roles of Tpz1/TPP1 phosphorylation might uncover a conserved mechanism for regulation of telomerase association with telomeres.

3.4 Materials and Methods

3.4.1 Fission yeast strains, plasmids and primers used in this chapter

The method of making *poz1:natMX4*, *rap1:ura4*$^+$ and *taz1:ura4*$^+$ strain has been described in 2.4.1. We introduced *tpz1-13myc* into *poz1:natMX4*, *rap1:ura4*$^+$ and *taz1:ura4*$^+$ backgrounds by genetic cross and dissection of tetrad spores (Alfa et al., 1993). All strains, plasmids and primers used in this chapter were listed in Table 3.1-3.3.

3.4.2 Tpz1-TER1 RNA co-immunoprecipitation assay

Exponentially growing *tpz1-13myc* cells were harvested and re-suspended by TMG-100 buffer [10mM Tris 1mM $MgCl_2$,100mM NaCl, 10% Glycerol, 1mM EDTA, 0.1mM DTT, 2mM PMSF, 0.2mM APMSF, 1U/ul RNaseOUT™ (Invitrogene),1x cOmplete Protease Inhibitor Cocktail (Roche)] +0.5% NP-40. Cells were mixed with glass beads and broken by genie vortex 3 minutes for four times at 4^{o}C. Lysates were obtained by spun at 13200rpm for 10 minutes. Protein concentration was measured by BioRad BCA assay. Preparing 4mg lysate and taking 1/40 of 4mg lysate as input. 2μg anti-Myc antibody (Cell Signaling, 9B11) was added to the rest of 4mg lysate and the whole antibody-

lysate mixture was kept on nutator at 4^{o}C for 2 hour, followed by adding 60μl Dynabeads Protein G to each reaction at 4^{o}C for 1 hour. The beads were washed by Wash by TMG-100 buffer 1ml for three times, TMG-100 + 0.5% Tween-20 1ml for three times. TER1 RNA was extracted by total RNA isolation kit (Clontech), and TER1 RNA was subject to reverse transcription reaction. Real time RT-PCR with telomere specific primers (listed in table 3.3) was used to quantify cDNA amount.

3.4.3 λ phosphatase treatment and western blot

Lysates of Tpz1-13myc strains were made as described in 3.4.2, and taken for λ protein phosphatase treatment (P0753, New England Biolabs) at 30 ^{o}C for 50 minutes. Reactions were stopped after boiling with 2 x sample buffer for 3 minutes and analyzed by western blot analysis, which was described in 2.4.2 section.

3.4.4 Southern blot of telomere length

This experiment has been described in Chapter 2 Materials and Methods 2.4.2 section.

3.4.5 Protein purification of Tpz1 and Mass Spectrometry analysis

3X FLAG sequence was introduced to pREP41-Tpz1 plasmid (Maundrell, 1993) by using Phusion® Site-Directed Mutagenesis Kit PCR (New England Biolabs) with primers carrying 3x FLAG ® (Sigma) sequence. The plasmid was transformed into yeast strains (*wt*, *rap1Δ*, *taz1Δ*, *rad3Δ tel1Δ*) and selected for *ura+* on the plate. Western blot confirmed the good expression levels of Tpz1 proteins in the cells. We then collected 500ml culture (~ 5 x 10^{9} cells) exponentially growing in the selective media (PMG media

containing Histidine, Leucine, and Alanine). Pelleted cells were re-suspended in 2x lysis buffer (50mM Tris pH8.0, 150mM NaCl, 10% Glycerol, 5mM EDTA, 50mM NaF, 1mM DTT, 1mM Na_3VO_4, 1mM PMSF,1x cOmplete Protease Inhibitor Cocktail (Roche)) and made as ice balls for the cryo-grinding process (Retsch Ball Mill mm301, 25ml Jar, 1/25 s, 5 minutes for four times). The following procedure was done on ice or 4^{o}C and Tpz1 protein was monitored by western blot in the purification process. Ground powdered cells were thawed on ice and lysates were obtained after spun at 13200 rpm for 10 minute at 4^{o}C. Before Tpz1-3FLAG protein immunoprecipitation, lysates went on the pre-clean step with Protein A sepharose for 1 hour at 4^{o}C to eliminate non-specific binding to agarose beads. The lysates then incubated with ANTI-FLAG® M2 Magnetic Agarose Beads (Sigma, M8823) for 2 hours at 4^{o}C. Beads were washed by lysis buffer with 100mM KCl for 5 minutes and repeated two times, and by lysis buffer for three times. Tpz1-3FLAG proteins were eluted by incubating with 100 μg/ml 3X FLAG® Peptide (Sigma, F4799) for 1 hour, and concentrated by Trichloroacetic acid-induced protein precipitation. Air-dried pellets were submitted to our collaborator Dr. Aaron Aslanian of The Scripps Research Institute. Mass Spectrometry data were analyzed by DTASelect v2.0.49 (Cociorva et al., 2007) and residues with AScore >13 were considered to be trustworthy *in vivo* phosphorylation sites (Figure 3.7A).

3.4.6 Site-directed mutagenesis on Tpz1 phosphorylation sites in fission yeast

Target sites on Tpz1 were mutated to Alanine using QuikChange Lightning Multi Site-Directed Mutagenesis Kit (Agilent Technologies) on pBS-Tpz1-13myc plasmid. Mutated tpz1-13myc:kanMX6 gene was derived from the *SalI*/*BglI* digested plasmids, and

transformed to yeast cells. Desired strains were obtained by the selection of G418 resistance.

Table 3.1 Fission yeast strains used in this study

Figure		Strain	Full Genotype[a]
3.1A	*wt (no tag)*	SS5264	*h- ura4-D18 cdc25-22*
	tpz1-myc	TN7467	*h- ura4-D18 tpz1-13myc:KanMX6 cdc25-22*
	tpz1-myc poz1Δ	YTC9362	*h- ura4-D18 tpz1-13myc:KanMX6 poz1::natMX6 cdc25-22*
	tpz1-myc rap1Δ	YTC9307	*h- ura4-D18 rap1::ura4+ tpz1-13myc:KanMX6 cdc25-22*
	tpz1-myc rap1Δ	YTC9327	*h- ura4-D18 taz1-2::ura4+ tpz1-13myc:KanMX6 cdc25-22*
3.1B	*tpz1-myc*	TN7196	*h- ura4-D18 tpz1-13myc:KanMX6*
	tpz1-myc poz1Δ	YTC9366	*h- ura4-D18 tpz1-13myc:KanMX6 poz1::natMX6*
	tpz1-myc rap1Δ	YTC9310	*h- ura4-D18 rap1::ura4+ tpz1-13myc:KanMX6*
	tpz1-myc taz1Δ	YTC9331	*h- ura4-D18 taz1-2::ura4+ tpz1-13myc:KanMX6*
3.2A	*wt (no tag)*	TN2411	*h- ura4-D18*
	tpz1-myc	TN7196	*h- ura4-D18 tpz1-13myc:KanMX6*
	tpz1-myc ccq1-T93A	YTC11740	*h- ura4-D18 ade6-M210 tpz1-13myc:KanMX6 ccq1-T93A:natMX (early)*
3.2B	*wt (no tag)*	TN2411	*h- ura4-D18*
	tpz1-myc	JH11829	*h- ura4-D18 tpz1-13myc:KanMX6*
	tpz1-myc trt1Δ	YTC12763	*h- ura4-D18 ade6-M210 trt1-2::his3+ tpz1-13myc:KanMX6*
	tpz1-myc trt1Δ ccq1Δ	YTC13026	*h- ura4-D18 ade6-M216 trt1-2::his3+ tpz1-13myc:KanMX6 ccq1::hphMX*
3.2C	*wt (no tag)*	TN2411	*h- ura4-D18*
	tpz1-myc	TN7196	*h- ura4-D18 tpz1-13myc:KanMX6*
	tpz1-myc ccq1Δ	TN9009	*h+ ura4-D18 tpz1-13myc:KanMX6 ccq1::hphMX*
	tpz1-myc poz1Δ	YTC9366	*h- ura4-D18 tpz1-13myc:KanMX6 poz1::natMX6*
	tpz1-myc rap1Δ	YTC9310	*h- ura4-D18 rap1::ura4+ tpz1-13myc:KanMX6*
	tpz1-myc taz1Δ	YTC9331	*h- ura4-D18 taz1-2::ura4+ tpz1-13myc:KanMX6*
	tpz1-myc rap1Δ ccq1Δ	LK9883	*h- ura4-D18 rap1::ura4+ tpz1-13myc:KanMX6 ccq1::hphMX*
3.3A	*tpz1-myc rap1Δ*	YTC9310	*h- ura4-D18 rap1::ura4+ tpz1-13myc:KanMX6*
	tpz1-myc rap1Δ tel1Δ	YTC10326[b]	*h- ura4-D18 ade6-M210 rap1::ura4+ tpz1-13myc:KanMX6 tel1::LEU2*
	tpz1-myc rap1Δ rad3Δ	TN10472[b]	*h- ura4-D18 rap1::ura4+ tpz1-13myc:KanMX6 rad3::LEU2*
	tpz1-myc rap1Δ tel1Δ rad3Δ	YTC10356[b]	*h- ura4-D18 ade6-M210 rap1::ura4+ tpz1-13myc:KanMX6 tel1::LEU2 rad3::LEU2 //pREP41H-rad3 (NO) (nmt:rad3; his3+)*
3.3B	*tpz1-myc*	TN7196	*h- ura4-D18 tpz1-13myc:KanMX6*
	tpz1-myc poz1Δ tel1Δ rad3Δ	YTC10296[b]	*h- ura4-D18 ade6-M210 tpz1-13myc:KanMX6 poz1::natMX6 tel1::LEU2 rad3::LEU2 //pREP41H-rad3 (NO) (nmt:rad3; his3+)*
	tpz1-myc rap1Δ tel1Δ rad3Δ	YTC10356[b]	*h- ura4-D18 ade6-M210 rap1::ura4+ tpz1-13myc:KanMX6 tel1::LEU2 rad3::LEU2 //pREP41H-rad3 (NO) (nmt:rad3; his3+)*
	tpz1-myc taz1Δ tel1Δ rad3Δ	YTC10354[b]	*h- ura4-D18 ade6-M210 taz1-2::ura4+ tpz1-13myc:KanMX6 tel1::LEU2 rad3::LEU2 //pREP41H-rad3 (NO) (nmt:rad3; his3+)*
3.3C	*wt (no tag)*	TN2411	*h- ura4-D18*
	tpz1-myc	TN7196	*h- ura4-D18 tpz1-13myc:KanMX6*
	tpz1-myc rap1Δ	YTC9310	*h- ura4-D18 rap1::ura4+ tpz1-13myc:KanMX6*
	tpz1-myc rap1Δ tel1Δ rad3Δ	YTC10356[b]	*h- ura4-D18 ade6-M210 rap1::ura4+ tpz1-13myc:KanMX6 tel1::LEU2 rad3::LEU2 //pREP41H-rad3 (NO) (nmt:rad3; his3+)*

	tpz1-myc taz1Δ	YTC9331	*h- ura4-D18 taz1-2::ura4+ tpz1-13myc:KanMX6*
	tpz1-myc taz1Δ tel1Δ rad3Δ	YTC10354[b]	*h- ura4-D18 ade6-M210 taz1-2::ura4+ tpz1-13myc:KanMX6 tel1::LEU2 rad3::LEU2 //pREP41H-rad3 (NO) (nmt:rad3; his3+)*
3.4B	*wt (no tag)*	TN2411	*h- ura4-D18*
	tpz1-myc rap1Δ	YTC9310	*h- ura4-D18 rap1::ura4+ tpz1-13myc:KanMX6*
	tpz1-myc (6AQ) rap1Δ	TN10643	*h- ura4-D18 ade6-M210 rap1::ura4+ tpz1-S63A,S97A,S164A,S309A,S340A,T354A-13myc:kanMX6*
	tpz1-myc (3AQ-N) rap1Δ	TN10635	*h- ura4-D18 ade6-M210 rap1::ura4+ tpz1-S63A,S97A,S164A-13myc:kanMX6*
	tpz1-myc (4AQ) rap1Δ	TN10552	*h- ura4-D18 ade6-M210 rap1::ura4+ tpz1-S164A,S309A,S340A,T354A-13myc:kanMX6*
	tpz1-myc (3AQ-C) rap1Δ	TN10553	*h- ura4-D18 ade6-M210 rap1::ura4+ tpz1-S309A,S340A,T354A-13myc:kanMX6*
3.4C	*tpz1-myc*	TN7196	*h- ura4-D18 tpz1-13myc:KanMX6*
	tpz1-myc (6AQ)	TN10629	*h- ura4-D18 ade6-M210 tpz1-S63A,S97A,S164A,S309A,S340A,T354A-13myc:kanMX6*
	tpz1-myc (3AQ-N)	TN10623	*h- ura4-D18 ade6-M210 tpz1-S63A,S97A,S164A-13myc:kanMX6*
	tpz1-myc (4AQ)	TN10550	*h- ura4-D18 ade6-M210 tpz1-S164A,S309A,S340A,T354A-13myc:kanMX6*
	tpz1-myc (3AQ-C)	TN10551	*h- ura4-D18 ade6-M210 tpz1-S309A,S340A,T354A-13myc:kanMX6*
3.4D	*tpz1-myc rap1Δ*	YTC9310	*h- ura4-D18 rap1::ura4+ tpz1-13myc:KanMX6*
	tpz1-myc (3AQ-C) rap1Δ	TN10553	*h- ura4-D18 ade6-M210 rap1::ura4+ tpz1-S309A,S340A,T354A-13myc:kanMX6*
	tpz1-myc (4AQ) rap1Δ	TN10552	*h- ura4-D18 ade6-M210 rap1::ura4+ tpz1-S164A,S309A,S340A,T354A-13myc:kanMX6*
	tpz1-myc (3AQ-N) rap1Δ	YTC10639	*h- ura4-D18 ade6-M210 rap1::ura4+ tpz1-S63A,S97A,S164A-13myc:kanMX6 (backup)*
	tpz1-myc (3AQ-N) rap1Δ	YTC10641	*h- ura4-D18 rap1::ura4+ tpz1-S63A,S97A,S164A-13myc:kanMX6 (backup)*
	tpz1-myc (3AQ-N) rap1Δ	YTC10635	*h- ura4-D18 ade6-M210 rap1::ura4+ tpz1-S63A,S97A,S164A-13myc:kanMX6*
	tpz1-myc (3AQ-N) rap1Δ	YTC10637	*h- ura4-D18 rap1::ura4+ tpz1-S63A,S97A,S164A-13myc:kanMX6*
	tpz1-myc (6AQ) rap1Δ	YTC10643	*h- ura4-D18 ade6-M210 rap1::ura4+ tpz1-S63A,S97A,S164A,S309A,S340A,T354A-13myc:kanMX6*
	tpz1-myc (6AQ) rap1Δ	YTC10644	*h- ura4-D18 ade6-M210 rap1::ura4+ tpz1-S63A,S97A,S164A,S309A,S340A,T354A-13myc:kanMX6*
	tpz1-myc (6AQ) rap1Δ	YTC10647	*h- ura4-D18 ade6-M210 rap1::ura4+ tpz1-S63A,S97A,S164A,S309A,S340A,T354A-13myc:kanMX6*
	tpz1-myc (6AQ) rap1Δ	YTC10649	*h- ura4-D18 rap1::ura4+ tpz1-S63A,S97A,S164A,S309A,S340A,T354A-13myc:kanMX6*
3.4E	*tpz1-myc*	TN7196	*h- ura4-D18 tpz1-13myc:KanMX6*
	tpz1-myc rap1Δ	YTC9310	*h- ura4-D18 rap1::ura4+ tpz1-13myc:KanMX6*
	tpz1-myc (6AQ) rap1Δ	YTC10643	*h- ura4-D18 ade6-M210 rap1::ura4+ tpz1-S63A,S97A,S164A,S309A,S340A,T354A-13myc:kanMX6*
3.5A-D	*wt/vector*	TN2411+(499)	*h- ura4-D18//pREP42*
	wt/tpz1-3FLAG plasmid	TN2411+(897)	*h- ura4-D18//pREP42-3FLAG*
	rad3Δ tel1Δ/tpz1-3FLAG plasmid	TN4328+(897)	*h- ura4-D18 ade6-M210 tel1::LEU2 rad3::LEU2//pREP42-3FLAG*
	rap1Δ/tpz1-3FLAG plasmid	YTC13531+(897)	*h+ ura4-D18 rap1::KanMX6 //pREP42-3FLAG*
	taz1Δ/tpz1-3FLAG plasmid	LS6957+(897)	*h- ura4-D18//pREP42-3FLAG*

3.8B-C	*wt (no tag)*	TN2411	*h- ura4-D18*
	tpz1-myc	TN7196	*h- ura4-D18 tpz1-13myc:KanMX6*
	tpz1-myc (S138A)	YTC13545	*h- ura4-D18 ade6-M210 tpz1-S138A-13myc:kanMX6 (early)*
	tpz1-myc (S162A, S164A)	YTC13956	*h+ ura4-D18 ade6-M210 tpz1-S162,S164A-13myc:KanMX6*
	tpz1-myc (S194A)	YTC13787	*h- ura4-D18 ade6-M210 tpz1-S194A-13myc:kanMX6 (early)*
	tpz1-myc (S162A, S164A, S194A)	YTC13959	*h- ura4-D18 ade6-M216 tpz1-S162,S164A,S194A-13myc:KanMX6*
	tpz1-myc (S234A)	YTC13713	*h- ura4-D18 ade6-M210 tpz1-S234A-13myc:kanMX6 (early)*
	tpz1-myc (T238A)	YTC13547	*h- ura4-D18 ade6-M210 tpz1-T238A-13myc:kanMX6 (early)*
	tpz1-myc (S234A, T238A)	YTC13714	*h- ura4-D18 ade6-M210 tpz1-S234A,T238A-13myc:kanMX6 (early)*
	tpz1-myc (S/T-N)	YTC13712	*h- ura4-D18 ade6-M210 tpz1-S309A,S318A,S327A,T328A,S333A,S334A,S340A,T354A-13myc:KanMX6 (early)*
	tpz1-myc (S/T-C)	YTC14012	*h- ura4-D18 tpz1-T378A,T379A,S383A,S397A,S404A,S407A,S410A-13myc:KanMX6 (early)*
	tpz1-myc (S/T-N+C)	YTC14013	*h- ura4-D18 ade6-M210 tpz1-S309A,S318A,S327A,T328A,S333A,S334A,S340A,T354A, T378A,T379A,S383A,S397A,S404A,S407A,S410A-13myc:KanMX6 (early)*
	tpz1-myc (S410A, T412A)	YTC13573	*h- ura4-D18 ade6-M210 tpz1-S410A,T412A-13myc:KanMX6 (early)*
3.9A-B	*wt (no tag)*	TN2411	*h- ura4-D18*
	tpz1-myc rap1Δ	YTC9310	*h- ura4-D18 rap1::ura4+ tpz1-13myc:KanMX6*
	tpz1-myc (S/T-N) rap1Δ	YTC14041	*h+ ura4-D18 ade6-M210 rap1::ura4+ tpz1-S309A,S318A,S327A,T328A,S333A,S334A,S340A,T354A-13myc:KanMX6 (early)*
	tpz1-myc (S/T-C) rap1Δ	YTC14033	*h- ura4-D18 rap1::ura4+ tpz1-T378A,T379A,S383A,S397A,S404A,S407A,S410A-13myc:KanMX6 (early)*
	tpz1-myc (S/T-N+C) rap1Δ	YTC14031	*h+ ura4-D18 rap1::ura4+ tpz1-S309A,S318A,S327A,T328A,S333A,S334A,S340A,T354A, T378A,T379A,S383A,S397A,S404A,S407A,S410A-13myc:KanMX6 (early)*
	tpz1-myc (S410A, T412A) rap1Δ	YTC14037	*h+ leu1-32 ura4-D18 ade6-M210 his3-D1 rap1::ura4+ tpz1-S410A,T412A-13myc:KanMX6 (early)*

[a]All strains are *leu1-32 his3-D1*

[b]Strains are collected after plasmid loss and show HU sensitive.

Table 3.2 DNA primers used in this study

Primer Name	Primer Sequence (5' to 3')	Description
5'TER1-T1	CAGTGTACGTGAGTCTTCTGCCTT	For RT-PCR for telomerase IP.
3'TER1-B1	GATCCATGGATCTCACGTAATG	
275-Ter1	CAAAAATTCGTTGTGATCTGACAAGC	

Table 3.3 Plasmids used in this study

Plasmid (Lab stock #)	Genes	Description
pRep42-Tpz1-3FLAG (879)	tpz1-3FLAG; ura4+, ars1, nmt1; *ampR*	S. pombe expression vector with medium nmt1 promoter & ura4+ marker.
pRep42 (499)	ura4+, ars1, nmt1; ampR	

References

Adams-Martin, A., Dionne, I., Wellinger, R.J., and Holm, C. (2000). The function of DNA polymerase alpha at telomeric G tails is important for telomere homeostasis. Mol Cell Biol *20*, 786-796.

Alfa, C., Fantes, P., Hyams, J., McLoed, M., and Warbrick, E. (1993). Experiments with Fission Yeast (Cold Spring Harbor, NY: Cold Spring Harbor Laboratory Press).

Armanios, M., and Blackburn, E.H. (2012). The telomere syndromes. Nat Rev Genet *13*, 693-704.

Arnoult, N., Schluth-Bolard, C., Letessier, A., Drascovic, I., Bouarich-Bourimi, R., Campisi, J., Kim, S.H., Boussouar, A., Ottaviani, A., Magdinier, F*., et al.* (2010). Replication timing of human telomeres is chromosome arm-specific, influenced by subtelomeric structures and connected to nuclear localization. PLoS Genet *6*, e1000920.

Azzalin, C.M., Reichenbach, P., Khoriauli, L., Giulotto, E., and Lingner, J. (2007). Telomeric repeat containing RNA and RNA surveillance factors at mammalian chromosome ends. Science *318*, 798-801.

Bae, N.S., and Baumann, P. (2007). A RAP1/TRF2 complex inhibits nonhomologous end-joining at human telomeric DNA ends. Mol Cell *26*, 323-334.

Bah, A., Wischnewski, H., Shchepachev, V., and Azzalin, C.M. (2012). The telomeric transcriptome of Schizosaccharomyces pombe. Nucleic Acids Res *40*, 2995-3005.

Baumann, P., and Cech, T.R. (2001). Pot1, the putative telomere end-binding protein in fission yeast and humans. Science *292*, 1171-1175.

Beernink, H.T., Miller, K., Deshpande, A., Bucher, P., and Cooper, J.P. (2003). Telomere maintenance in fission yeast requires an Est1 ortholog. Curr Biol *13*, 575-580.

Bentley, N.J., Holtzman, D.A., Flaggs, G., Keegan, K.S., DeMaggio, A., Ford, J.C., Hoekstra, M., and Carr, A.M. (1996). The *Schizosaccharomyces pombe rad3* checkpoint gene. EMBO J *15*, 6641-6651.

Bi, X., Srikanta, D., Fanti, L., Pimpinelli, S., Badugu, R., Kellum, R., and Rong, Y.S. (2005). *Drosophila* ATM and ATR checkpoint kinases control partially redundant pathways for telomere maintenance. Proc Natl Acad Sci U S A *102*, 15167-15172.

Bianchi, A., and Shore, D. (2007a). Early replication of short telomeres in budding yeast. Cell *128*, 1051-1062.

Bianchi, A., and Shore, D. (2007b). Increased association of telomerase with short telomeres in yeast. Genes Dev *21*, 1726-1730.

Boltz, K.A., Leehy, K., Song, X., Nelson, A.D., and Shippen, D.E. (2012). ATR cooperates with CTC1 and STN1 to maintain telomeres and genome integrity in Arabidopsis. Mol Biol Cell *23*, 1558-1568.

Canudas, S., Houghtaling, B.R., Bhanot, M., Sasa, G., Savage, S.A., Bertuch, A.A., and Smith, S. (2011). A role for heterochromatin protein 1gamma at human telomeres. Genes Dev *25*, 1807-1819.

Casteel, D.E., Zhuang, S., Zeng, Y., Perrino, F.W., Boss, G.R., Goulian, M., and Pilz, R.B. (2009). A DNA polymerase-α•primase cofactor with homology to replication protein A-32 regulates DNA replication in mammalian cells. J Biol Chem *284*, 5807-5818.

Chandra, A., Hughes, T.R., Nugent, C.I., and Lundblad, V. (2001). Cdc13 both positively and negatively regulates telomere replication. Genes Dev *15*, 404-414.

Chang, Y.T., Moser, B.A., and Nakamura, T.M. (2013). Fission Yeast Shelterin Regulates DNA Polymerases and Rad3^{ATR} Kinase to Limit Telomere Extension. PLoS Genet *9*, e1003936.

Chen, L.Y., Majerska, J., and Lingner, J. (2013). Molecular basis of telomere syndrome caused by CTC1 mutations. Genes Dev *27*, 2099-2108.

Chen, L.Y., Redon, S., and Lingner, J. (2012). The human CST complex is a terminator of telomerase activity. Nature *488*, 540-544.

Chen, Y., Rai, R., Zhou, Z.R., Kanoh, J., Ribeyre, C., Yang, Y., Zheng, H., Damay, P., Wang, F., Tsujii, H.*, et al.* (2011). A conserved motif within RAP1 has diversified roles in telomere protection and regulation in different organisms. Nat Struct Mol Biol *18*, 213-221.

Chikashige, Y., and Hiraoka, Y. (2001). Telomere binding of the Rap1 protein is required for meiosis in fission yeast. Curr Biol *11*, 1618-1623.

Cociorva, D., D, L.T., and Yates, J.R. (2007). Validation of tandem mass spectrometry database search results using DTASelect. Curr Protoc Bioinformatics *Chapter 13*, Unit 13 14.

Cooper, J.P., Nimmo, E.R., Allshire, R.C., and Cech, T.R. (1997). Regulation of telomere length and function by a Myb-domain protein in fission yeast. Nature *385*, 744-747.

Cooper, J.P., Watanabe, Y., and Nurse, P. (1998). Fission yeast Taz1 protein is required for meiotic telomere clustering and recombination. Nature *392*, 828-831.

Cornacchia, D., Dileep, V., Quivy, J.P., Foti, R., Tili, F., Santarella-Mellwig, R., Antony, C., Almouzni, G., Gilbert, D.M., and Buonomo, S.B. (2012). Mouse Rif1 is a key regulator of the replication-timing programme in mammalian cells. EMBO J *31*, 3678-3690.

Dahlen, M., Sunnerhagen, P., and Wang, T.S. (2003). Replication proteins influence the maintenance of telomere length and telomerase protein stability. Mol Cell Biol *23*, 3031-3042.

de Lange, T. (2005). Shelterin: the protein complex that shapes and safeguards human telomeres. Genes Dev *19*, 2100-2110.

Dehe, P.M., Rog, O., Ferreira, M.G., Greenwood, J., and Cooper, J.P. (2012). Taz1 enforces cell-cycle regulation of telomere synthesis. Mol Cell *46*, 797-808.

Denchi, E.L., and de Lange, T. (2007). Protection of telomeres through independent control of ATM and ATR by TRF2 and POT1. Nature *448*, 1068-1071.

Deng, Y., Guo, X., Ferguson, D.O., and Chang, S. (2009). Multiple roles for MRE11 at uncapped telomeres. Nature *460*, 914-918.

Evans, S.K., and Lundblad, V. (1999). Est1 and Cdc13 as comediators of telomerase access. Science *286*, 117-120.

Feng, J., Funk, W.D., Wang, S.S., Weinrich, S.L., Avilion, A.A., Chiu, C.P., Adams, R.R., Chang, E., Allsopp, R.C., Yu, J.*, et al.* (1995). The RNA component of human telomerase. Science *269*, 1236-1241.

Ferreira, M.G., and Cooper, J.P. (2001). The fission yeast Taz1 protein protects chromosomes from Ku-dependent end-to-end fusions. Mol Cell *7*, 55-63.

Fujita, I., Tanaka, M., and Kanoh, J. (2012). Identification of the functional domains of the telomere protein Rap1 in *Schizosaccharomyces pombe*. PLoS One *7*, e49151.

Gao, H., Cervantes, R.B., Mandell, E.K., Otero, J.H., and Lundblad, V. (2007). RPA-like proteins mediate yeast telomere function. Nat Struct Mol Biol *14*, 208-214.

Gelinas, A.D., Paschini, M., Reyes, F.E., Heroux, A., Batey, R.T., Lundblad, V., and Wuttke, D.S. (2009). Telomere capping proteins are structurally related to RPA with an additional telomere-specific domain. Proc Natl Acad Sci U S A *106*, 19298-19303.

Gilson, E., and Geli, V. (2007). How telomeres are replicated. Nat Rev Mol Cell Biol *8*, 825-838.

Grandin, N., Damon, C., and Charbonneau, M. (2001). Ten1 functions in telomere end protection and length regulation in association with Stn1 and Cdc13. EMBO J *20*, 1173-1183.

Grandin, N., Reed, S.I., and Charbonneau, M. (1997). Stn1, a new Saccharomyces cerevisiae protein, is implicated in telomere size regulation in association with Cdc13. Genes Dev *11*, 512-527.

Greenwood, J., and Cooper, J.P. (2012). Non-coding telomeric and subtelomeric transcripts are differentially regulated by telomeric and heterochromatin assembly factors in fission yeast. Nucleic Acids Res *40*, 2956-2963.

Greider, C.W., and Blackburn, E.H. (1985). Identification of a specific telomere terminal transferase activity in Tetrahymena extracts. Cell *43*, 405-413.

Greider, C.W., and Blackburn, E.H. (1989). A telomeric sequence in the RNA of Tetrahymena telomerase required for telomere repeat synthesis. Nature *337*, 331-337.

Grossi, S., Puglisi, A., Dmitriev, P.V., Lopes, M., and Shore, D. (2004). Pol12, the B subunit of DNA polymerase alpha, functions in both telomere capping and length regulation. Genes Dev *18*, 992-1006.

Haering, C.H., Nakamura, T.M., Baumann, P., and Cech, T.R. (2000). Analysis of telomerase catalytic subunit mutants *in vivo* and *in vitro* in *Schizosaccharomycespombe*. Proc Natl Acad Sci U S A *97*, 6367-6372.

Hang, L.E., Liu, X., Cheung, I., Yang, Y., and Zhao, X. (2011). SUMOylation regulates telomere length homeostasis by targeting Cdc13. Nat Struct Mol Biol *18*, 920-926.

Hayano, M., Kanoh, Y., Matsumoto, S., Renard-Guillet, C., Shirahige, K., and Masai, H. (2012). Rif1 is a global regulator of timing of replication origin firing in fission yeast. Genes Dev *26*, 137-150.

Hayashi, M., Katou, Y., Itoh, T., Tazumi, A., Yamada, Y., Takahashi, T., Nakagawa, T., Shirahige, K., and Masukata, H. (2007). Genome-wide localization of pre-RC sites and identification of replication origins in fission yeast. EMBO J *26*, 1327-1339.

Hector, R.E., Shtofman, R.L., Ray, A., Chen, B.R., Nyun, T., Berkner, K.L., and Runge, K.W. (2007). Tel1p preferentially associates with short telomeres to stimulate their elongation. Mol Cell *27*, 851-858.

Hedges, S.B. (2002). The origin and evolution of model organisms. Nat Rev Genet *3*, 838-849.

Hodson, J.A., Bailis, J.M., and Forsburg, S.L. (2003). Efficient labeling of fission yeast Schizosaccharomyces pombe with thymidine and BUdR. Nucleic Acids Res *31*, e134.

Huang, C., Dai, X., and Chai, W. (2012). Human Stn1 protects telomere integrity by promoting efficient lagging-strand synthesis at telomeres and mediating C-strand fill-in. Cell Res *22*, 1681-1695.

Hughes, T.R., Morris, D.K., Salinger, A., Walcott, N., Nugent, C.I., and Lundblad, V. (1997). The role of the EST genes in yeast telomere replication. Ciba Found Symp *211*, 41-47; discussion 47-52, 71-45.

Jia, X., Weinert, T., and Lydall, D. (2004). Mec1 and Rad53 inhibit formation of single-stranded DNA at telomeres of *Saccharomyces cerevisiae cdc13-1* mutants. Genetics *166*, 753-764.

Jun, H.I., Liu, J., Jeong, H., Kim, J.K., and Qiao, F. (2013). Tpz1 controls a telomerase-nonextendible telomeric state and coordinates switching to an extendible state via Ccq1. Genes Dev *27*, 1917-1931.

Kanoh, J., and Ishikawa, F. (2001). spRap1 and spRif1, recruited to telomeres by Taz1, are essential for telomere function in fission yeast. Curr Biol *11*, 1624-1630.

Kanoh, J., Sadaie, M., Urano, T., and Ishikawa, F. (2005). Telomere binding protein Taz1 establishes Swi6 heterochromatin independently of RNAi at telomeres. Curr Biol *15*, 1808-1819.

Khair, L., Subramanian, L., Moser, B.A., and Nakamura, T.M. (2009). Roles of heterochromatin and telomere proteins in regulation of fission yeast telomere recombination and telomerase recruitment. J Biol Chem *285*, 5327-5337.

Li, S., Makovets, S., Matsuguchi, T., Blethrow, J.D., Shokat, K.M., and Blackburn, E.H. (2009). Cdk1-dependent phosphorylation of Cdc13 coordinates telomere elongation during cell-cycle progression. Cell *136*, 50-61.

Liu, C.C., Gopalakrishnan, V., Poon, L.F., Yan, T., and Li, S. (2014). Cdk1 regulates the temporal recruitment of telomerase and cdc13-stn1-ten1 complex for telomere replication. Mol Cell Biol *34*, 57-70.

Liu, D., O'Connor, M.S., Qin, J., and Songyang, Z. (2004). Telosome, a mammalian telomere-associated complex formed by multiple telomeric proteins. J Biol Chem *279*, 51338-51342.

Luke, B., Panza, A., Redon, S., Iglesias, N., Li, Z., and Lingner, J. (2008). The Rat1p 5' to 3' exonuclease degrades telomeric repeat-containing RNA and promotes telomere elongation in Saccharomyces cerevisiae. Mol Cell *32*, 465-477.

Lydall, D. (2009). Taming the tiger by the tail: modulation of DNA damage responses by telomeres. EMBO J *28*, 2174-2187.

Mahaney, B.L., Meek, K., and Lees-Miller, S.P. (2009). Repair of ionizing radiation-induced DNA double-strand breaks by non-homologous end-joining. Biochem J *417*, 639-650.

Martin, V., Du, L.L., Rozenzhak, S., and Russell, P. (2007). Protection of telomeres by a conserved Stn1-Ten1 complex. Proc Natl Acad Sci U S A *104*, 14038-14043.

Martinez, P., and Blasco, M.A. (2010). Role of shelterin in cancer and aging. Aging Cell *9*, 653-666.

Maundrell, K. (1993). Thiamine-repressible expression vectors pREP and pRIP for fission yeast. Gene *123*, 127-130.

McClintock, B. (1941). The Association of Mutants with Homozygous Deficiencies in Zea Mays. Genetics *26*, 542-571.

Michelson, R.J., Rosenstein, S., and Weinert, T. (2005). A telomeric repeat sequence adjacent to a DNA double-stranded break produces an anticheckpoint. Genes Dev *19*, 2546-2559.

Miller, K.M., and Cooper, J.P. (2003). The telomere protein Taz1 is required to prevent and repair genomic DNA breaks. Mol Cell *11*, 303-313.

Miller, K.M., Ferreira, M.G., and Cooper, J.P. (2005). Taz1, Rap1 and Rif1 act both interdependently and independently to maintain telomeres. EMBO J *24*, 3128-3135.

Miller, K.M., Rog, O., and Cooper, J.P. (2006). Semi-conservative DNA replication through telomeres requires Taz1. Nature *440*, 824-828.

Min, B., and Collins, K. (2009). An RPA-related sequence-specific DNA-binding subunit of telomerase holoenzyme is required for elongation processivity and telomere maintenance. Mol Cell *36*, 609-619.

Miyake, Y., Nakamura, M., Nabetani, A., Shimamura, S., Tamura, M., Yonehara, S., Saito, M., and Ishikawa, F. (2009). RPA-like mammalian Ctc1-Stn1-Ten1 complex binds to single-stranded DNA and protects telomeres independently of the Pot1 pathway. Mol Cell *36*, 193-206.

Miyoshi, T., Kanoh, J., Saito, M., and Ishikawa, F. (2008). Fission yeast Pot1-Tpp1 protects telomeres and regulates telomere length. Science *320*, 1341-1344.

Moser, B.A., Chang, Y.T., Kosti, J., and Nakamura, T.M. (2011). Tel1^{ATM} and Rad3^{ATR} kinases promote Ccq1-Est1 interaction to maintain telomeres in fission yeast. Nat Struct Mol Biol *18*, 1408-1413.

Moser, B.A., Subramanian, L., Chang, Y.T., Noguchi, C., Noguchi, E., and Nakamura, T.M. (2009a). Differential arrival of leading and lagging strand DNA polymerases at fission yeast telomeres. EMBO J *28*, 810-820.

Moser, B.A., Subramanian, L., Khair, L., Chang, Y.T., and Nakamura, T.M. (2009b). Fission yeast Tel1^{ATM} and Rad3^{ATR} promote telomere protection and telomerase recruitment. PLoS Genet *5*, e1000622.

Müller, H. (1938). The remaking of chromosomes. . Collecting Net (Woods Hole) *13*, 181–198.

Naito, T., Matsuura, A., and Ishikawa, F. (1998). Circular chromosome formation in a fission yeast mutant defective in two ATM homologues. Nat Genet *20*, 203-206.

Nakamura, T.M., Cooper, J.P., and Cech, T.R. (1998). Two modes of survival of fission yeast without telomerase. Science *282*, 493-496.

Nakamura, T.M., Morin, G.B., Chapman, K.B., Weinrich, S.L., Andrews, W.H., Lingner, J., Harley, C.B., and Cech, T.R. (1997). Telomerase catalytic subunit homologs from fission yeast and human. Science *277*, 955-959.

Nakamura, T.M., Moser, B.A., and Russell, P. (2002). Telomere binding of checkpoint sensor and DNA repair proteins contributes to maintenance of functional fission yeast telomeres. Genetics *161*, 1437-1452.

Nakaoka, H., Nishiyama, A., Saito, M., and Ishikawa, F. (2012). *Xenopus laevis* Ctc1-Stn1-Ten1 (xCST) protein complex is involved in priming DNA synthesis on single-stranded DNA template in Xenopus egg extract. J Biol Chem *287*, 619-627.

Nimmo, E.R., Cranston, G., and Allshire, R.C. (1994). Telomere-associated chromosome breakage in fission yeast results in variegated expression of adjacent genes. EMBO J *13*, 3801-3811.

Noguchi, E., Noguchi, C., McDonald, W.H., Yates, J.R., 3rd, and Russell, P. (2004). Swi1 and Swi3 are components of a replication fork protection complex in fission yeast. Mol Cell Biol *24*, 8342-8355.

Nugent, C.I., Bosco, G., Ross, L.O., Evans, S.K., Salinger, A.P., Moore, J.K., Haber, J.E., and Lundblad, V. (1998). Telomere maintenance is dependent on activities required for end repair of double-strand breaks. Curr Biol *8*, 657-660.

Ohya, T., Kawasaki, Y., Hiraga, S., Kanbara, S., Nakajo, K., Nakashima, N., Suzuki, A., and Sugino, A. (2002). The DNA polymerase domain of polε is required for rapid, efficient, and highly accurate chromosomal DNA replication, telomere length maintenance, and normal cell senescence in Saccharomyces cerevisiae. J Biol Chem *277*, 28099-28108.

Olovnikov, A.M. (1971). [Principle of marginotomy in template synthesis of polynucleotides]. Dokl Akad Nauk SSSR *201*, 1496-1499.

Palm, W., and de Lange, T. (2008). How shelterin protects mammalian telomeres. Annu Rev Genet *42*, 301-334.

Pardo, B., and Marcand, S. (2005). Rap1 prevents telomere fusions by nonhomologous end joining. EMBO J *24*, 3117-3127.

Pennock, E., Buckley, K., and Lundblad, V. (2001). Cdc13 delivers separate complexes to the telomere for end protection and replication. Cell *104*, 387-396.

Price, C.M., Boltz, K.A., Chaiken, M.F., Stewart, J.A., Beilstein, M.A., and Shippen, D.E. (2010). Evolution of CST function in telomere maintenance. Cell Cycle *9*, 3157-3165.

Puglisi, A., Bianchi, A., Lemmens, L., Damay, P., and Shore, D. (2008). Distinct roles for yeast Stn1 in telomere capping and telomerase inhibition. EMBO J *27*, 2328-2339.

Qi, H., and Zakian, V.A. (2000). The *Saccharomyces* telomere-binding protein Cdc13p interacts with both the catalytic subunit of DNA polymerase α and the telomerase-associated Est1 protein. Genes Dev *14*, 1777-1788.

Rai, R., Li, J.M., Zheng, H., Lok, G.T., Deng, Y., Huen, M.S., Chen, J., Jin, J., and Chang, S. (2011). The E3 ubiquitin ligase Rnf8 stabilizes Tpp1 to promote telomere end protection. Nat Struct Mol Biol *18*, 1400-1407.

Reichenbach, P., Hoss, M., Azzalin, C.M., Nabholz, M., Bucher, P., and Lingner, J. (2003). A human homolog of yeast Est1 associates with telomerase and uncaps chromosome ends when overexpressed. Curr Biol *13*, 568-574.

Sabourin, M., Tuzon, C.T., and Zakian, V.A. (2007). Telomerase and Tel1p preferentially associate with short telomeres in *S. cerevisiae*. Mol Cell *27*, 550-561.

Sakaguchi, K., Ishibashi, T., Uchiyama, Y., and Iwabata, K. (2009). The multi-replication protein A (RPA) system--a new perspective. FEBS J *276*, 943-963.

Schoeftner, S., and Blasco, M.A. (2008). Developmentally regulated transcription of mammalian telomeres by DNA-dependent RNA polymerase II. Nat Cell Biol *10*, 228-236.

Sfeir, A., Kosiyatrakul, S.T., Hockemeyer, D., MacRae, S.L., Karlseder, J., Schildkraut, C.L., and de Lange, T. (2009). Mammalian telomeres resemble fragile sites and require TRF1 for efficient replication. Cell *138*, 90-103.

Singer, M.S., and Gottschling, D.E. (1994). TLC1: template RNA component of *Saccharomyces cerevisiae* telomerase. Science *266*, 404-409.

Sipiczki, M. (2000). Where does fission yeast sit on the tree of life? Genome Biol *1*, REVIEWS1011.

Sivakumar, S., Porter-Goff, M., Patel, P.K., Benoit, K., and Rhind, N. (2004). *In vivo* labeling of fission yeast DNA with thymidine and thymidine analogs. Methods *33*, 213-219.

Snow, B.E., Erdmann, N., Cruickshank, J., Goldman, H., Gill, R.M., Robinson, M.O., and Harrington, L. (2003). Functional conservation of the telomerase protein Est1p in humans. Curr Biol *13*, 698-704.

Subramanian, L., Moser, B.A., and Nakamura, T.M. (2008). Recombination-based telomere maintenance is dependent on Tel1-MRN and Rap1 and inhibited by telomerase, Taz1, and Ku in fission yeast. Mol Cell Biol *28*, 1443-1455.

Subramanian, L., and Nakamura, T.M. (2010). A kinase-independent role for the $Rad3^{ATR}$-$Rad26^{ATRIP}$ complex in recruitment of $Tel1^{ATM}$ to telomeres in fission yeast. PLoS Genet *6*, e1000839.

Sun, J., Yu, E.Y., Yang, Y., Confer, L.A., Sun, S.H., Wan, K., Lue, N.F., and Lei, M. (2009). Stn1-Ten1 is an Rpa2-Rpa3-like complex at telomeres. Genes Dev *23*, 2900-2914.

Surovtseva, Y.V., Churikov, D., Boltz, K.A., Song, X., Lamb, J.C., Warrington, R., Leehy, K., Heacock, M., Price, C.M., and Shippen, D.E. (2009). Conserved telomere maintenance component 1 interacts with STN1 and maintains chromosome ends in higher eukaryotes. Mol Cell *36*, 207-218.

Tazumi, A., Fukuura, M., Nakato, R., Kishimoto, A., Takenaka, T., Ogawa, S., Song, J.H., Takahashi, T.S., Nakagawa, T., Shirahige, K*., et al.* (2012). Telomere-binding protein Taz1 controls global replication timing through its localization near late replication origins in fission yeast. Genes Dev *26*, 2050-2062.

Teixeira, M.T., Arneric, M., Sperisen, P., and Lingner, J. (2004). Telomere length homeostasis is achieved via a switch between telomerase- extendible and -nonextendible states. Cell *117*, 323-335.

Tomaska, L., Willcox, S., Slezakova, J., Nosek, J., and Griffith, J.D. (2004). Taz1 binding to a fission yeast model telomere: formation of telomeric loops and higher order structures. J Biol Chem *279*, 50764-50772.

Tomita, K., and Cooper, J.P. (2008). Fission yeast Ccq1 is telomerase recruiter and local checkpoint controller. Genes Dev *22*, 3461-3474.

Tseng, S.F., Lin, J.J., and Teng, S.C. (2006). The telomerase-recruitment domain of the telomere binding protein Cdc13 is regulated by Mec1p/Tel1p-dependent phosphorylation. Nucleic Acids Res *34*, 6327-6336.

Tseng, S.F., Shen, Z.J., Tsai, H.J., Lin, Y.H., and Teng, S.C. (2009). Rapid Cdc13 turnover and telomere length homeostasis are controlled by Cdk1-mediated phosphorylation of Cdc13. Nucleic Acids Res *37*, 3602-3611.

Verdun, R.E., Crabbe, L., Haggblom, C., and Karlseder, J. (2005). Functional human telomeres are recognized as DNA damage in G2 of the cell cycle. Mol Cell *20*, 551-561.

Verdun, R.E., and Karlseder, J. (2007). Replication and protection of telomeres. Nature *447*, 924-931.

Vespa, L., Couvillion, M., Spangler, E., and Shippen, D.E. (2005). ATM and ATR make distinct contributions to chromosome end protection and the maintenance of telomeric DNA in Arabidopsis. Genes Dev *19*, 2111-2115.

Wach, A., Brachat, A., Pohlmann, R., and Philippsen, P. (1994). New heterologous modules for classical or PCR-based gene disruptions in *Saccharomyces cerevisiae*. Yeast *10*, 1793-1808.

Walker, J.R., and Zhu, X.D. (2012). Post-translational modifications of TRF1 and TRF2 and their roles in telomere maintenance. Mech Ageing Dev *133*, 421-434.

Wan, M., Qin, J., Songyang, Z., and Liu, D. (2009). OB fold-containing protein 1 (OBFC1), a human homolog of yeast Stn1, associates with TPP1 and is implicated in telomere length regulation. J Biol Chem *284*, 26725-26731.

Wang, F., Stewart, J.A., Kasbek, C., Zhao, Y., Wright, W.E., and Price, C.M. (2012). Human CST has independent functions during telomere duplex replication and C-strand fill-in. Cell Rep *2*, 1096-1103.

Watson, J.D. (1972). Origin of concatemeric T7 DNA. Nat New Biol *239*, 197-201.

Webb, C.J., and Zakian, V.A. (2008). Identification and characterization of the *Schizosaccharomyces pombe* TER1 telomerase RNA. Nat Struct Mol Biol *15*, 34-42.

Webb, C.J., and Zakian, V.A. (2012). Schizosaccharomyces pombe Ccq1 and TER1 bind the 14-3-3-like domain of Est1, which promotes and stabilizes telomerase-telomere association. Genes Dev *26*, 82-91.

Williams, R.S., Williams, J.S., and Tainer, J.A. (2007). Mre11-Rad50-Nbs1 is a keystone complex connecting DNA repair machinery, double-strand break signaling, and the chromatin template. Biochem Cell Biol *85*, 509-520.

Wu, P., Takai, H., and de Lange, T. (2012). Telomeric 3' overhangs derive from resection by Exo1 and Apollo and fill-in by POT1b-associated CST. Cell *150*, 39-52.

Wu, Y., Xiao, S., and Zhu, X.D. (2007). MRE11-RAD50-NBS1 and ATM function as co-mediators of TRF1 in telomere length control. Nat Struct Mol Biol *14*, 832-840.

Yamazaki, H., Tarumoto, Y., and Ishikawa, F. (2012a). $Tel1^{ATM}$ and $Rad3^{ATR}$ phosphorylate the telomere protein Ccq1 to recruit telomerase and elongate telomeres in fission yeast. Genes Dev *26*, 241-246.

Yamazaki, S., Ishii, A., Kanoh, Y., Oda, M., Nishito, Y., and Masai, H. (2012b). Rif1 regulates the replication timing domains on the human genome. EMBO J *31*, 3667-3677.

Yang, D., He, Q., Kim, H., Ma, W., and Songyang, Z. (2011). TIN2 protein dyskeratosis congenita missense mutants are defective in association with telomerase. J Biol Chem *286*, 23022-23030.

Ye, J.Z., Donigian, J.R., van Overbeek, M., Loayza, D., Luo, Y., Krutchinsky, A.N., Chait, B.T., and de Lange, T. (2004). TIN2 binds TRF1 and TRF2 simultaneously and stabilizes the TRF2 complex on telomeres. J Biol Chem *279*, 47264-47271.

Yu, G.L., Bradley, J.D., Attardi, L.D., and Blackburn, E.H. (1990). In vivo alteration of telomere sequences and senescence caused by mutated Tetrahymena telomerase RNAs. Nature *344*, 126-132.

Zhang, Y., Chen, L.Y., Han, X., Xie, W., Kim, H., Yang, D., Liu, D., and Songyang, Z. (2013). Phosphorylation of TPP1 regulates cell cycle-dependent telomerase recruitment. Proc Natl Acad Sci U S A *110*, 5457-5462.

Zhao, Y., Sfeir, A.J., Zou, Y., Buseman, C.M., Chow, T.T., Shay, J.W., and Wright, W.E. (2009). Telomere extension occurs at most chromosome ends and is uncoupled from fill-in in human cancer cells. Cell *138*, 463-475.

Zhong, Z., Shiue, L., Kaplan, S., and de Lange, T. (1992). A mammalian factor that binds telomeric TTAGGG repeats in vitro. Mol Cell Biol *12*, 4834-4843.

Zubko, M.K., and Lydall, D. (2006). Linear chromosome maintenance in the absence of essential telomere-capping proteins. Nat Cell Biol *8*, 734-740.

VITA

NAME	Ya-Ting Chang
PROFESSIONAL MEMBERSHIP	American Society for Microbiology
HONORS	Hsu Chien-Tien Award, 2003 Annual Thesis Competition, Taiwan
	Yin Hsun-Ruo Scholarship, First Place, 2003 Academic Competition of Master Thesis of National Yang-Ming University, Taiwan
	Student Presenter Awards of UIC, 2013
ABSRACTS	Fission Yeast EMBO Meeting in London 2013, poster.
	UIC Student Research Forum 2009-10 and 2011, poster.
	Midwest Yeast Meeting 2010, poster.
	Cold Spring Harbor Laboratory Telomeres & Telomerase Meeting 2009, poster.
PUBLICATION	Moser, B.A., Subramanian, L., **Chang, Y.-T.**, Noguchi, C., Noguchi, E. and Nakamura, T.M. Differential arrival of leading and lagging strand DNA polymerases at fission yeast telomeres. *EMBO J*. 28(7): 810-820, 2008.
	Moser, B.A., Subramanian, L., Khair, L., **Chang, Y.-T**. and Nakamura, T.M. Fission yeast $Tel1^{ATM}$ and $Rad3^{ATR}$ promote telomere protection and telomerase recruitment. *PLoS Genet*. 5(8): e1000622, 2009.
	Khair, L., **Chang, Y.-T.**, Subramanian, L., Russell, P. and Nakamura, T.M. Roles of the checkpoint sensor clamp Rad9-Rad1-Hus1 (911)-complex and the clamp loaders Rad17-RFC and Ctf18-RFC in *Schizosaccharomyces pombe* telomere maintenance. *Cell Cycle* 9(11): 2237-2248, 2010.
	Moser, B.A., **Chang, Y.-T.**, Kosti, J. and Nakamura, T.M. $Tel1^{ATM}$ and $Rad3^{ATR}$ kinases promote Ccq1-Est1 interaction to maintain telomeres in fission yeast. *Nat. Struct. Mol. Biol*. 18: 1408-1413, 2011.
	Chang,Y.-T., Moser, B.A. and Nakamura, T.M. Fission yeast shelterin regulates DNA polymerases and Rad3ATR kinase to limit telomere extension. *PLoS Genet*. 9(11): e1003936, 2013.
	Moser, B.A., **Chang, Y.-T.**, Nakamura, T. M. Telomere regulation during cell cycle in fission yeast. Methods Mol. Biol. : Cell Cycle Control, Mechanisms and Protocols, 2nd Edition (Eds. Noguch, E. and Gadaleta, M.) In Press, 2014.